1 OF 2

N75 12775

UNCLAS

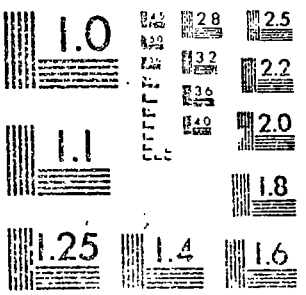

MICROCOPY RESOLUTION TEST CHART
NATIONAL BUREAU OF STANDARDS-1963-A

Princeton University

DEI SUB NUMINE VIGET

Department of Aerospace and Mechanical Sciences

National Aeronautics and Space Administration
NGL 31-001-005

PULSED ELECTROMAGNETIC GAS ACCELERATION

1 January 1974 to 30 June 1974

Semi-annual Report 634w

Prepared by:

Robert G. Jahn
Dean, School of Engineering and
Principal Investigator

and

Woldemar E. von Jaskowsky
Sr. Research Engineer and
Lecturer

Kenn E. Clark
Research Engineer

July 1974

School of Engineering and Applied Science
Department of Aerospace and Mechanical Sciences
Guggenheim Aerospace Propulsion Laboratories
PRINCETON UNIVERSITY
Princeton, NJ 08540

ABSTRACT

Detailed measurements of the axial velocity profile and electromagnetic structure of a high power, quasi-steady MPD discharge are used to formulate a gasdynamic model of the acceleration process. Conceptually dividing the accelerated plasma into an inner flow and an outer flow, it is found that more than two-thirds of the total power in the plasma is deposited in the inner flow, accelerating it to an exhaust velocity of 12.5 km/sec. The outer flow, which is accelerated to a velocity of only 6.2 km/sec, appears to provide a current conduction path between the inner flow and the anode.

Related cathode studies have shown that the critical current for the onset of terminal voltage fluctuations, which was recently shown to be a function of the cathode area, appears to reach an asymptote for cathodes of very large surface area. Detailed floating potential measurements show that the fluctuations are confined to the vicinity of the cathode and hence reflect a cathode emission process rather than a fundamental limit on MPD performance.

A 45-cm wide parallel plate configuration produces a two-dimensional discharge which replicates the essential features of the conventional three-dimensional MPD discharge. Magnetic probe studies show that for a total current of 65 kA, the current distribution is uniform to better than 10% across the entire electrode width with no evidence of instabilities. Using a recently constructed resonant optical cavity which will straddle this configuration and a newly designed and calibrated mass feed system capable of injecting a uniformly distributed mass flow of more than 10 g/sec with a risetime of only 2 msec, this device will be capable of determining directly whether lasing can be obtained in the MPD flow.

Axial floating potential and enclosed current distributions have been measured for several hollow cathode configurations using an extended current pulse of 500 μsec duration. For a cathode cavity which diverges with a 10^{o} half-angle, the characteristic features of the distributions are the same as for previous cylindrical hollow cathodes: a surface current density greater than 1000 A/cm^2 at the downstream end of the cavity accompanied by a weak axial electric field of less than 10 V/cm. For a configuration where the cavity diverges at a 45^{o} half-angle, the equipotential plateau recedes further inside the cavity and drops to only +4 volts with respect to the cathode, as compared to approximately +20 volts for the cylindrical cathode. In addition, preliminary data indicate that the current density peaks on the 45^{o} face rather than at the downstream end of the cavity. Based on the results of these and previous tests, a cylindrical hollow cathode with refractory insulation has been selected for a more detailed series of diagnostic measurements.

TABLE OF CONTENTS

LIST OF ILLUSTRATIONS

LIST OF ILLUSTRATIONS (Cont'd)

CURRENT STUDENT PARTICIPATION

Student	Period	Degree	
BOYLE, Michael J.	1968-1969 1971-	B.S.E. Ph.D. Cand.	Velocity and Acceleration Patterns in the MPD Exhaust
CAMPBELL, Edward M.	1972-	Ph.D. Cand.	Plasmadynamic Laser Studies
DUTT, Gautam S.	1971-	Ph.D. Cand.	Stimulated Emission of Argon Ion Lines in High Current Discharges
KRISHNAN, Mahadevan	1972-	Ph.D. Cand.	Hollow Cathode Discharges
RUDOLPH, L. Kevin	1973-		Cathode Studies in MPD Discharges
VILLANI, Daniel D.	1969-	Ph.D. Cand.	Power Deposition in MPD Discharges

I. INTRODUCTION

During this past spring, the Electric Propulsion Lab was moved from the Forrestal Campus, approximately four miles outside of Princeton, to the Engineering Quadrangle on the main campus. The move was undertaken to facilitate collaboration with several related research programs already housed in the Quadrangle, and to provide more accessible facilities for student participation in independent research programs during their undergraduate years. The relocation was totally financed by the University, which continues to regard the Princeton program in electric propulsion as one of the principal vehicles for undergraduate and graduate research education within the Engineering School, and one of the selected areas of engineering research in which it can best serve the national aerospace needs. The new laboratory was officially opened on Tuesday, May 21 in a brief ceremony attended by the President of the University, William Bowen, Mr. James Lazar from NASA Headquarters, and approximately 50 members of the Engineering faculty, staff and students. Figure 1 shows Mr. Lazar triggering the initial plasma discharge in the new laboratory.

During Mr. Lazar's visit, the various phases of the laboratory research program were reviewed in detail. After discussing the on-going studies of power deposition into the MPD anode and the insulator ablation and cathode emission problems, the suggestion was made that the MPD discharge work be broadened to serve as a basis for further arc physics studies. Accordingly, the MPD effort now encompasses the Ph.D. programs of three graduate students and the independent research topic of one undergraduate student. Of these, the work on the acceleration mechanisms in an MPD discharge free of ablated species, and two aspects of the study of the cathode emission processes are reviewed in this semi-annual report.

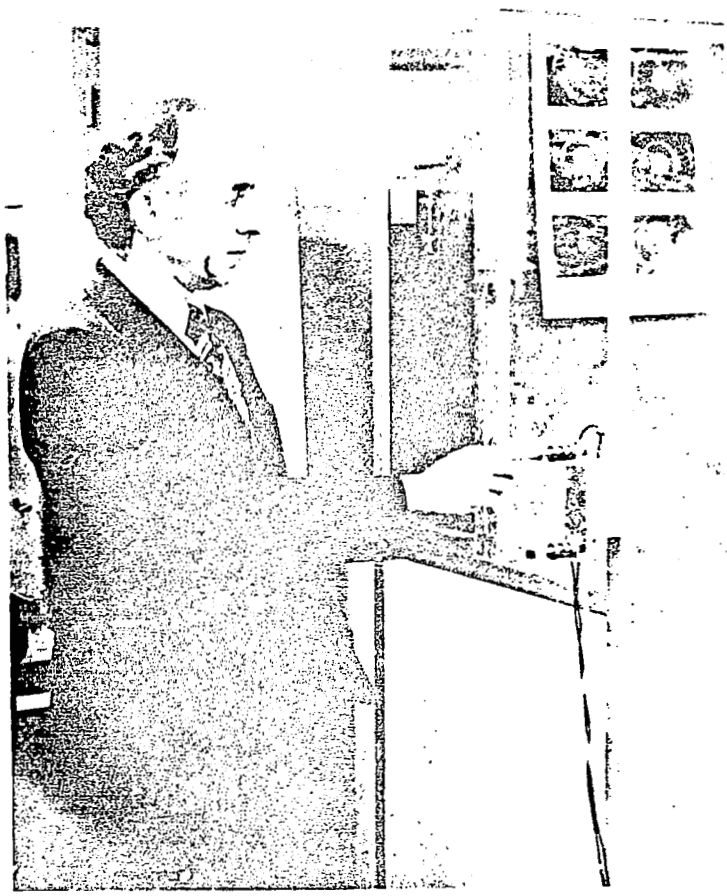

FIRST FIRING OF DISCHARGE APPARATUS BY
J. LAZAR, NASA HEADQUARTERS

FIGURE 1
AP25-P-539

The plasmadynamic laser program is an example of the development of a new avenue of research from a more general study of the physics of high current MPD discharges. Earlier measurements of the radiation environment in the discharge revealed several levels of ionization in the expanding exhaust flow. Use of operating conditions where this radiation is optimized gives rise to the possibility of high power lasing in the visible and ultraviolet. Of the two Ph.D. programs in this topical area, one is centered on the examination of the optical depth of selected argon ion and neutral lines in the exhaust of the conventional three-dimensional discharge geometry. The second program examines the gain of selected lines directly by using an optical cavity in conjunction with a unique two-dimensional plasma accelerator geometry. This latter program has progressed rapidly and will be described in detail. In addition and at the sponsor's request, technical contact in this area has been initiated with F. C. Schwenk and K. Thom of NASA Headquarters.

The program to determine the physics of hollow cathode operation has completed its first phase. This work, which is reviewed herein, has examined various hollow cathode geometries and the extent to which they influence the current distribution within the cavity and the equipotential profile along the cathode centerline. Based on these results, a cathode has been selected with which to begin a series of more detailed measurements of the plasma properties within the cavity.

II. LABORATORY RELOCATION

Following the recent move, the Electric Propulsion Laboratory is now located on the main campus in the Engineering Quadrangle, shown in Fig. 2. This building houses the classrooms, experimental and support facilities for the Electrical Engineering, Chemical Engineering, Civil Engineering, and Aerospace and Mechanical Sciences Departments, as well as several interdisciplinary programs in energy conversion, bioengineering, environmental studies and transportation.

The move proved to be an advantageous time to redesign the laboratory layout for optimum service of the present and future needs and for incorporating several modifications and improvements to the existing discharge equipment. Figures 3, 4 and 5 show three views of the new laboratory arrangement. As can be seen, large areas are now available around each machine for improved accessibility and specialized diagnostic equipment. In addition, sufficient flexibility has been built in to allow repositioning each machine within its area for special tests or discharge configurations. The photos also show an optics room connected to the main lab and a conference area, two features that were not present in the previous laboratory arrangement due to space limitations. Not shown but immediately adjoining the optics room is a photographic dark room.

All of the capacitor power supplies are located on the floor below the laboratory with the connection to the discharge devices provided by bundles of coaxial cable (RG 8/U). Figure 6 shows the two principal capacitor banks. The bank on the left provides currents from 1 to 20 kA for hollow cathode experiments, and the bank on the right supplies up to 120 kA for MPD discharges associated with either propulsion, arc

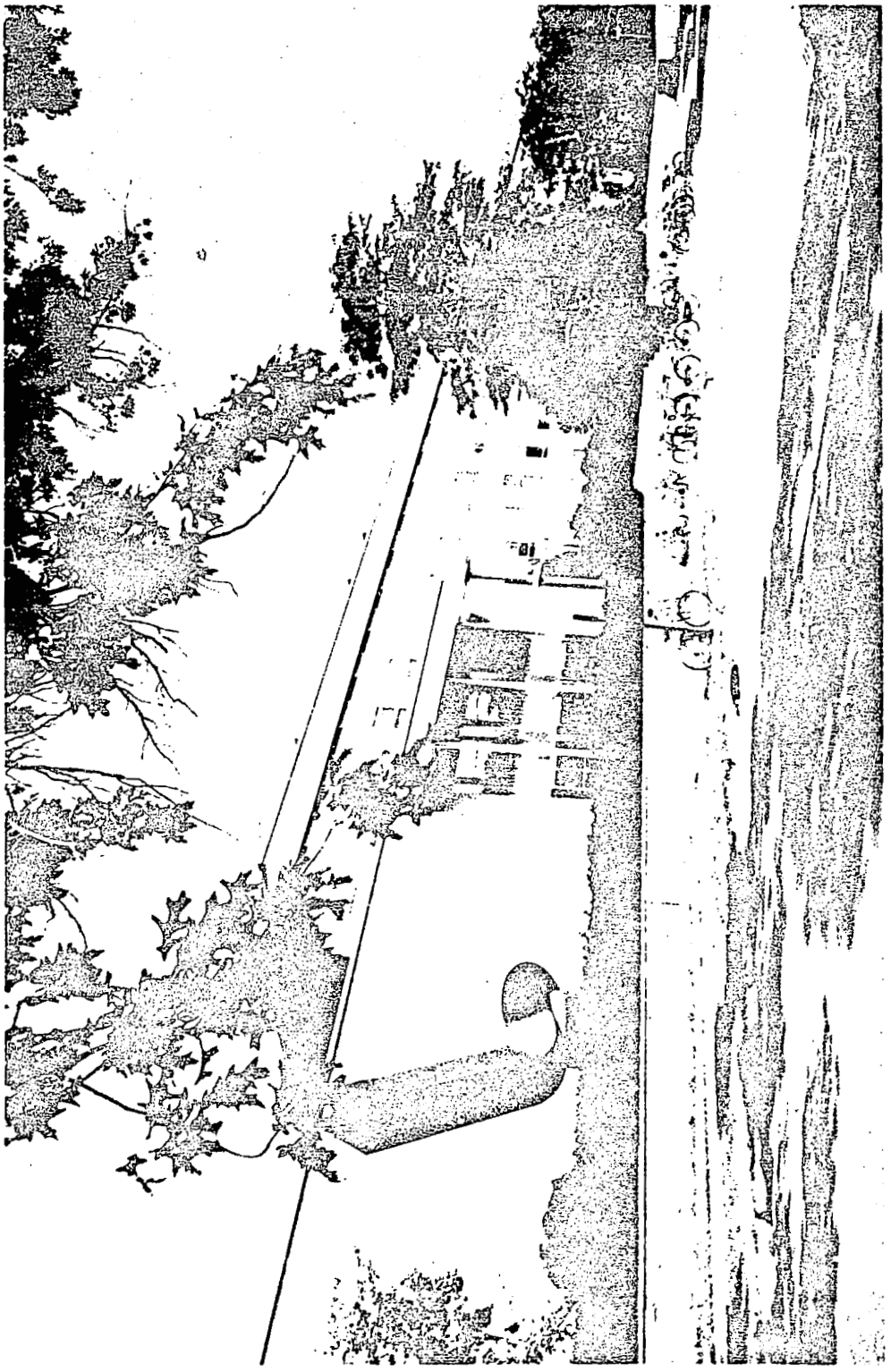

FIGURE - 2
AP25-P-528

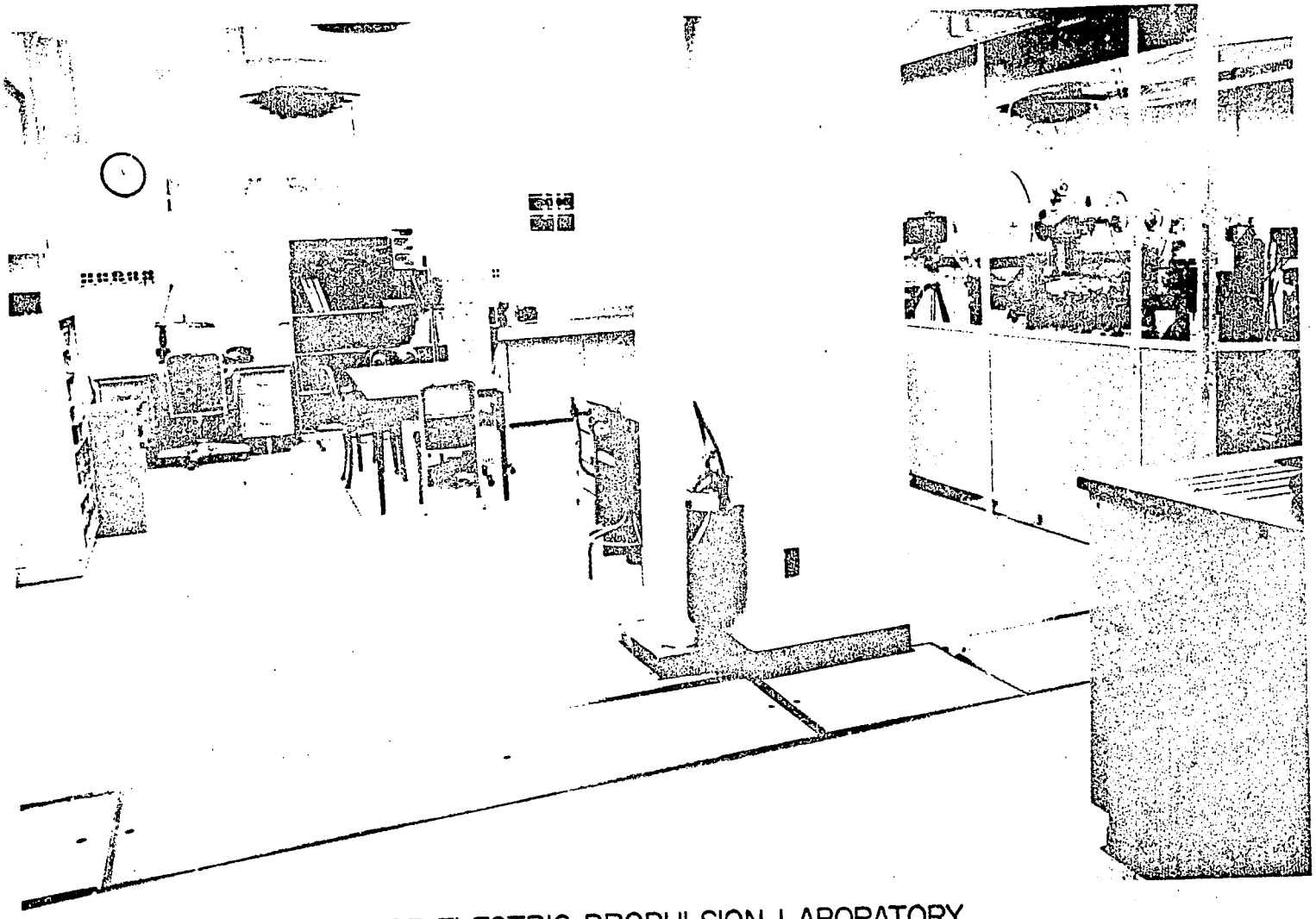

FIGURE 3
AP25-P-529

VIEW OF ELECTRIC PROPULSION LABORATORY

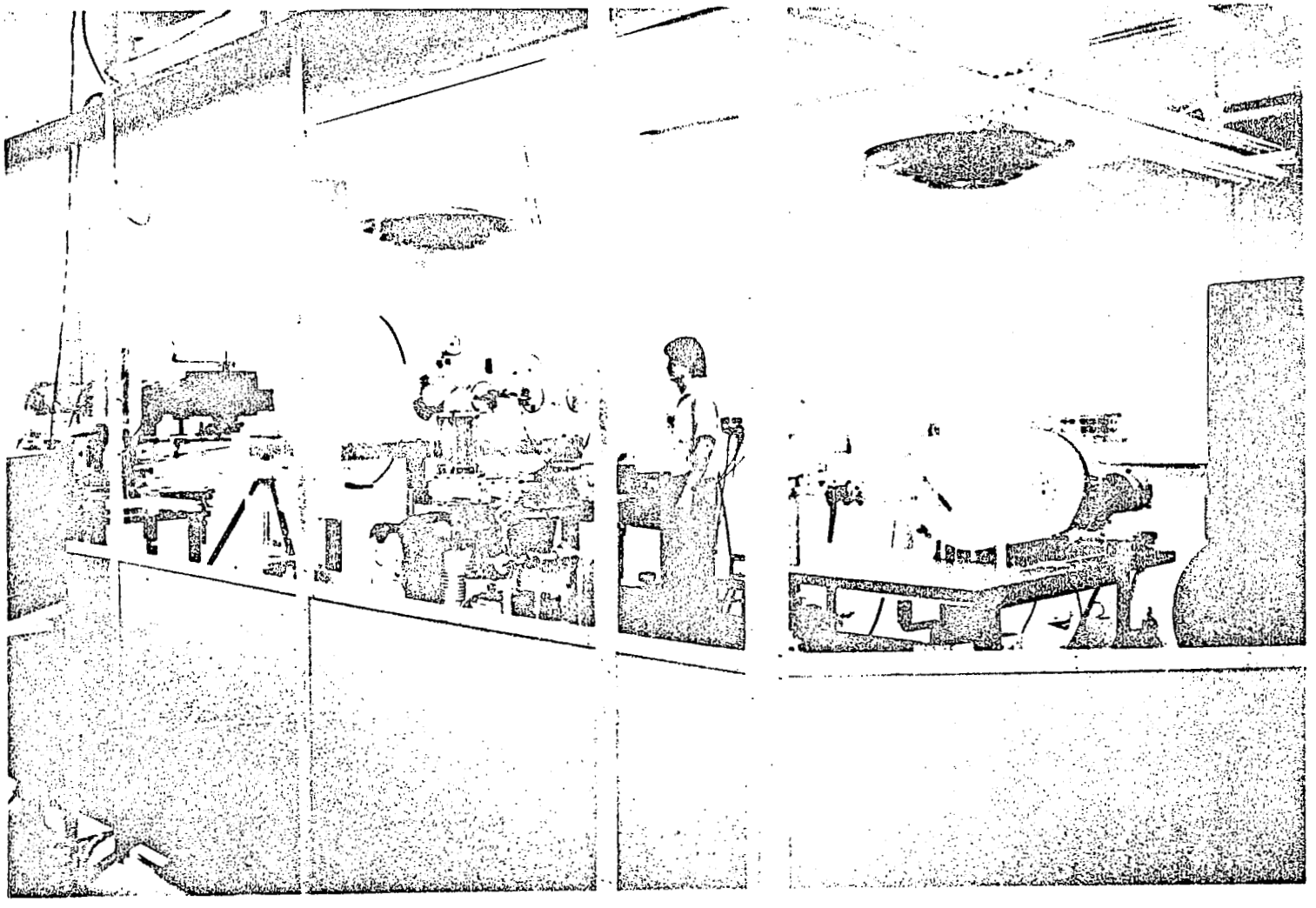

VIEW OF MPD FACILITIES

FIGURE 4
AP25-P-530

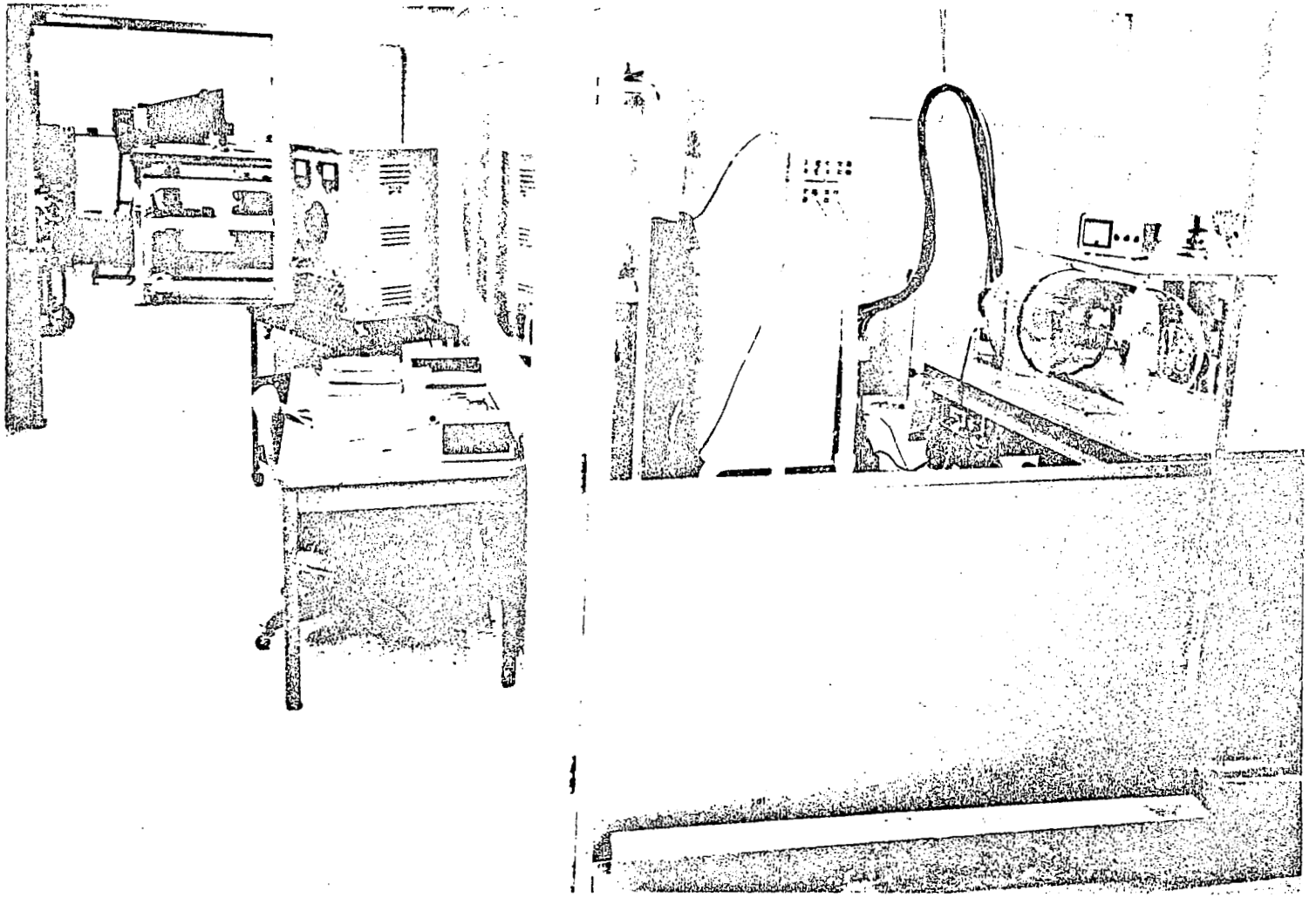

FIGURE 5
AP25-P-531

VIEW OF HOLLOW CATHODE FACILITY

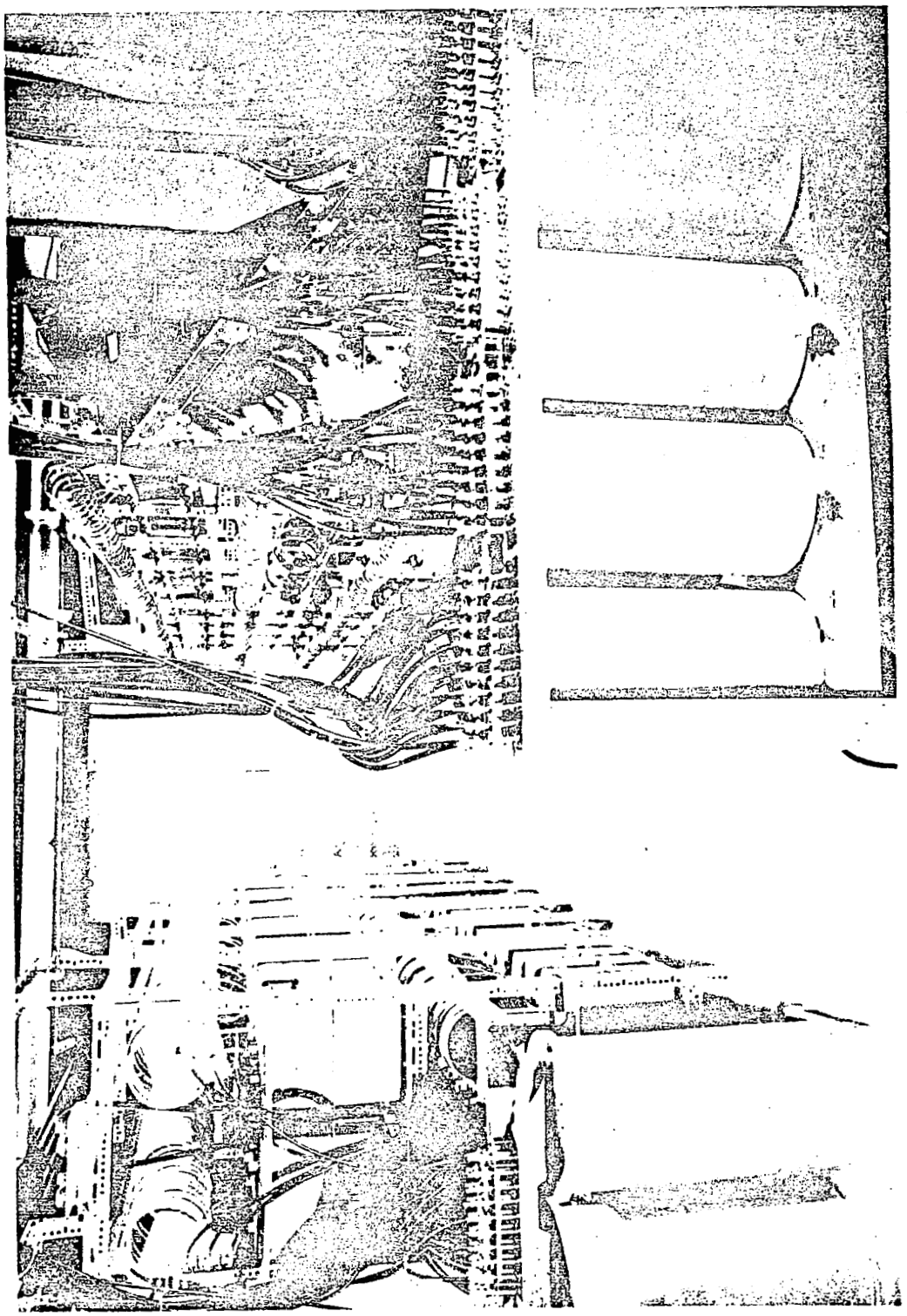

VIEW OF THE POWER SUPPLY ROOM

FIGURE 6
AP25-P-532

physics or plasmadynamic laser studies. Both capacitor banks and all experimental facilities in the main lab are now fully operational following this relocation.

III. QUASI-STEADY MPD DISCHARGE

A. Plasma Acceleration Processes (Boyle)

In order to determine the maximum performance capability of the MPD accelerator, it is necessary to understand completely the plasma acceleration mechanisms within the discharge. However, previous semi-annual reports have shown that the effects of insulator ablation and cathode surface area can greatly alter arc behavior and thus obscure this evaluation.[151,155] With these effects reduced to a minimum, it is now possible to proceed systematically toward acquiring this understanding.

In principle, the total velocity vector field, and thus the acceleration pattern, of the MPD device may be determined by the simultaneous solution of the mass, momentum and energy conservation equations for given initial and boundary conditions. The electromagnetic variables responsible for the Lorentz body force in the momentum equation and the Joule heating term in the energy equation must be consistent with Maxwell's equations. In addition, a generalized Ohm's law which describes the coupling between the electromagnetic and gasdynamic variables must be prescribed. An appropriate equation of state and expressions for the plasma transport properties including a plasma conductivity law are required to complete the set. In practice the coupled nonlinear nature of the governing partial differential equations presents a problem of extreme mathematical complexity.

By contrast, the quasi-steady plasma acceleration problem becomes more tractable when discussed in a semi-empirical manner. In this section the measured exhaust velocity profile and the electromagnetic discharge structure are presented for an accelerator operating at an arc current of 15.3 kA and an

argon mass flow of 6 g/sec. These data are combined in a quasi-phenomenological model of the acceleration process and finally discussed in relation to the fundamental capability of the quasi-steady accelerator.

Experimental Conditions

The plasma acceleration process may be studied for any desired combination of arcjet parameters so long as the accelerator operation is uninfluenced by ablation or cathode surface area effects. There is particular interest, however, in examining the exhaust velocity profile of the quasi-steady accelerator for operating conditions such that the parameter $J^2/\dot{m}$, the arc current squared divided by the argon propellant mass flow rate, equals approximately 40 kA^2-sec/g. Claims have been made previously that the acceleration mechanisms are fundamentally limited at these conditions.[A-1] Furthermore, results in the last semi-annual report indicate that arcjet operation free from (boron nitride insulator) ablation is restricted to $J^2/\dot{m}$ less than or equal to 40 kA^2-sec/g.

This condition is realized experimentally with an arc current of 15.3 kA and a total argon mass flow rate of 6 g/sec. The mass injection configuration equally divides the total propellant flow between inner and outer injection orifices. Three grams per second are injected directly about the cathode through an inner cathode base annulus. The remaining 3 g/sec enter the discharge chamber through twelve 0.32 cm holes symmetrically distributed about the 3.81 cm radius.

To prevent voltage fluctuations, a cathode area greater than 20 cm^2 is required for this combination of arc current and mass flow.[155] A thoriated tungsten cathode 1.91 cm in diameter, 7.62 cm in length, with a 2.54 cm conical tip provides sufficient electrode area ($\approx$ 41 cm^2) to insure stable arcjet operation. The terminal arc voltage for this configuration equals 115 volts. Typical current and voltage signatures at these conditions are shown in Fig. 7.

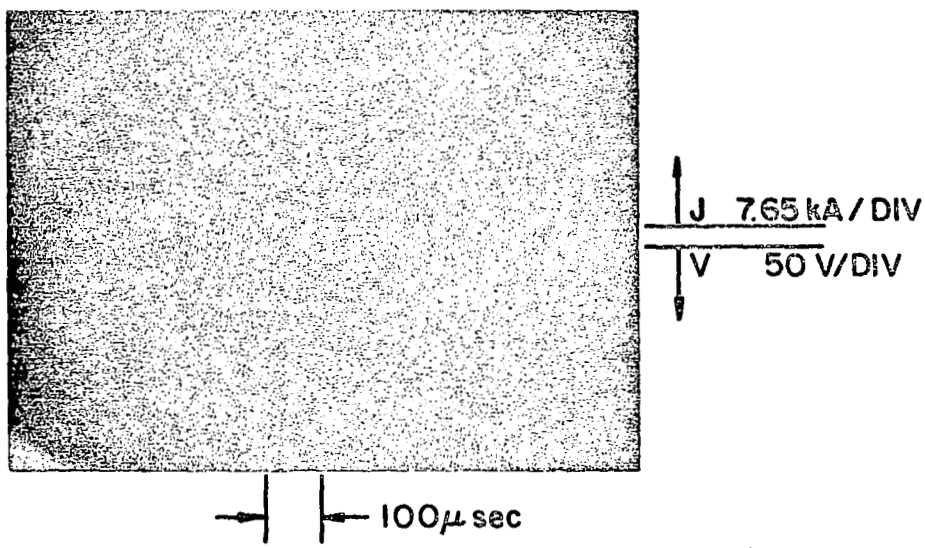

ARC CURRENT AND VOLTAGE SIGNATURES

FIGURE 7
AP25-P-526

Axial Velocity Profile

The axial velocity profile measured using the time-of-flight probe technique on the accelerator's centerline is presented in Fig. 8. The axial distance z is measured downstream from the anode plane. Velocity measurements within the discharge chamber were precluded due to the lack of discernable ion density fluctuations required by the time-of-flight technique. The plasma leaves the discharge chamber at a velocity less than 9.0 km/sec. Final exhaust velocities of 12.5 km/sec are observed several anode orifice diameters downstream. This final exhaust velocity exceeds by nearly 50% the Alfvén critical speed of 8.7 km/sec for argon, previously suggested as the upper limit to which propellant may be accelerated by a quasi-steady MPD arc operating at these conditions.

Electromagnetic Structure of the MPD Discharge

The exhaust velocity profile results primarily from the combined action of electromagnetic body forces upon the accelerated propellant mass. The magnitude and direction of the electromagnetic body forces may be ascertained from measured distributions of current density and magnetic field. In this way the local acceleration processes may be related to the local $\bar{j} \times \bar{B}$ distribution. Alternatively, the plasma acceleration process may be viewed as the conversion of some portion of the electrical input power $(\bar{j} \cdot \bar{E})$ into directed motion of the propellant. Evaluation of the local $\bar{j} \cdot \bar{E}$ power deposition within the arc discharge requires knowledge of the electric fields as well as the current density distribution. From these distributions of magnetic field, current density and electric field, a qualitative model of the quasi-steady acceleration mechanisms will emerge.

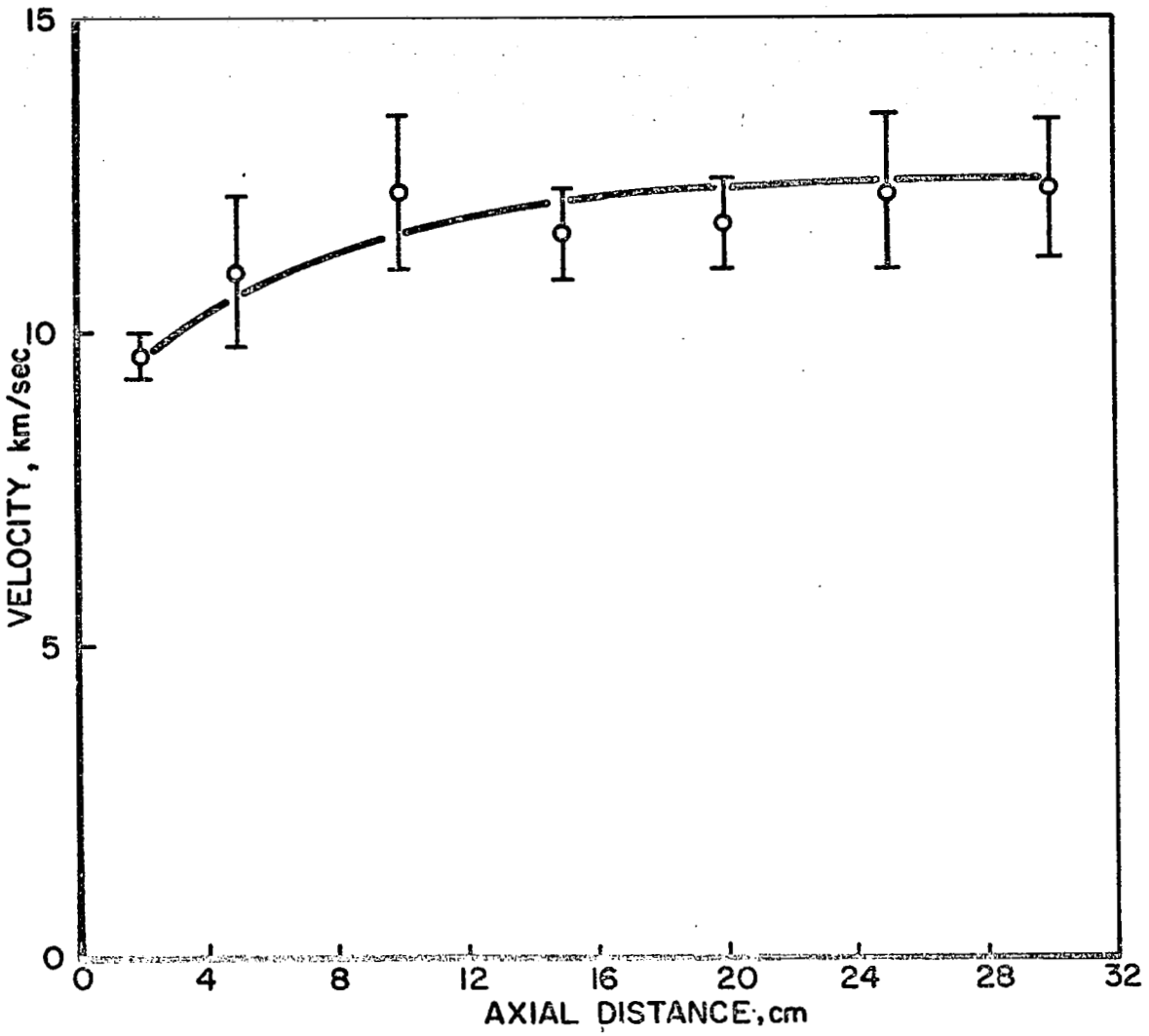

CENTERLINE AXIAL VELOCITY PROFILE

FIGURE 8
AP25-5050

Because the arc discharge is cylindrically symmetric, the induced self magnetic field (B) is azimuthal. The B field distribution is determined from axial and radial induction coil surveys. Azimuthal probe surveys for selected radial locations within the discharge confirm the presumed cylindrical symmetry of the magnetic field. The magnetic field distribution stabilizes in two characteristic times. Approximately 200 μsec after discharge initiation, the magnetic field within the discharge chamber assumes a quasi-steady distribution. At a somewhat later time, approximately 450 μsec into the 1000 μsec current pulse, a quasi-steady distribution throughout the entire flow field is achieved. This quasi-steady distribution, presented in Fig. 9, is maintained for the duration of the current pulse. In this figure, lines of constant magnetic induction are superimposed upon a schematic of the accelerator chamber.

The quasi-steady current distribution is derived directly from the magnetic field data employing Ampere's law and the azimuthal symmetry of the discharge. The resulting distribution of enclosed current for the total discharge current of 15.3 kA is illustrated in Fig. 10. Each current contour represents a current streamline and is labelled with the amount of current in kiloamperes which flows downstream of it. The magnitude of the local current density vector may be estimated by dividing the current between two adjacent current contours by the normal area through which it flows.

A significant fraction of the total arc current flows in the region exterior to the discharge chamber. The current streamlines within the accelerator chamber emerge from the cathode with a density distribution peaked at both ends of the cathode as shown in Fig. 11. The current contours then bend axially downstream before turning radially toward the anode. Anode current attachment concentrates about the lip region of the anode.

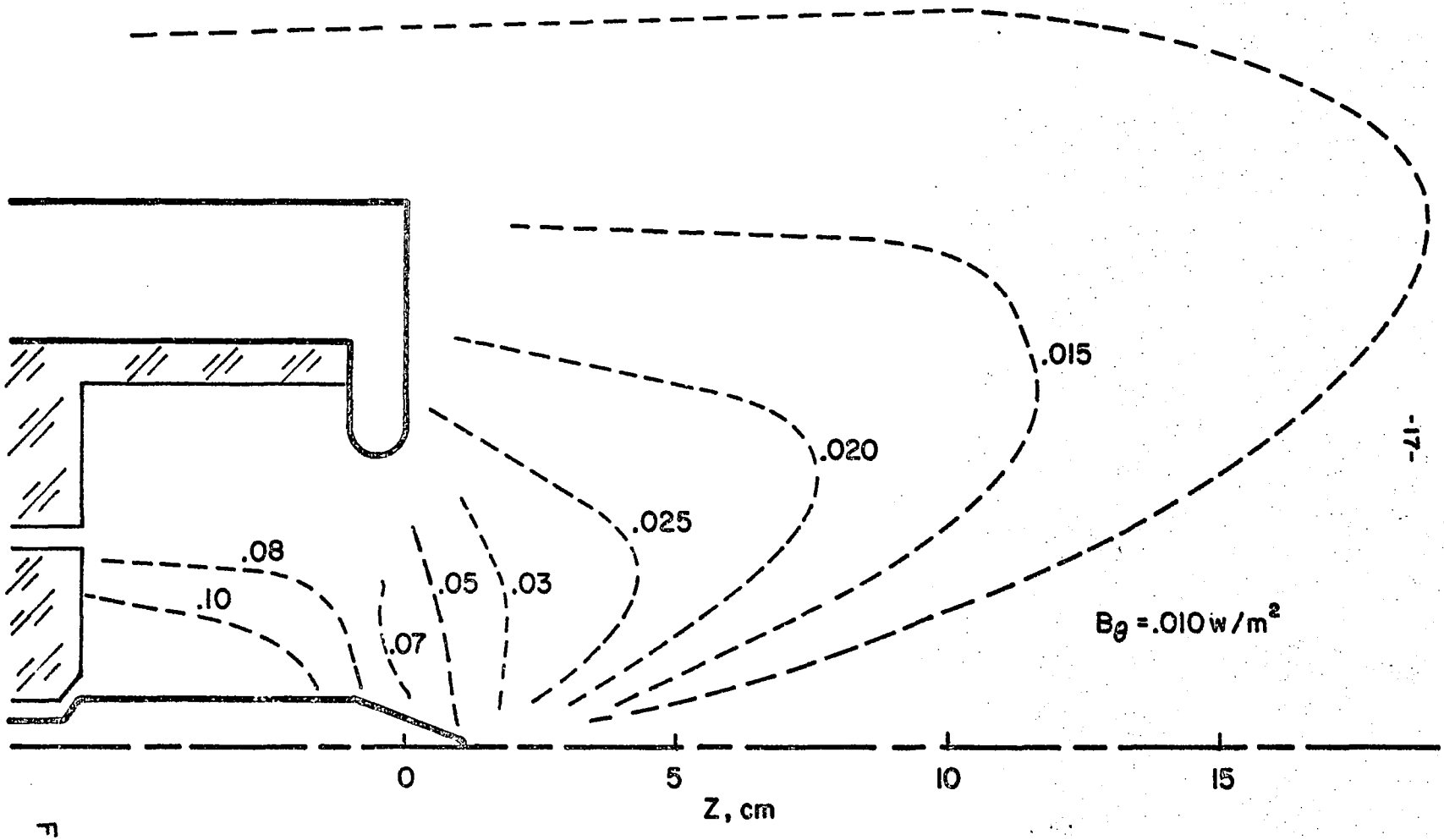

FIGURE 9
AP25-5051

QUASI - STEADY MAGNETIC FIELD DISTRIBUTION

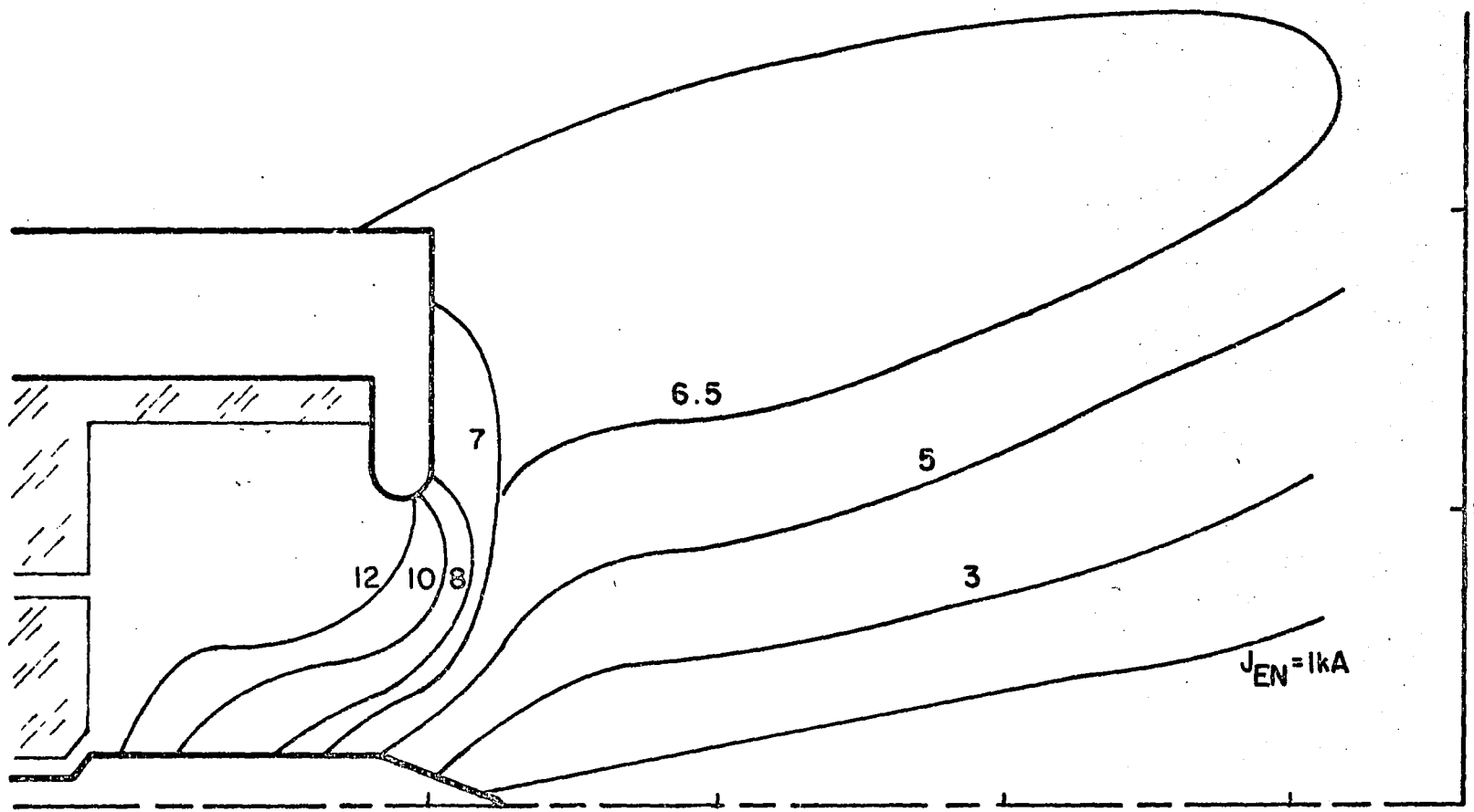

QUASI-STEADY ENCLOSED CURRENT CONTOURS
J = 15.3 kA

FIGURE 10
AP25.5052

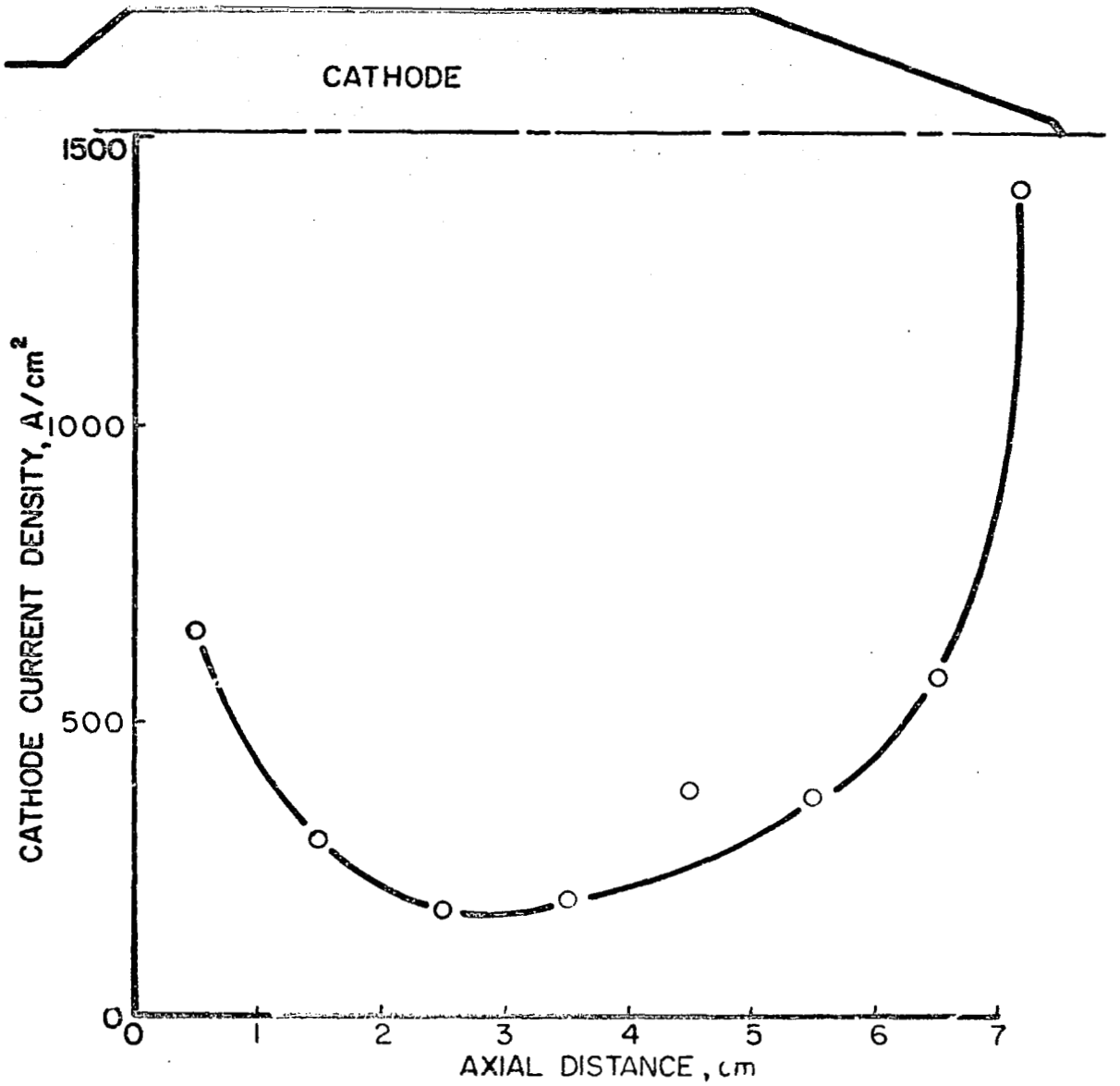

CATHODE CURRENT DENSITY DISTRIBUTION

FIGURE 11
AP25-5053

Outside the discharge chamber nearly fifty percent of the total arc current billows far downstream in the exhaust plume before returning and attaching on the outer surfaces of the anode barrel. The current density vector within several centimeters of the accelerator's centerline in this exhaust region is primarily axial. This current density pattern is characteristic of the moderate magnetic Reynolds number, O(1-10), associated with the discharge flow.

The local electric fields, which integrate to the terminal arc voltage, arise as a result of current conduction across the flowing, finite conductivity discharge plasma. Current conduction processes across the electrode-plasma interface also create potential gradients commonly referred to as electrode falls.

The local electric field equals the gradient in plasma potential which, in turn, is related to the experimentally measurable floating potential. For small distances over which the gradients in electron temperature, flow vector, and collision frequencies are negligible, the electric field may be evaluated from the difference in floating potential. The quasi-steady distribution of floating potential contours is shown in Fig. 12. The cathode is at 115 volts negative with respect to the anode ground. The labelled equipotential contours are also negative with respect to the ground, the negative signs being omitted from Fig. 12 for convenience. The 20 and 90 volt contours envelope the anode and cathode regions respectively. The equipotential contours in the outer radial regions of the downstream exhaust are approximately parallel to the current streamlines.

Evaluation of the total arcjet power distribution throughout the MPD accelerator requires local evaluation of $\bar{j}\cdot\bar{E}$, the dot product between the current density and electric field vectors. For this purpose, the accelerator may be sub-divided into several separate regions, A through F, as is done in Fig. 13.

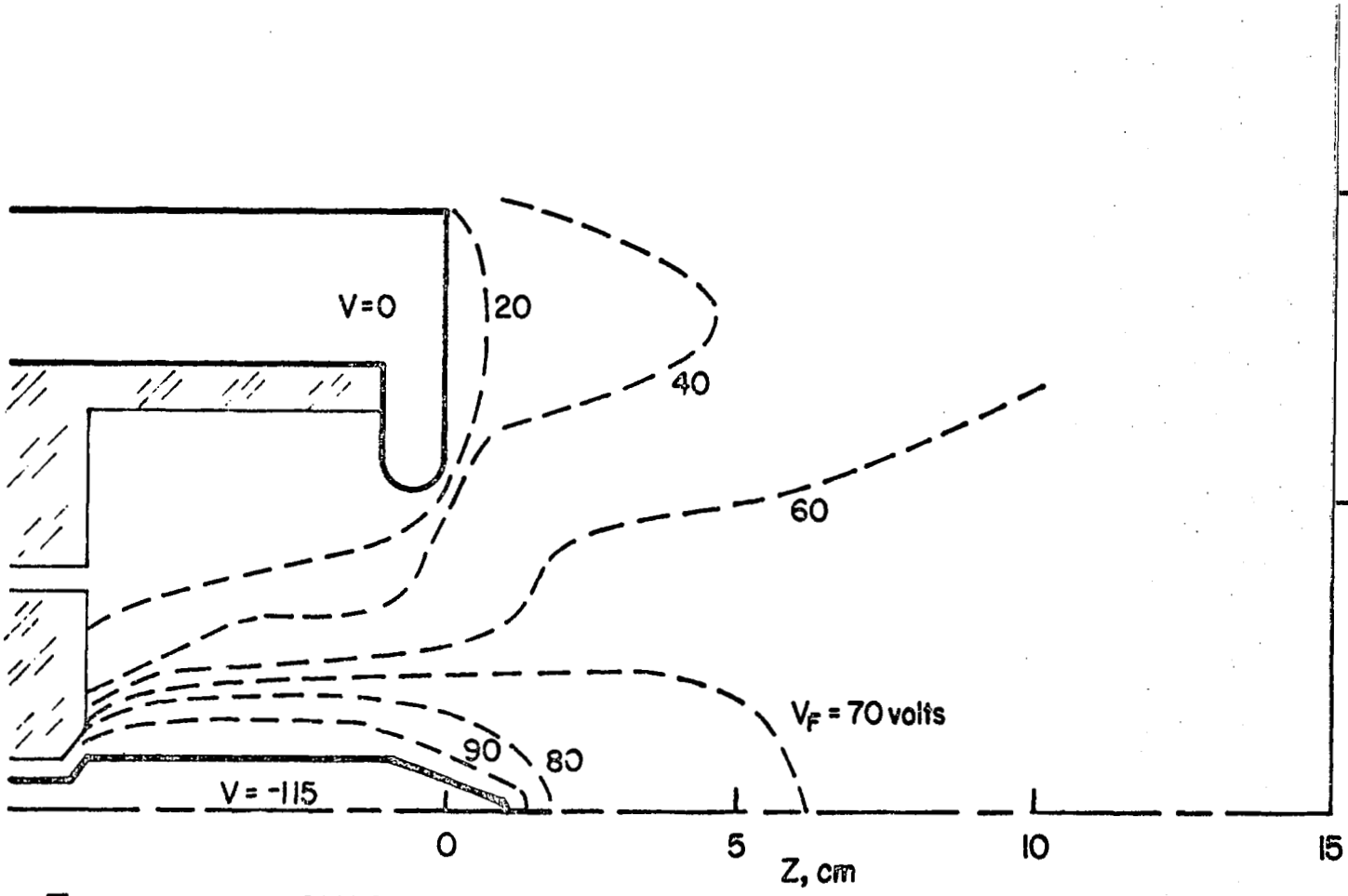

QUASI - STEADY FLOATING POTENTIAL CONTOURS

FIGURE 12
AP25-5055

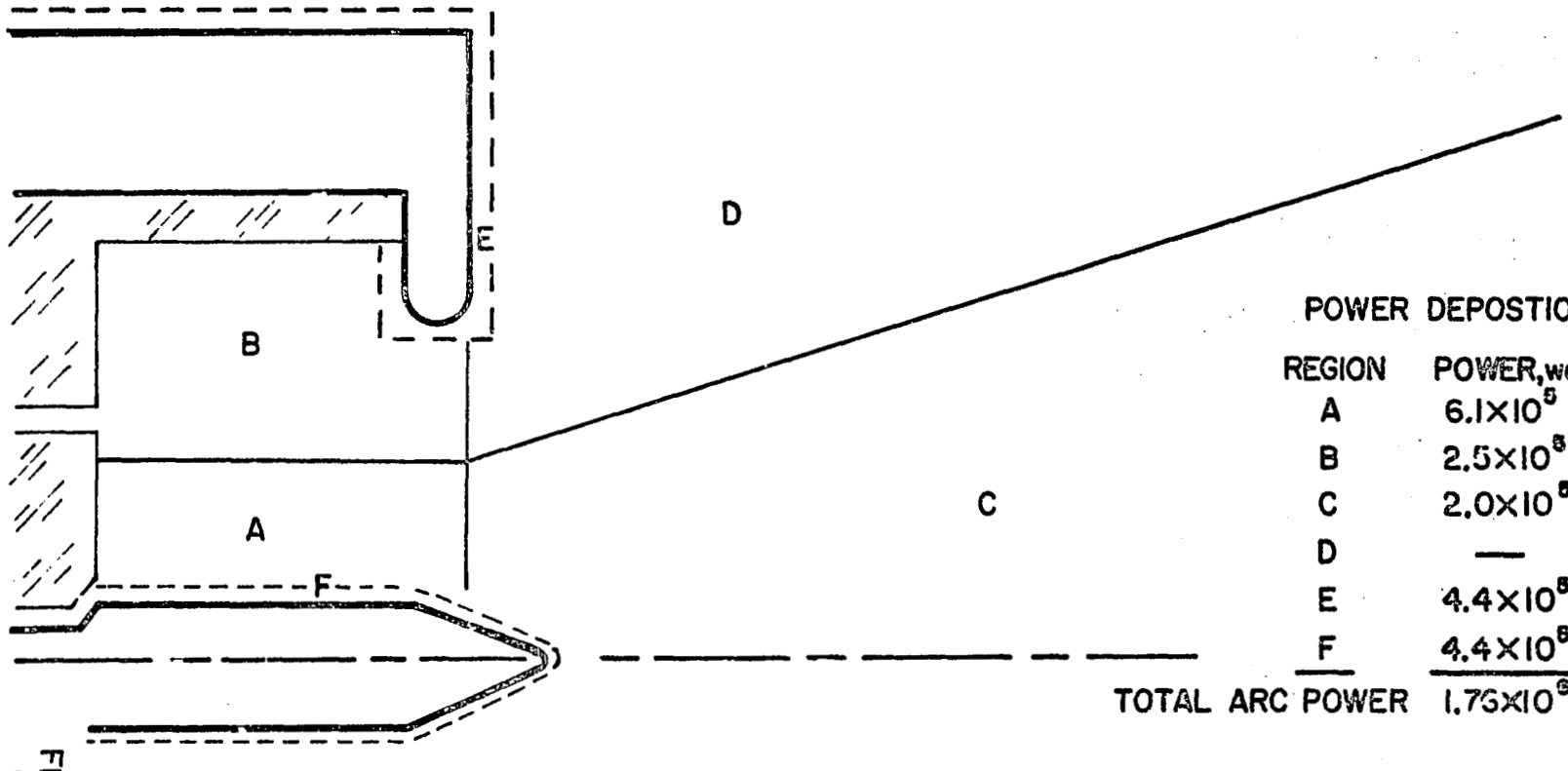

POWER DEPOSTION

REGION	POWER, watts
A	6.1×10^{5}
B	2.5×10^{6}
C	2.0×10^{6}
D	—
E	4.4×10^{6}
F	4.4×10^{6}
TOTAL ARC POWER	1.76×10^{6}

$\bar{j}\cdot\bar{E}$ POWER DISTRIBUTION

FIGURE 13
AP25-5070

These regions, excluding the electrode fall regions E and F, are further divided into incremental volume elements in which average values for the magnitude and direction of the $\bar{j}$ and $\bar{E}$ vectors are assigned. The product of local power density and incremental volume element when summed over each region represents the total electrical power deposited in that region. This regional power deposition is summarized in Table I. At 15.3 kA and 6 g/sec the total arc power is 1.76 megawatts.

Table I

Region	$(\bar{j}\cdot\bar{E})$(vol), watts	Region description
A	6.1×10^5	inner chamber flow
B	2.5×10^5	outer chamber flow
C	2.0×10^4	inner exhaust flow
D	----	outer exhaust flow
E	4.4×10^5	anode fall
F	4.4×10^5	cathode fall
Total Arc Power	1.76×10^6	

To first order, no power addition appears in region D of the discharge because the electric field is perpendicular to the current density vector, thereby making $\bar{j}\cdot\bar{E}$ zero throughout the volume. The power lost to the anode in region E is estimated from recent work relating anode power fraction to total arc power in the quasi-steady MPD discharge.[156] For $J^2/\dot{m} = 40$ kA^2-sec/g, these results extrapolate to an anode power fraction of 25%; i.e. 25% of the total arc power or 4.4×10^5 watts is accounted for by loss mechanisms in the vicinity of the anode. With the anode fall and bulk plasma flow regions accounted for, the remaining input power must appear in the cathode fall region F to provide an overall power balance of the arc.

The distribution of local power deposition for the MPD accelerator operating at 15.3 kA and 6 g/sec may now be summarized: Approximately fifty percent of the total arc power is invested in the plasma flow which occupies regions A, B, and C in Fig. 13. The major power addition to the plasma flow occurs within the discharge chamber, with negligible power addition ensuing in the downstream exhaust. The remaining fifty percent of the total power appears in the electrode fall regions of the discharge.

Flow Field Characteristics of the MPD Discharge

The flow pattern in the exhaust of the accelerator is determined from velocity vector measurements using the double probe.[85] The mass streamlines constructed from these local flow angles parallel the current streamlines in the inner exhaust region C depicted in Fig. 13. Precise flow vector measurements in the outer exhaust region D are difficult to obtain due to a decrease in the probe's sensitivity to the flow orientation. Despite this decreased accuracy, flow vectors not parallel to the current streamlines are identified. The mass streamlines appear to diverge more rapidly than the current streamlines in the outer exhaust region.

The flow in region C of the exhaust is supersonic. Bow shocks are photographed off the hemispherical tips of rods introduced into this inner flow several centimeters downstream of the anode orifice. Oblique shocks attached to wedges of different turning angles are also observed. As these wedges are moved axially inward towards the anode plane, the oblique shock angles increase indicative of lower incident flow Mach numbers. Finally no shocks are seen in the vicinity of the anode orifice indicating near sonic conditions there.

Insufficient knowledge of the shocked plasma's thermodynamic state precludes exact Mach number calculations from the shock angle data. However, the oblique shock relations for a perfect gas with an appropriate ratio of specific heats provide a first order estimate.[A-2] Using this method, the flow Mach number seven centimeters downstream of the anode orifice is estimated between two and three.

Photographs through narrow band spectral filters display the luminosity patterns of the discharge. Spectrograms of the discharge reveal singly ionized argon (A-II) as the predominant species. Argon II line radiation in the downstream exhaust extends to radii beyond the anode barrel of the accelerator although the spectral intensity monotonically decreases with radius. Referring again to Fig. 13, the predominant argon II radiation photographed through a 4880 Å filter is confined to the inner flow regions A and C. The outer edge of the A-II luminosity in region C coincides with a mass streamline previously defined by the velocity vector measurements. The correspondence among the 4880 Å A-II luminosity boundary, the mass streamline and the demarcation of the A-C and B-D flow regions is illustrated in Fig. 14.

The remaining regions of the discharge, B and D, are essentially dark, except for a small toroidal volume located in the anode plane between the anode lip and region A.

Quasi-Steady MPD Acceleration Processes

Having discussed the pertinent electromagnetic and flow field characteristics of the MPD discharge, a model of the acceleration mechanisms responsible for the measured plasma velocity profile may be constructed. A complete description of the flow processes would require additional profiles of

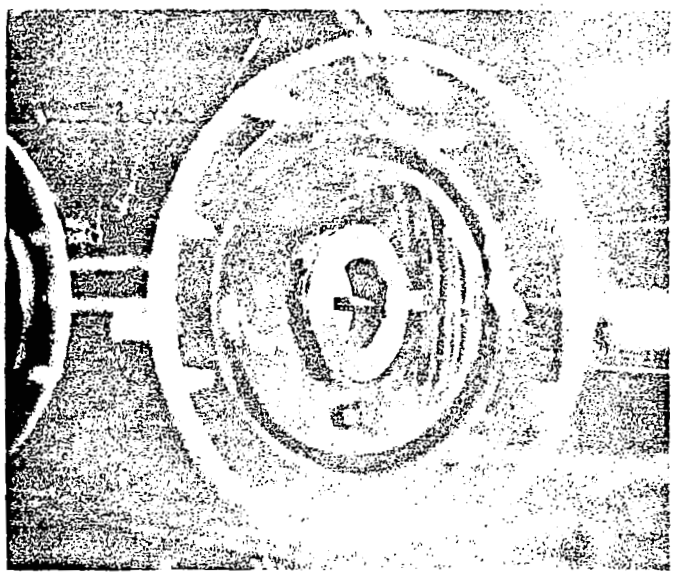

a) REFERENCE PERSPECTIVE

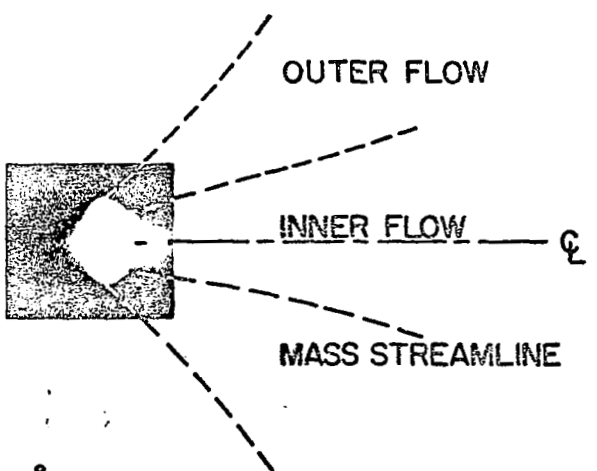

b) 4880Å LUMINOSITY

ARGON II LUMINOSITY PATTERNS

FIGURE 14

AP25-P-527

number density, ion and electron temperatures, and pressure throughout the discharge. For this arcjet configuration, these profiles have not yet been determined. However, reasonable estimates of these variables based upon previous measurements for other configurations can be made. This allows a phenomenological model of the plasma acceleration process to be formulated.

Two-Flow Plasma Acceleration Model

The total injected argon propellant is divided into two independent mass flows associated with chamber injection at large and small radii. The local power deposition and luminosity profiles in regions A and B of the discharge chamber suggest this flow division is essentially maintained as the two flows are accelerated axially downstream out of the chamber and into the exhaust regions. The plasma acceleration process will thus be modelled in terms of two separate inner and outer propellant flows, schematically illustrated in Fig. 15.

Inner and outer flow separation is consistent with the observed electromagnetic discharge structure within the accelerator chamber. In particular, there are substantial differences between the axial power deposition profiles for the two flow regions. Figure 16 compares the incremental power addition to each flow as a function of axial distance downstream from their respective injection orifices. Approximately 180 kW are deposited immediately in the inner flow as it emerges from the cathode base injection annulus. This power level is commensurate with complete single ionization of the injected 3 g/sec argon. Once ionized, the prevailing $\bar{j} \times \bar{B}$ body forces tend to confine radially and accelerate axially the inner flow. Only after leaving the discharge chamber does the inner flow expand radially.

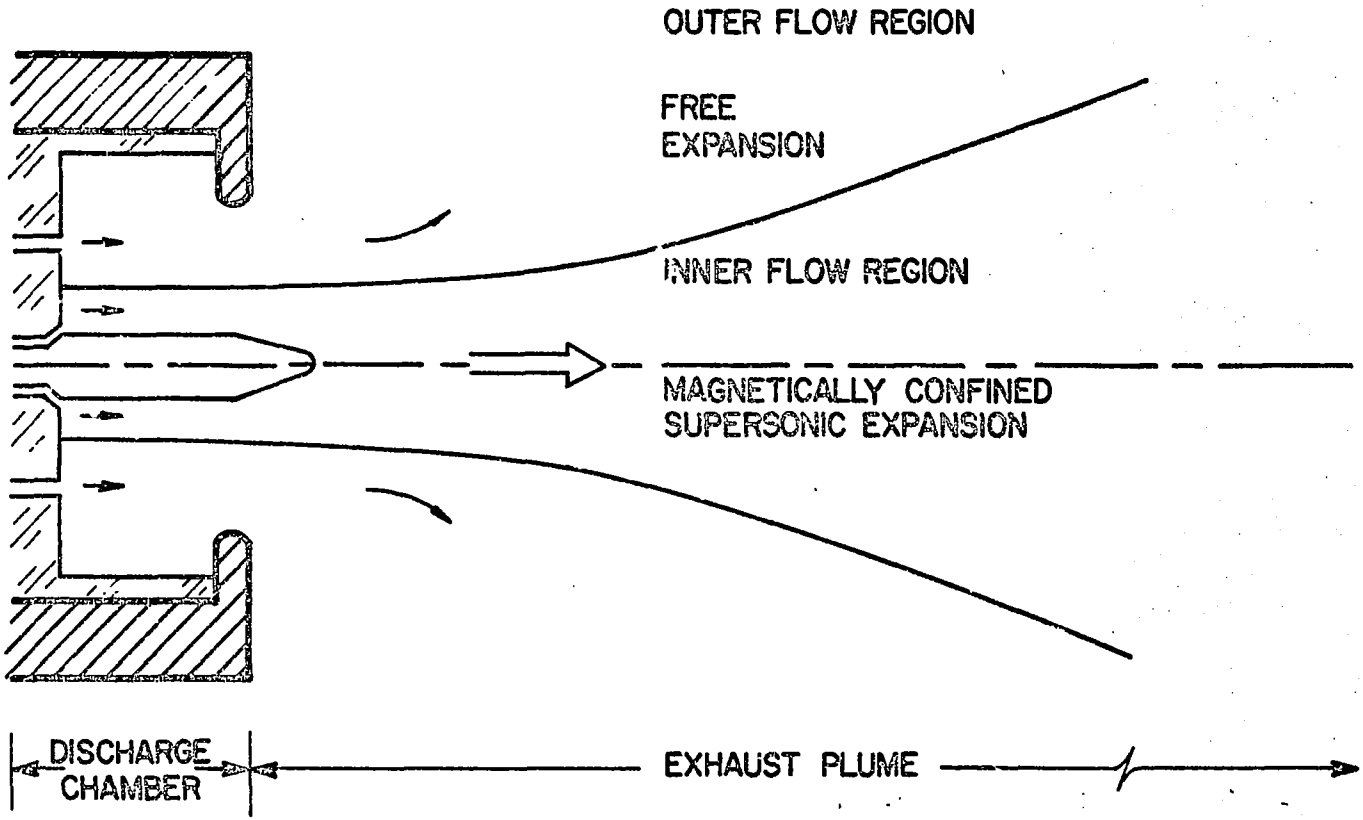

TWO-FLOW ACCELERATION MODEL

FIGURE 4-9
AP25-5059

FIGURE 15
AP25-5059

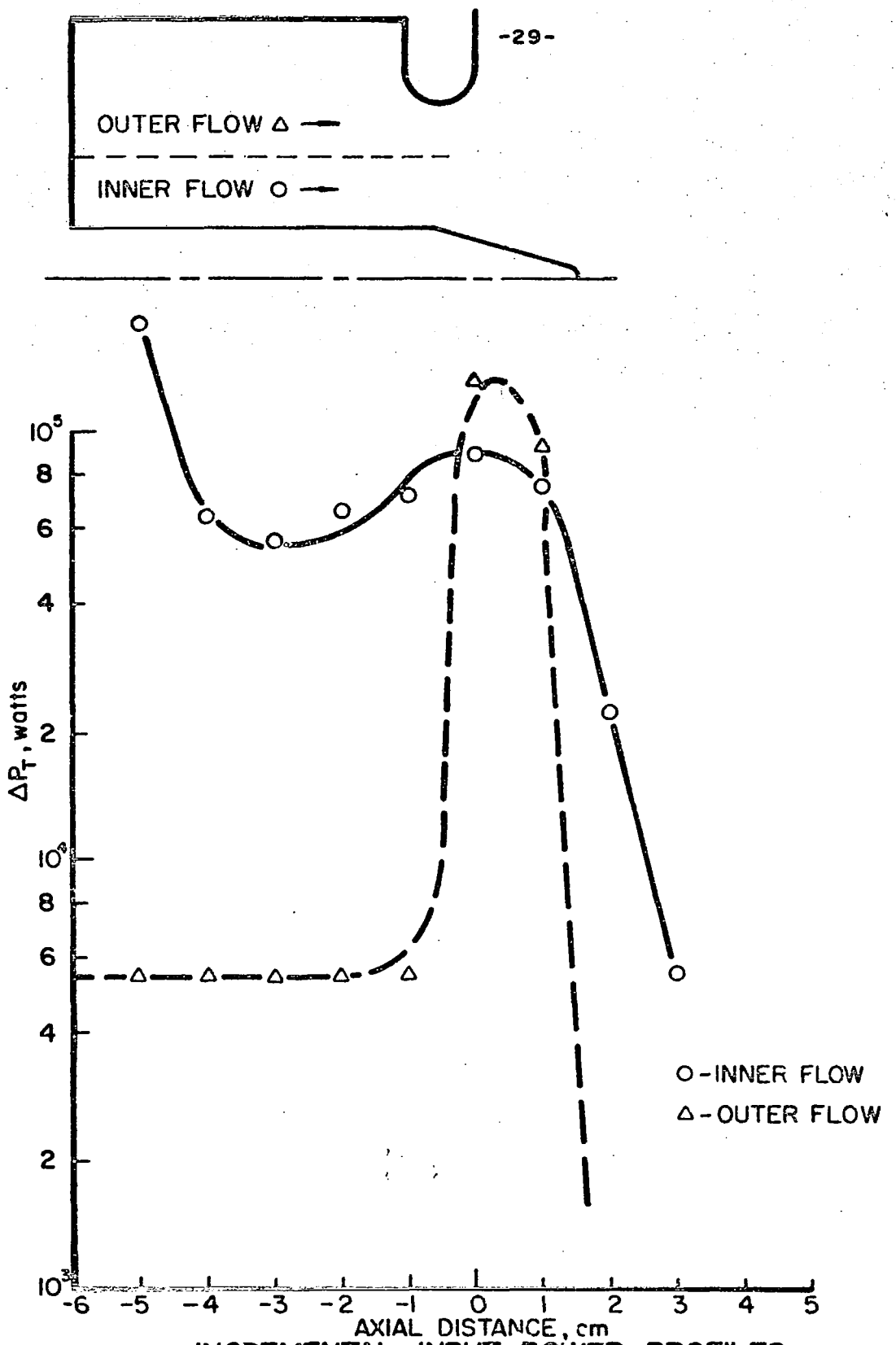

INCREMENTAL INPUT POWER PROFILES

FIGURE 16

AP25-5054

In contrast, negligible input power appears in the outer flow upstream of the anode lip region. A total of only 27 kW is deposited in this region. Thus, it may be inferred that only a small fraction of the 3 g/sec outer mass flow rate is ionized upstream of the anode. This is also consistent with the absence of ionized argon line radiation in this region of the discharge. In addition the local current density and magnetic field are substantially lower in this region. As a consequence of the weak local Lorentz forces, the initial axial flow direction of the outer propellant stream will be only slightly perturbed. To this approximation, the integrity of the two concentric inner and outer flows is preserved as they are accelerated downstream.

Inner Flow Region. Two-thirds of the electrical input power invested in all the plasma flow regions appears as total enthalpy of the inner propellant flow. In addition, nearly 100 percent of this inner flow power addition is accomplished within the discharge chamber as shown in Fig. 17. Negligible power addition occurs in the exhaust. The discharge chamber and exhaust plume regions of the inner flow are distinguishable by this localization of power input. As such, the flow processes within each will be treated separately.

Inner Flow, Discharge Chamber. The inner propellant mass flow is ionized, heated, and accelerated through the sonic point within the discharge chamber. The net result of these processes may be examined in terms of a power balance across the region.

The total input power, P_T, invested in the inner flow within the discharge chamber is 6.1×10^5 watts, exclusive of the cathode fall power. Of this total, a certain amount, P_R, is lost through radiative processes. The remaining power appears directly in the flow.

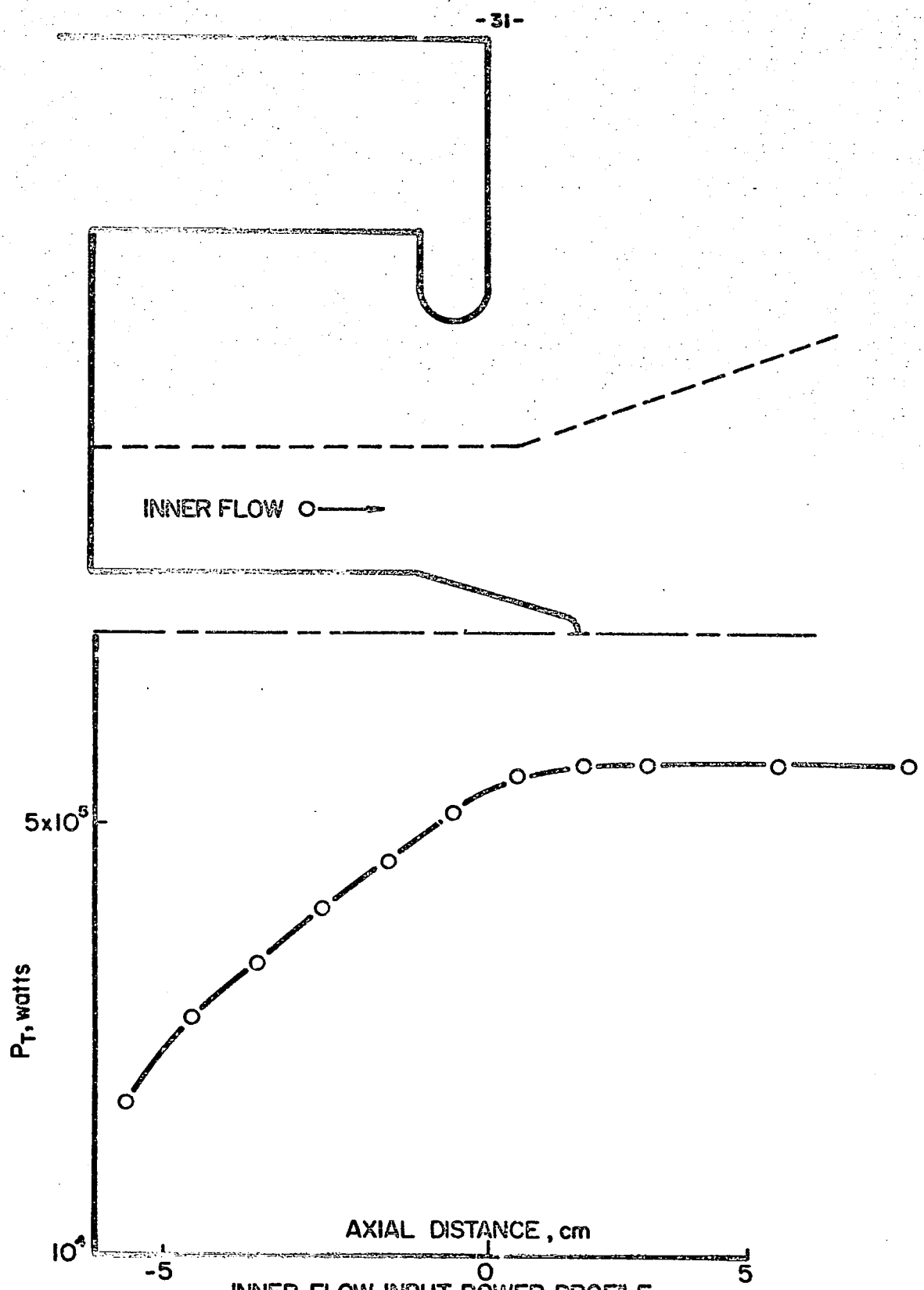

INNER FLOW INPUT POWER PROFILE
FIGURE 17
AP25-5056

$$P_{FLOW} = P_T - P_R \qquad \text{(III-1)}$$

This flow power is partitioned between enthalpic and kinetic modes.

$$P_{FLOW} = \dot{m}\left(h + u^2/2\right) \qquad \text{(III-2)}$$

where $\dot{m}$ is the accelerated mass flow rate, h the flow enthalpy, and u the mean flow velocity.

A quasi-equilibrium expression for the flow enthalpy is assumed, in the form,

$$h = \int_0^{T_e} C_p(T,p)\,dT + \frac{5}{2}R\int_{T_e}^{T_i} dT \qquad \text{(III-3)}$$

where T_e and T_i are the electron and ion temperatures, C_p is the heat capacity at constant pressure and R equals the argon gas constant. The first integral in Eqn. III-3 represents the contribution to the flow enthalpy from both excitation and ionization as well as the energy content of the ion and electron random motion at temperature T_e.[A-3] Generally the excitation and ionization processes in devices of this type limit the electron temperature to between one and two volts. After initially being ionized, the plasma experiences a significant axial acceleration. The resulting high velocities are characterized by flow times short compared to characteristic electron-ion energy equipartition times[A-4] thereby establishing a non-equilibrium situation. Because electron-ion collisions are unable to establish an equilibrium temperature distribution in time, additional enthalpy appears in ion random motion alone, thereby raising the ion temperature above the electron temperature. This non-equilibrium effect is accounted for by the second integral in Eqn. III-3.

Equations III-1, 2 and 3 may be rearranged to express the flow velocity in terms of input and radiated power, accelerated mass flow rate, pressure, and electron and ion temperatures such that:

$$u = \left[2\left(\frac{P_T - P_R}{\dot{m}} + \frac{5R}{2}(T_e - T_i) - \int_0^{T_e} C_p(T,p)\,dT \right) \right]^{1/2} \qquad \text{(III-4)}$$

Order of magnitude estimates of P_R, p, T_e and T_i at a given axial location are required to calculate the local flow velocity from the measured power input up to that point. The measurement techniques for any one of these variables require a major experimental effort in terms of the sophistication and time demanded by the particular measurement. In lieu of their actual measurement, these estimates must rely upon previous data obtained at similar operating conditions, albeit for different arcjet configurations.

Plasma radiation phenomena in an environment of this type are extremely complex. An exact formulation of the input power radiated away by bremmstrahlung and line radiation is beyond the scope of this work. The power density radiated in free-free transitions for a Maxwellian electron distribution is given by Spitzer as:

$$P_{ff}\ (W/cm^3) = 1.42(10^{-34}) Z^2 n_e n_i \bar{T}_e^{1/2} \qquad \text{(III-5)}$$

where Z is the ion charge number and $n_{e,i}$ are the electron and ion number densities.[A-4] For a singly ionized argon plasma with an electron number density equal to 10^{15} cm^{-3} and T_e between one and two volts:

$$P_{ff} = O(1\ W/cm^3)$$

The power radiated away by bremmstrahlung from the 10^2 cm^3 inner flow volume may thus be approximated as:

$$P_R^{ff} = P_{ff}(Vol) = O(10^2 W)$$

a negligible amount relative to the total input power. However, power losses from bound-bound transitions may be significant. A line radiation flux of 2000 watts/cm^2 has previously been found typical of this plasma environment.[125] The luminous inner flow region within the discharge chamber radiates from a surface area of $O(10^2$ cm$^2)$. From this surface,

$$P_R^{bb} = O(2 \times 10^5 W)$$

will be radiated away. The assumption of no recombination within this discharge region implies the power loss from free-bound transitions is negligible. The total input power lost to radiation is therefore

$$P_R = P_R^{ff} + P_R^{bb} = O(2 \times 10^5 W)$$

Electron temperatures consistent with previous probe measurements and observed levels of ionization, pressures inferred from static pressure measurements in the discharge chamber, and argon ion temperatures extrapolated from Doppler width data are listed below.[125,134,141]

$$T_e = O(19{,}000\ ^{\circ}K)$$
$$p = O(10^{-2}\text{-}10^{-1}\ \text{atm})$$
$$T_i = O(60{,}000\ ^{\circ}K)$$

For $P_T = 6.1 \times 10^5$ watts just outside the discharge chamber and an accelerated inner mass flow rate of 3 g/sec, the corresponding exit velocity is calculated from Eqn. III-4 to be $8.0 \leq u_e \leq 10.4$ km/sec. The experimentally measured plasma velocity 2 centimeters downstream is 9.6 ± 0.4 km/sec. The inner propellant flow thus is slightly supersonic as it departs the discharge chamber with an elevated ion temperature

and an electron temperature consistent with the conductivity requirements of the discharge.

Inner Flow, Exhaust Plume. The flow in the inner exhaust plume of the discharge is accelerated supersonically to a final velocity of 12.5 km/sec. This acceleration region extends several anode orifice diameters downstream. Within this region the electromagnetic body forces are normal to the flow streamlines. Thus, electromagnetic body forces tend to confine rather than accelerate the flow in the streamwise direction. The axial acceleration, however, may be accounted for by the radial divergence of the hot, electromagnetically confined inner plasma flow.

The mathematical description of the expansion process is significantly simplified for one-dimensional flows. Radial profiles of velocity and number density at several axial locations justify the 1-D assumption as a first approximation of the flow field. The one-dimensional mass, momentum, and energy relations for a given streamtube may be written as:[A-5]

$$d(\rho u A) = 0 \qquad \text{(III-6)}$$

$$\rho u\, du + dp = 0 \qquad \text{(III-7)}$$

$$dh + u\, du = dq \qquad \text{(III-8)}$$

where A is the normal streamtube area, dq the energy addition per unit mass from Joule heating, and ρ, u, p, and h the common nomenclature for density, velocity, pressure, and enthalpy. The flow enthalpy may be expressed as

$$h = \frac{5}{2}\, p/\rho + h_I \qquad \text{(III-9)}$$

where h_I is the internal energy content due to excitation and ionization. The energy addition, dq, to the expanding flow was found to be insignificant compared to the total energy content. Thus, dq may be approximated as zero.

Significant argon ion recombination (AIII→AII or AII→AI) in this exhaust region of the discharge has not been experimentally observed.[A-6] Recombination times for these processes are characteristically long, compared to local flow times. This suggests the plasma flow may be treated as frozen, i.e.,

$$dh_I = 0$$

Hence, the one-dimensional energy equation becomes

$$d\left(\frac{5}{2}\, p/\rho\right) + u\, du = 0 \qquad \text{(III-10)}$$

Equation III-10 integrates to

$$\frac{5}{2}\, p/\rho + u^2/2 = K \qquad \text{(III-11)}$$

where the integration constant K represents the total specific flow enthalpy exclusive of excitation and ionization energies. The constant K may be evaluated from either the sonic velocity u^* or the maximum velocity u_{max} according to Eqn. III-12.

$$K = \frac{5+\gamma}{2\gamma}\, u^{*2} = \frac{u_{max}^2}{2} \qquad \text{(III-12)}$$

where the sonic condition $\gamma p^*/\rho^* = u^{*2}$ has been used.

Equations III-6,7, 10 and 12 may be solved for the streamline area as a function of u, K, and the minimum area A^*. It is easily shown that

$$\frac{A}{A^*} = \left[\frac{K - u^{*2}/2}{K - u^2/2}\right]^{3/2} \left(\frac{u^*}{u}\right) \qquad \text{(III-13)}$$

or, in terms of the streamtube radius r,

$$r = r^* \left[\frac{K - u^{*2}/2}{K - u^2/2}\right]^{3/4} \left(\frac{u^*}{u}\right)^{1/2} \qquad \text{(III-14)}$$

Mass streamline coordinates r(z) for given r^* values may be calculated when the measured axial velocity profile u(z) in Fig. 8 is substituted into Eqn. III-14. K and u^* are evaluated from u_{max} = 12.5 km/sec. The flow streamlines associated with r^* = 1.0, 1.5, and 2.0 centimeters are shown in Fig. 13. Circular and triangular data symbols represent two experimentally measured streamlines. The circular data symbols also represent the outermost boundary of the AII luminosity photographed through the 4880 Å filter. Streamline agreement between the one-dimensional expansion model and the experimental data is excellent. Thus, the downstream acceleration of the inner propellant flow may be accounted for by the radial expansion of the high enthalpy plasma discharged from the accelerator chamber.

Questions may arise as to the sensitivity of these results to the shape of the measured velocity profile and the assumption of negligible recombination in the expanding flow. The above calculations were repeated for an arbitrarily chosen linear velocity profile substituted for the measured profile of Fig. 8. The corresponding streamline shapes calculated from Eqn III-14 for the linear profile differed noticeably from the experimentally measured flow directions. Recombination enthalpy was arbitrarily introduced onto the flow by including dh_I in Eqn. III-10. Even for relatively small degrees of assumed recombination, the calculated streamlines bore no resemblance to the measured flow patterns.

Outer Flow Region. Plasma acceleration appears qualitatively less significant in the outer flow regions of the discharge. Reduced levels of power addition, local $\bar{j} \times \bar{B}$, and luminosity suggest lower velocities, densities, and ion temperatures in the outer flow. Estimates of these temperatures and velocities may be made in the same spirit as with the inner flow.

Outer Flow, Discharge Chamber. The interesting feature of the outer flow within the discharge chamber is the localization

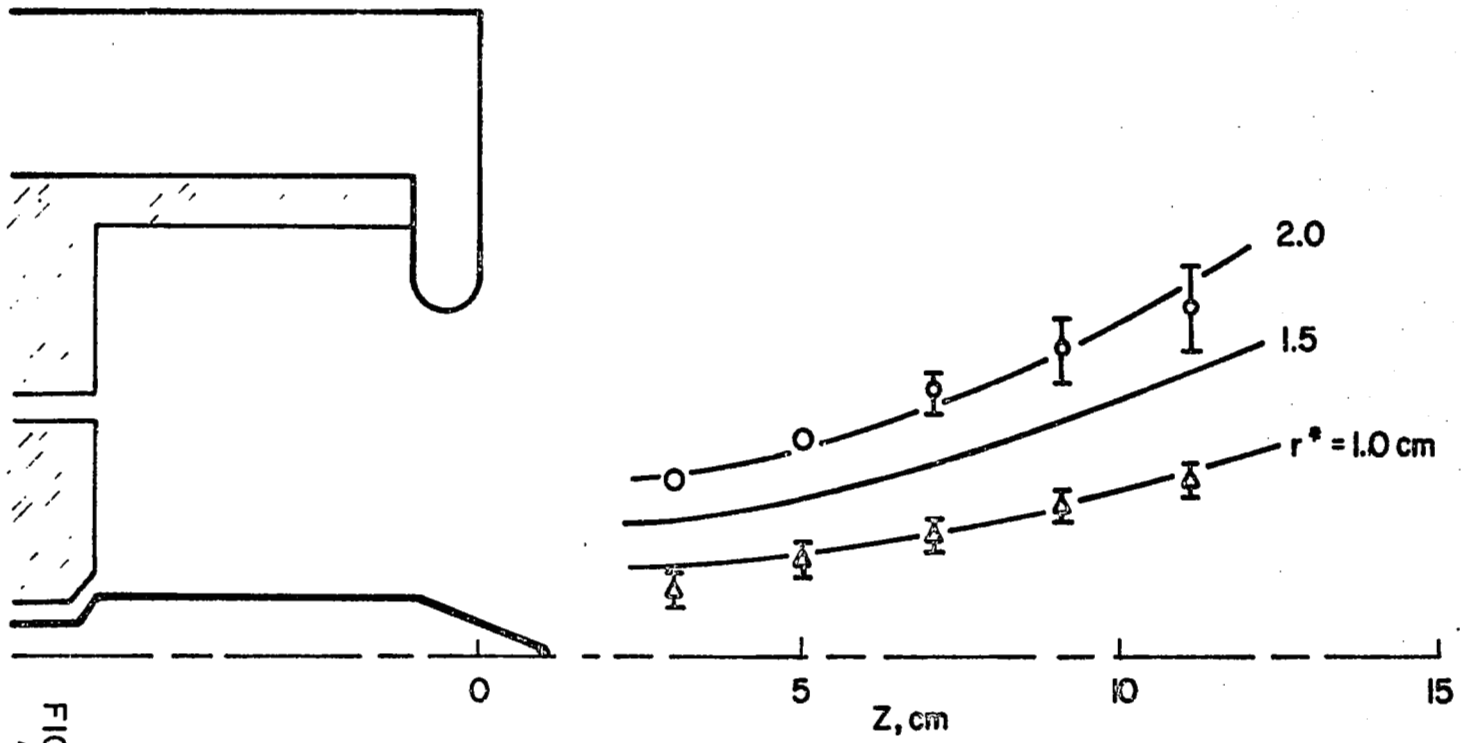

FIGURE 18
AP25-5057

CALCULATED AND EXPERIMENTAL MASS STREAMLINES

of power addition off the tip of the anode previously illustrated in Fig. 16. Because of this, significant ionization of the injected propellant is delayed until the flow enters the vicinity of the anode orifice. The local power addition there is commensurate with full ionization of the incident propellant flux. It should be recalled that outer flow mass injection was originally required to prevent severe terminal voltage fluctuations and minimize the total arc voltage.[151] Similar behavior has been reported for different arcjet configurations operating at conditions where the anode region appears locally "starved" of propellant. One may speculate that the outer flow functions primarily to provide a source of conduction electrons in the vicinity of the plasma-anode interface.

The outer flow plasma velocity in the anode plane may be estimated using the power balance Eqn. III-4. However, ion temperatures in this region of the discharge have not been previously measured. To circumvent this problem, advantage may be made of the near sonic conditions existing in the vicinity of the anode orifice. The ion temperature may be expressed in terms of the acoustic speed c_s,

$$c_s^2 = R\left(\gamma_e T_e + \gamma_i T_i\right)$$

where $\gamma_{e,i}$ are the respective electron and ion specific heat ratios. Since the acoustic speed equals the flow velocity at the sonic point, the ion temperature may be expressed as,

$$T_i = \frac{u^{*2}}{\gamma_i R} - \frac{\gamma_e}{\gamma_i} T_e \qquad \text{(III-15)}$$

Using Eqn. III-15, Eqn. III-4 may be rearranged to express the flow velocity u^* in terms of P^*_{FLOW}, $\dot{m}$, and T_e^* evaluated at the sonic point. Electron temperatures on the same order

as the inner flow are assumed, i.e. 0(19,000 ^{o}K). The electrical power input to the outer flow within the discharge chamber is 2.5 x 10^5 watts. This input power level accordingly accelerates the 3 g/sec outer flow rate to velocities less than 4500 m/sec and heats the ions to temperatures below 40,000 ^{o}K. Both these values are approximately a factor of two less than the inner flow velocity and ion temperature at a similar axial station.

Outer Flow, Exhaust Plume. The mass streamlines measured in the outer exhaust plume flow of the accelerator do not parallel the local current streamlines. The more rapid radial divergence of the outer exhaust flow indicates only partial magnetic confinement. The expansion process in this region of the discharge should therefore more closely resemble that of a free expansion from a sonic orifice. The details of the outer exhaust flow field were not considered.

Specific Impulse of the MPD Discharge Flow

The specific impulse of the quasi-steady plasma accelerator, defined by Eqn. III-16, is an important parameter used to evaluate thruster performance.

$$I_{sp} = T/\dot{m}g \qquad \text{(III-16)}$$

where T is the thrust produced by the acceleration of the mass flow rate $\dot{m}$, and g is the standard acceleration of gravity. The AVCO critical $J^2/\dot{m}$ model implies an upper limit of 890 seconds for the quasi-steady acceleration of argon propellant.[A-1] The foregoing results of the two-flow plasma acceleration model may be examined in light of this claim. In order to do this the thrust producing regions of the discharge must first be identified.

The thrust produced by the quasi-steady MPD arcjet is both electromagnetic and electrothermal in origin. Electromagnetic

thrust arises from the coupling among the vector components of the current density and azimuthal self-magnetic field of the discharge. Both axial and radial Lorentz body forces result from radial and axial current flow respectively. The $j_r B_\theta$ body forces ("electromagnetic blowing") directly accelerate the propellant downstream imparting thrust to the arcjet through the interaction between the current flow in the discharge plasma and the accelerator circuitry. The magnitude of the "blowing" thrust component may be calculated by integrating the Maxwell stress tensor over any convenient surface which encloses the discharge current pattern.[61] The radial or "pumping" $j_x B_\theta$ forces confine the discharge plasma and support radial pressure gradients similar to those found in classical pinch discharges. The thrust contribution from these "electromagnetic pumping" forces may be evaluated by integrating the pressure distributions caused by this magnetic confinement over those surfaces normal to the accelerator's symmetry axis. Thrust results from the overpressure generated on these surfaces.

Electrothermal or aerodynamic thrust generation is a consequence of the discharge plasma being resistively heated. As a result, the unbalanced pressure on the discharge chamber walls and any subsequent nozzle-like flow expansion in the exhaust, will impart additional thrust to the device. The proper evaluation of the electrothermal thrust component is not straightforward. Conventionally, aerodynamic thrust is expressed in terms of a nozzle discharge coefficient. However, the appropriate discharge coefficients and chamber pressures for the quasi-steady MPD arc are generally unknown. Usually therefore, one must rely upon specific experimental results to estimate the magnitude of the electrothermal thrust component.

The thrust attributable to the inner and outer flows may be estimated from the experimental data taken at J = 15.3 kA and $\dot{m}$ = 6 g/sec. The results are summarized below.[158]

Inner flow:

$$T^I = T^I_{em} + T^I_{et}$$
$$= 28.0 + 9.5$$
$$= 37.5 \text{ N}$$

Outer flow:

$$T^O = T^O_{em} + T^O_{et}$$
$$= 16.0 + 2.7$$
$$= 18.7 \text{ N}$$

where the superscripts I and O denote the inner and outer flows and the subscripts em and et imply electromagnetic and electrothermal thrust components. The total thrust generated by the MPD discharge at these conditions is the sum of T^I and T^O and equals,

$$T = T^I + T^O$$
$$= 56.2 \text{ N}$$

It is interesting to note that approximately 22% of this total calculated thrust is electrothermal in origin. This T_{et}/T ratio is consistent with previous experimental thrust data which implied the electrothermal thrust fraction of the quasi-steady MPD arcjet was constant and equal to 20% over a wide range of conditions.[125]

Several implications of these thrust data may now be discussed. Since each flow region accelerates three grams per second argon, the mass-averaged velocities corresponding to the inner and outer flow thrusts are,

$$\bar{u}^I = T^I / \dot{m}_I = 12.5 \text{ km/sec}$$

$$\bar{u}^O = T^O / \dot{m}_O = 6.2 \text{ km/sec}$$

Comparison between these mass averaged velocities and the anode orifice exit velocities of the inner and outer flows suggests that approximately 28% of the arcjet's thrust is derived from the flow expansion in the downstream exhaust. In addition, the mass averaged velocity $\bar{u}^I$ is in close agreement with the terminal exhaust velocity of 12.3 $\pm$ 1.1 km/sec measured in the plume of the inner flow. This velocity also equals the maximum velocity obtainable from the 1-D, nozzle-like expansion of the inner flow discussed previously. From this correspondence, it may be inferred that thrust recovery in the downstream exhaust regions of the discharge results from the experimentally observed electromagnetic confinement of the flow.

Finally, the specific impulse of the two propellant streams may be calculated.

$$I^I_{sp} = T^I / \dot{m}_I g = 1280 \text{ sec.}$$

$$I^O_{sp} = T^O / \dot{m}_O g = 640 \text{ sec.}$$

The inner and outer flow regions delineated by the two-flow plasma acceleration model may be further characterized by the disparity between their specific impulses. The inner flow region generates thrust with a specific impulse which considerably exceeds the AVCO limiting I_{sp} of 890 seconds for the quasi-steady acceleration of argon propellant. In contrast, the specific impulse associated with the outer propellant flow falls beneath this limiting value. On combining these two flows, the overall specific impulse of the thruster, equal to the total thrust divided by g times the total mass flow, becomes,

$$I_{sp} = (T^I + T^O) / g(\dot{m}_I + \dot{m}_O) = 960 \text{ sec.}$$

which, although lower than I_{sp}^I, still exceeds the minimum power model's fundamental limit of 890 seconds.

The implications of the two-flow model and the above results, with respect to improving the performance of the quasi-steady MPD thruster, are clear. Namely, higher accelerator thrust densities and specific impulses should be achieved if the relative importance of the outer flow region is reduced. This could seem to be accomplished by reducing the anode and chamber radii such that the outer flow discharge chamber region is physically eliminated. If as a result of the chamber geometry change, the inner flow properties remain the same, the specific impulse of the accelerator would increase from ≈ 960 to ≈ 1280 seconds. It must be recalled, however, that previous variations in the mass injection geometry resulted in increased terminal voltages and erratic arcjet behavior when the outer anode regions were deprived of injected mass.[151] Furthermore, power density and luminosity measurements imply ionization phenomena are important in the vicinity of the anode. These data all tend to suggest the function of the outer flow may be primarily related to current conduction processes in the anode region. Since these phenomena and their connection and influence upon the plasma acceleration process are not well understood at this time, it is not clear that this flow region can be eliminated without inducing other significant consequences throughout the remainder of the discharge. Improved MPD thruster performance realized by enhancing the inner flow characteristics of the discharge at the expense of the outer flow, thus remains to be shown.

B. Cathode Studies (Rudolph)

In previous photographic and diagnostic studies of the MPD discharge, it was observed that an intensely luminous plasma was formed in the region immediately downstream of the cathode tip.[141] It was postulated that this plasma was a result of the high axial current densities at the cathode tip which caused a large, radially inward "pumping" force, increasing the number densities and temperatures in this region.

The role of this intense plasma in the overall acceleration process is unclear. According to the self-field thrust equation, a positive thrust increment is generated within this region by the plasma pressure acting against the conical cathode surface. On the other hand, the high temperature and pressure in this volume elevates the propellant to excited states which in turn leads to radiation and frozen flow losses.

In order to clarify the role of this cathode tip plasma, a much longer cathode was installed in the MPD apparatus. It was anticipated that with this cathode, the current would be distributed such that the axial current component causing the radial pumping would be eliminated, and the operation of an accelerator of a purely "sweeping" type could be studied.

An additional advantage of this long cathode configuration arises from its relation to a series of experiments recently conducted by Boyle.[155] In this work, the discharge current J^* at which the arc reached a seeming limitation on quiescent operation (as indicated by a rapidly fluctuating or "hashy" terminal voltage V^*) was found to be a linear function of the cathode surface area over a range of areas from 5 to 40 cm^2. Throughout this investigation, the discharge current (typically 10 to 20 kA) was determined to attach over the entire cathode surface, indicating a decreasing surface current density for larger cathodes. The new long cathode provides an opportunity to examine the "critical" current for a cathode with a surface area much larger than those previously tested.

The cathode configuration initially used in this study is shown in Fig. 19a. It consists of a 13.6 cm long, 1.9 cm diameter cylinder with a conical tip, 2.54 cm in length. The diameter is the same as previous cathodes in order to maintain the same geometric constant in the self-field thrust equation.[61] The cathode is made of type 304 stainless steel instead of the usual thoriated tungsten due to the former's availability and relative ease of machining. The rest of the discharge configuration was kept the same as Boyle's to facilitate a comparison with his data. The mass flow was 6 g/sec of argon propellant.

A current-voltage characteristic for this configuration is shown in Fig. 20. Two interesting features of this graph are the discharge voltage of 115 volts at a current of 16 kA, and the voltage, V^*, at the initiation of the "hashy" voltage of 216 volts. These values can be immediately compared to Boyle's data.

A graph of discharge terminal voltage versus cathode surface area is shown in Fig. 21 for all previously tested tungsten cathodes, which were limited to surface areas of 40 cm^2. The points at 75 cm^2 represent the present 13.6 cm long stainless steel cathode. The dashed lines show that the present data are not inconsistent with an extrapolation of the Boyle data.

In Fig. 22, the onset of the "hashy" voltage is graphed versus cathode surface area. The value for the 13.6-cm long cathode is also shown and again agrees with a reasonable extrapolation of previous data. Both graphs indicate that the cathode emission processes may be independent of cathode material.

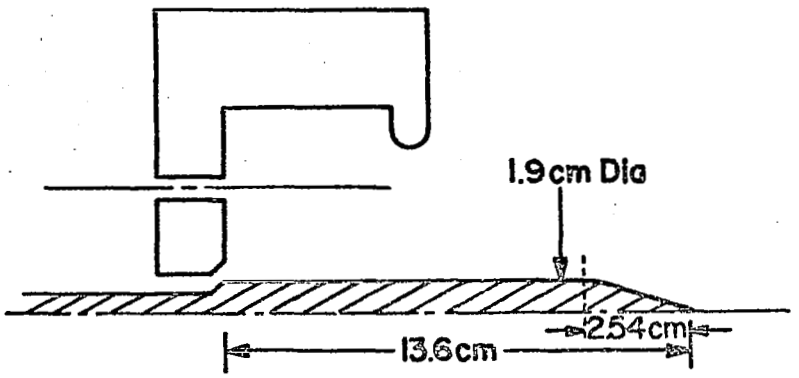

a) 13.6 cm CATHODE

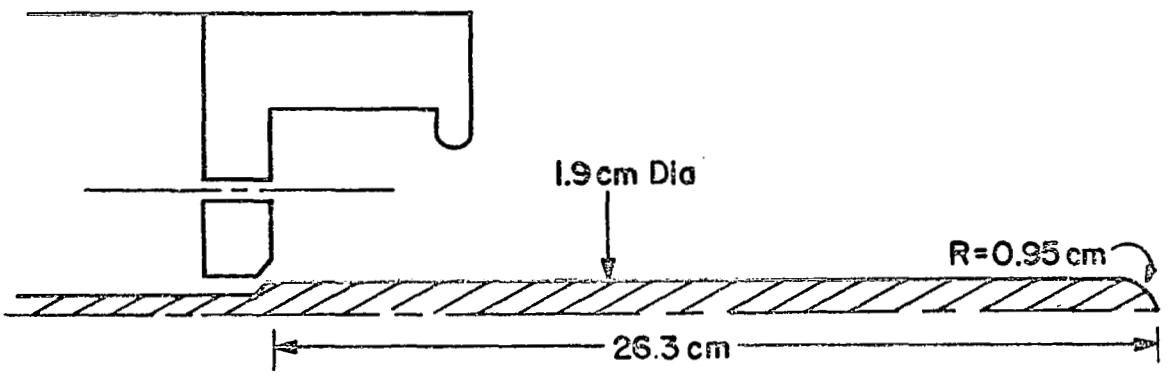

b) 26.3 cm CATHODE

CATHODE GEOMETRIES

FIGURE 19
AP25-5071

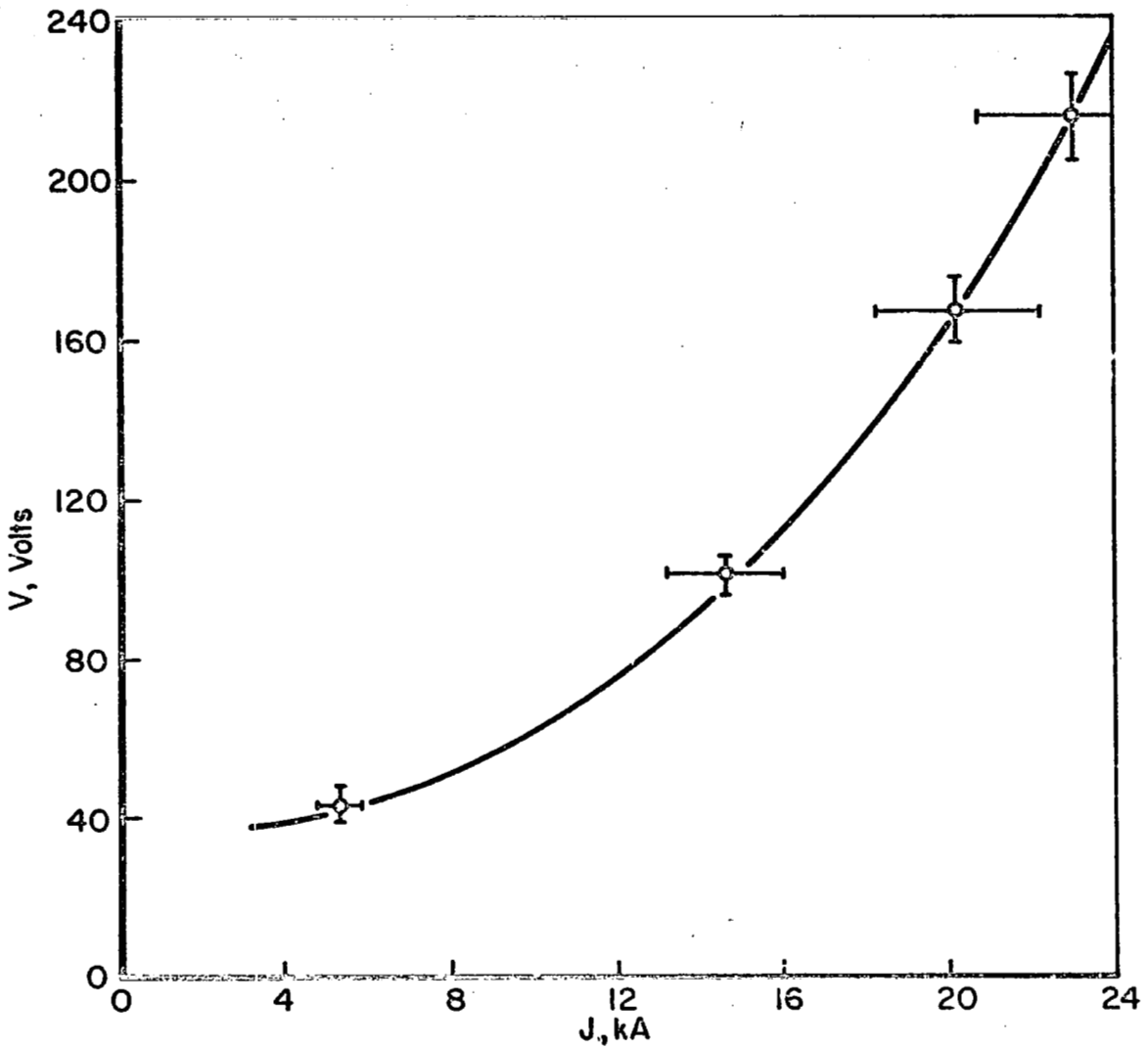

VOLTAGE CURRENT CHARACTERISTIC

FIGURE 20
AP25-5072

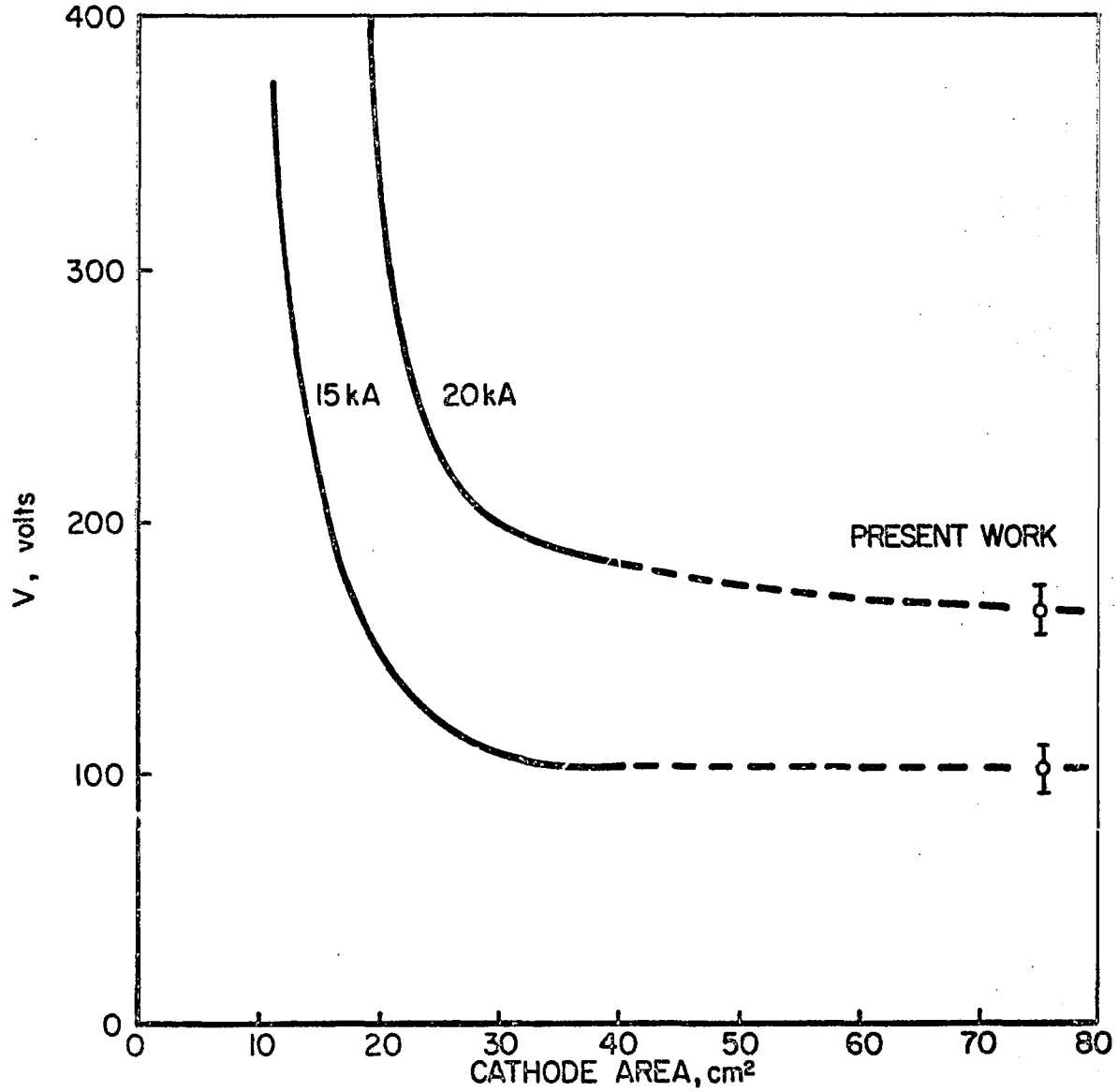

FIGURE 21
AP25-5073

TERMINAL VOLTAGE VS. CATHODE AREA

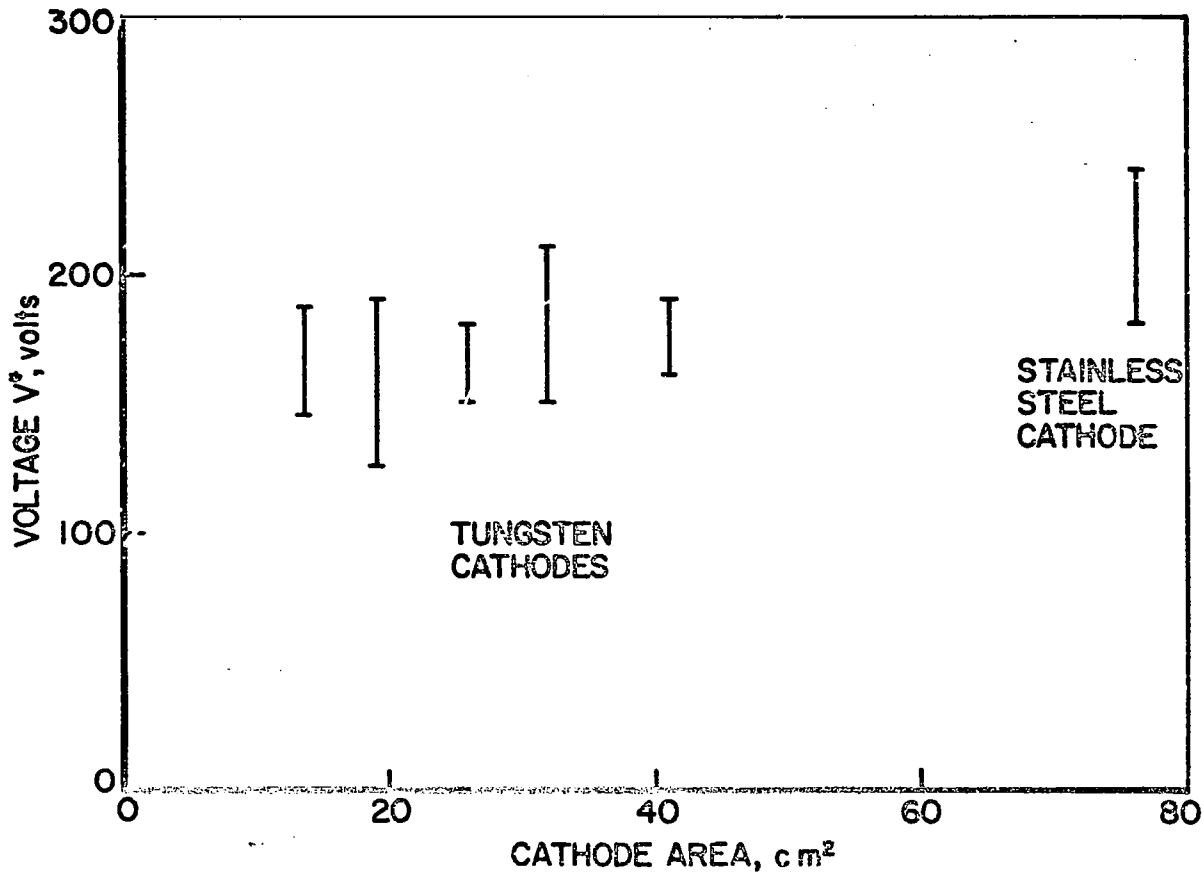

CRITICAL VOLTAGE vs CATHODE AREA

FIGURE 22
AP 25-5074

The graph of the critical current versus the cathode area is shown in Fig. 23. Again, the data for areas below 40 cm^2 are from Boyle while the bar at 75 cm^2 represents the cathode used in the present study. If the cathode material is unimportant, the new point indicates that as the cathode area increases, the previously rising critical current approaches an asymptotic value of about 25 kA. Further data are required to verify this trend.

In order to determine whether the previously mentioned electromagnetic compression region off the cathode tip was eliminated using this larger cathode, the local magnetic field distribution was measured for a total current of 16 kA. The resulting current contour map is shown in Fig. 24. It is noted that at the cathode tip, there is a sizeable fraction of the total current (approximately 4 kA) that has a significant axial component. This indicates that the "pumping" force has not been completely eliminated in this downstream region. Current conduction upstream of the 6 kA line is virtually radial, however, and seems to indicate that a completely radial current distribution is possible if the cathode attachment is allowed to spread out over a larger area.

The total current attachment downstream of a point on the cathode surface versus the axial coordinate of that point is shown in Fig. 25. As can be seen, a straight line can be drawn through the data on the cylindrical part of the cathode, which is consistent with a uniform attachment.

The 2 kA attachment on the conical cathode tip and the large axial component of the current downstream of the 4 kA streamline both tend to indicate that a longer cathode is needed to provide a current attachment free of cathode tip influence and to eliminate the radial $\bar{j} \times \bar{B}$ force. Consequently, a larger stainless steel cathode, 26.4 cm in length, has been built and is shown in Fig. 19b. This cathode is presently undergoing the same tests as the previous 13.6 cm cathode.

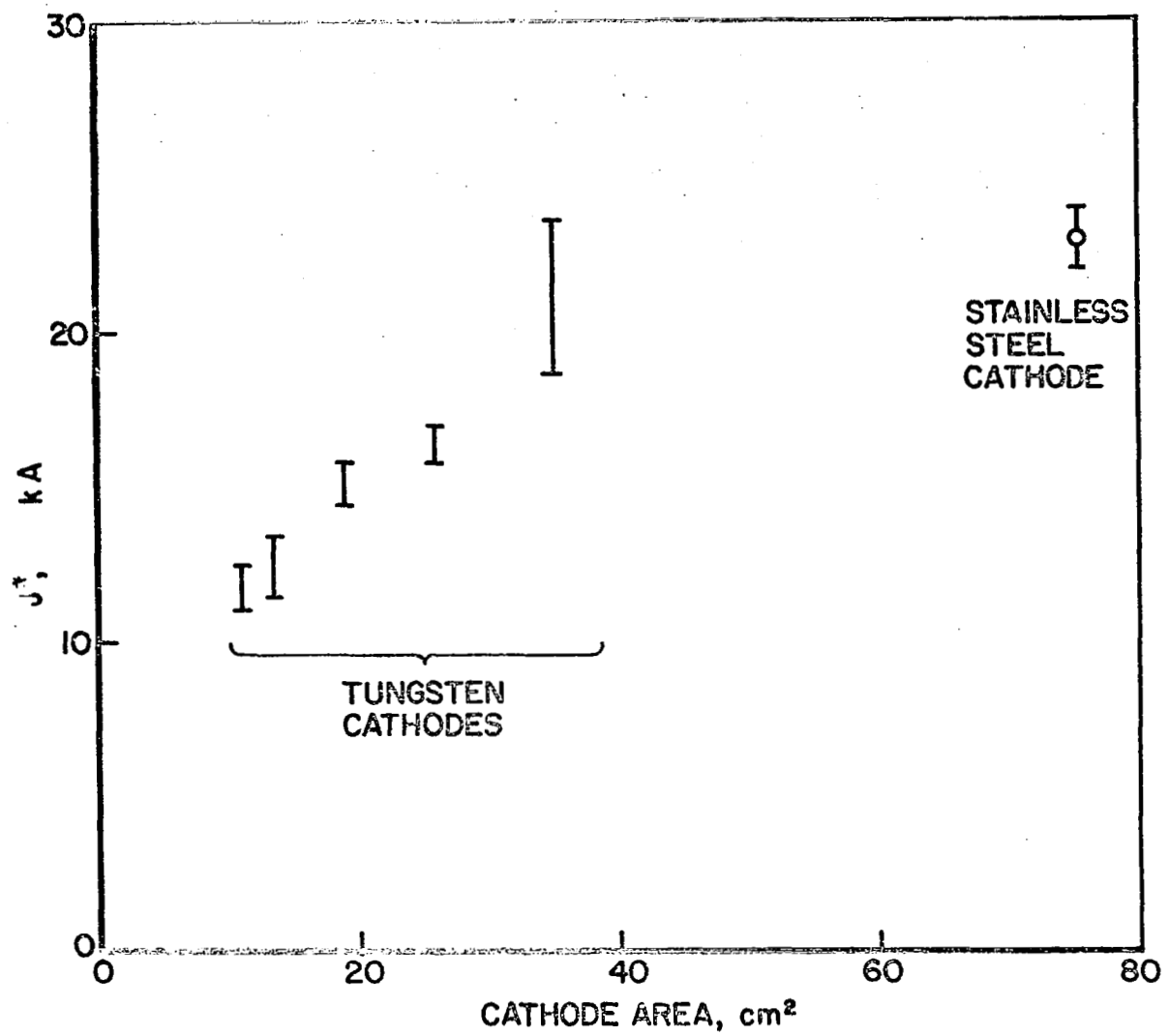

CRITICAL CURRENT vs CATHODE AREA

FIGURE 23
AP25-5075

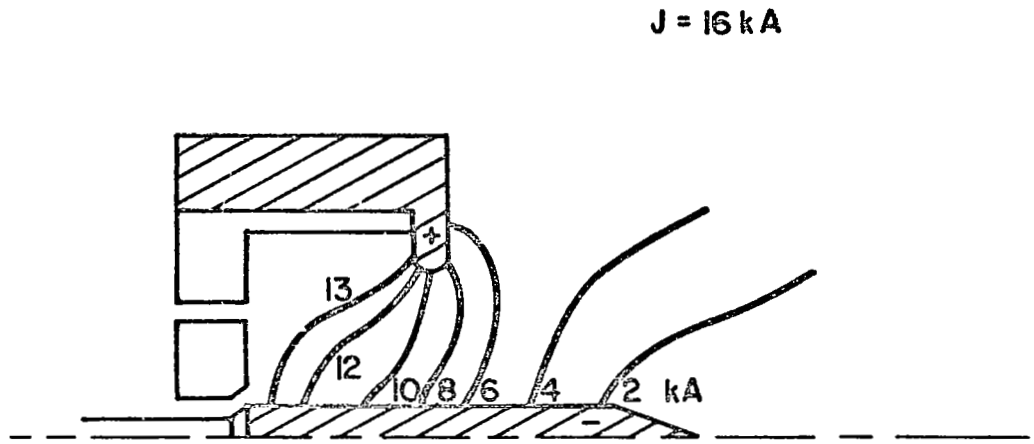

ENCLOSED CURRENT CONTOURS

FIGURE 24
AP 25 5076

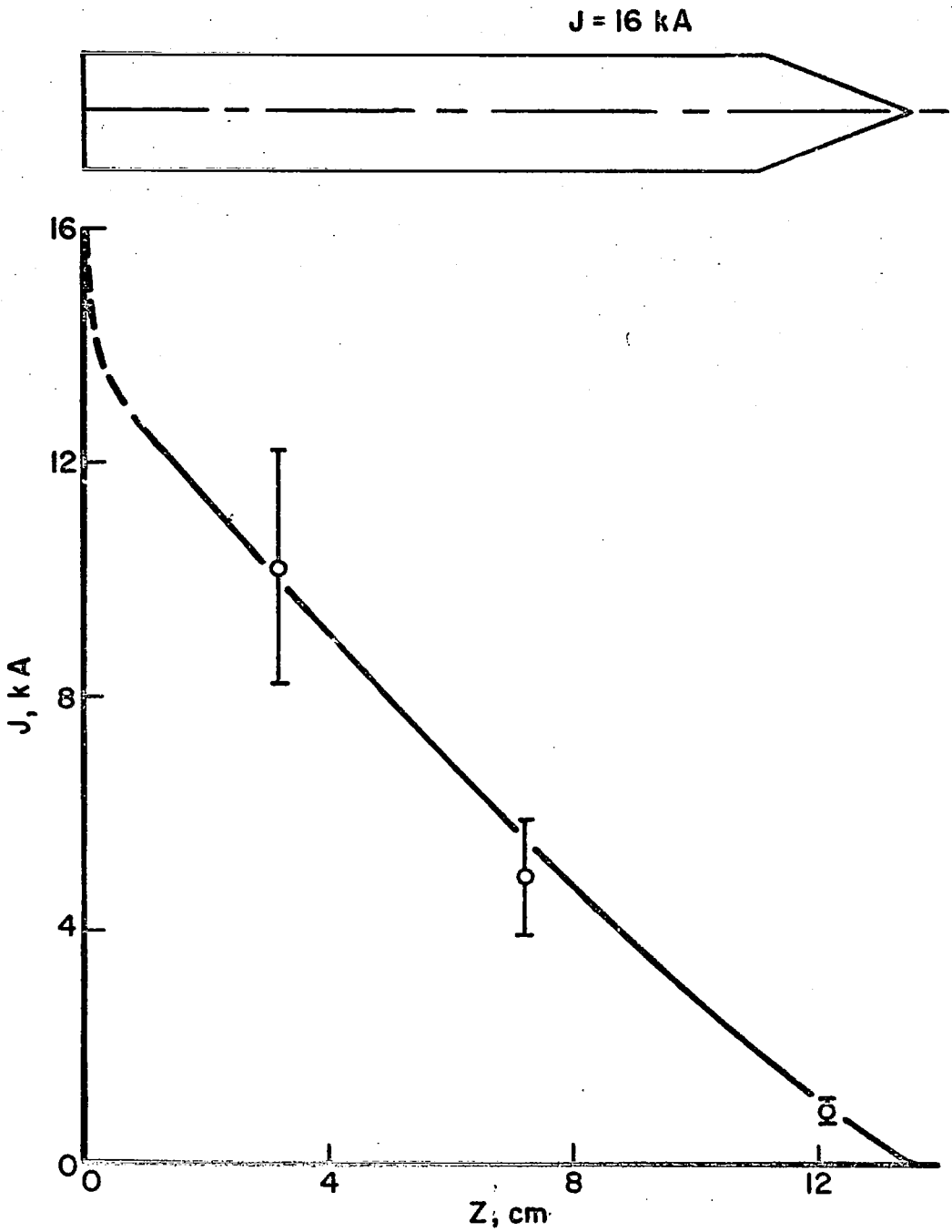

ENCLOSED CURRENT ON CATHODE SURFACE

FIGURE 25
AP25-5077

C. Terminal Voltage Fluctuations in Quasi-Steady MPD Discharges (Boyle)

The onset of fluctuations in the terminal arc voltage of the quasi-steady MPD accelerator has been reported previously. Originally this behavior was interpreted as indicative of a fundamental limitation imposed upon the quasi-steady acceleration of a plasma flow. This arcjet model proposed nominal MPD discharge operation was restricted to arc currents and injected mass flow rates for which the parameter $J^2/\dot{m}$, the arc current squared divided by the propellant flow rate, was equal to a critical constant dependent only upon accelerator geometry and propellant species. Empirically this critical $J^2/\dot{m}$ value equalled $(J^*)^2/\dot{m}$, where J^* is the arc current at which the onset of terminal voltage fluctuations is observed.

Recent experiments however suggest the critical $(J^*)^2/\dot{m}$ parameter is neither constant nor unique.[155] In fact, J^* is found to be functionally dependent upon both cathode surface area and mass injection geometry for a given propellant flow rate. These data also suggest the phenomena responsible for the voltage fluctuations occur in the vicinity of the cathode electrode.

As part of a preliminary investigation to determine the nature and significance of these phenomena, local potential measurements about the electrode regions of the discharge were made. The accelerator configuration for these measurements included a 7.62-cm-long tungsten cathode, 50:50 flow division between cathode base annulus and outer injector holes and 6 g/sec total mass flow rate. Two floating potential probes are positioned close to the central cathode and outer anode lip. The potential drop between the cathode and the potential probe several millimeters off the cathode surface is measured differentially and labelled V_C. The floating potential several millimeters off the anode lip is simultaneously recorded with respect to the anode ground and is labelled V_A. The potential difference across the plasma

flow region, V_p, may be expressed as:

$$V_p = V - V_A - V_C$$

where V is the terminal arc voltage. This experimental arrangement is schematically reproduced in Fig. 26.

Figure 27 compares the oscillogram signatures of V, V_A and V_C for an arc current greater than the onset current J^*. The cathode voltage signal V_C clearly reproduces the onset time, frequency, and amplitude of the terminal voltage fluctuation. This 1:1 correspondence implies the fluctuations in the terminal voltage signal are localized about the vicinity of the cathode.

The onset of terminal voltage fluctuations is further characterized by a sudden increase in the local electric field about the cathode. Figure 28 presents V_C, V_A and the terminal voltage V as a function of current. The current at which the cathode voltage V_C sharply increases corresponds exactly with J^* determined from the terminal voltage-current characteristic. The anode voltage V_A also exhibits a similar sharp increase in magnitude although at a lower current of 8 kA. Coincidentally, this value approximately equals the ion current which would be generated by the complete single ionization of the outer 3 g/sec argon mass flow rate. No such sharp voltage increases are evident in the terminal voltage and V_p characteristics.

It is interesting to note that the terminal voltages at which the sudden increase in cathode potential and discharge instability occur, V^*, are insensitive to the cathode surface area. Preliminary stainless steel large cathode results suggest that V^* is also insensitive to cathode material (section III-B). Referring back to Fig. 22, the common voltage associated with the onset of the voltage fluctuations is 180 volts ± 30%. Thus it would appear that for arc conditions such that the terminal voltage exceeds V^*, the local electric field about the cathode sharply

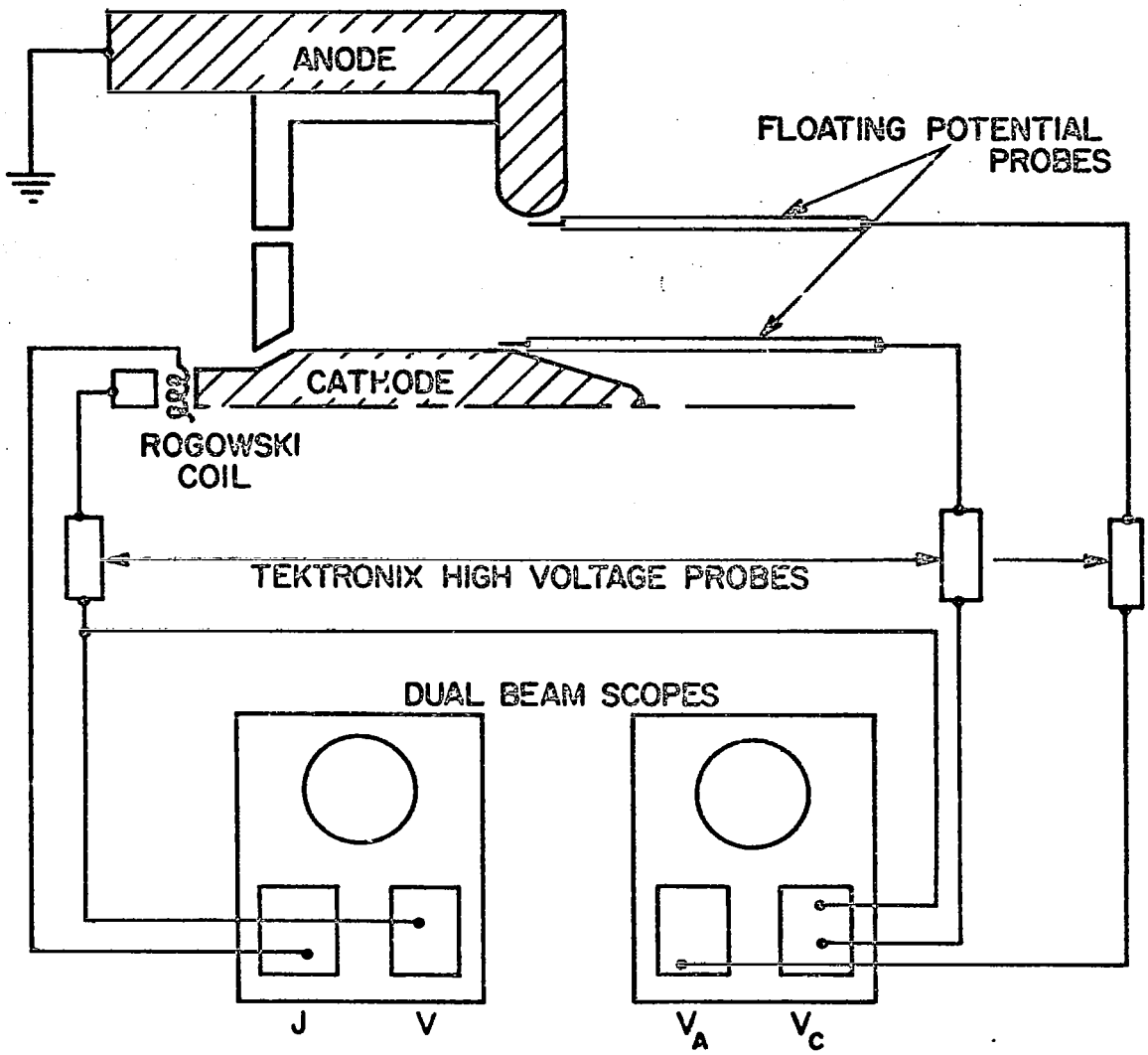

FLOATING POTENTIAL MEASUREMENT

FIGURE 26
AP 25-5078

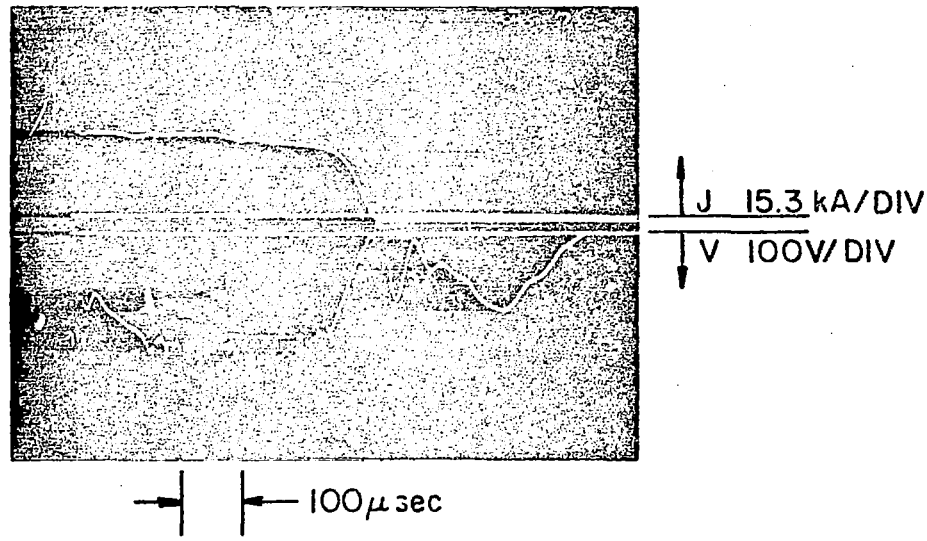

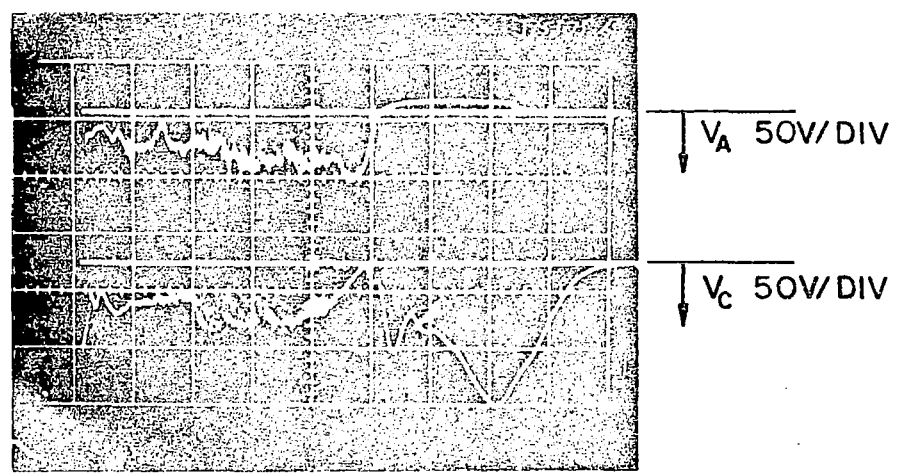

TERMINAL VOLTAGE AND FLOATING POTENTIAL SIGNATURES

FIGURE 27
AP25-P-525

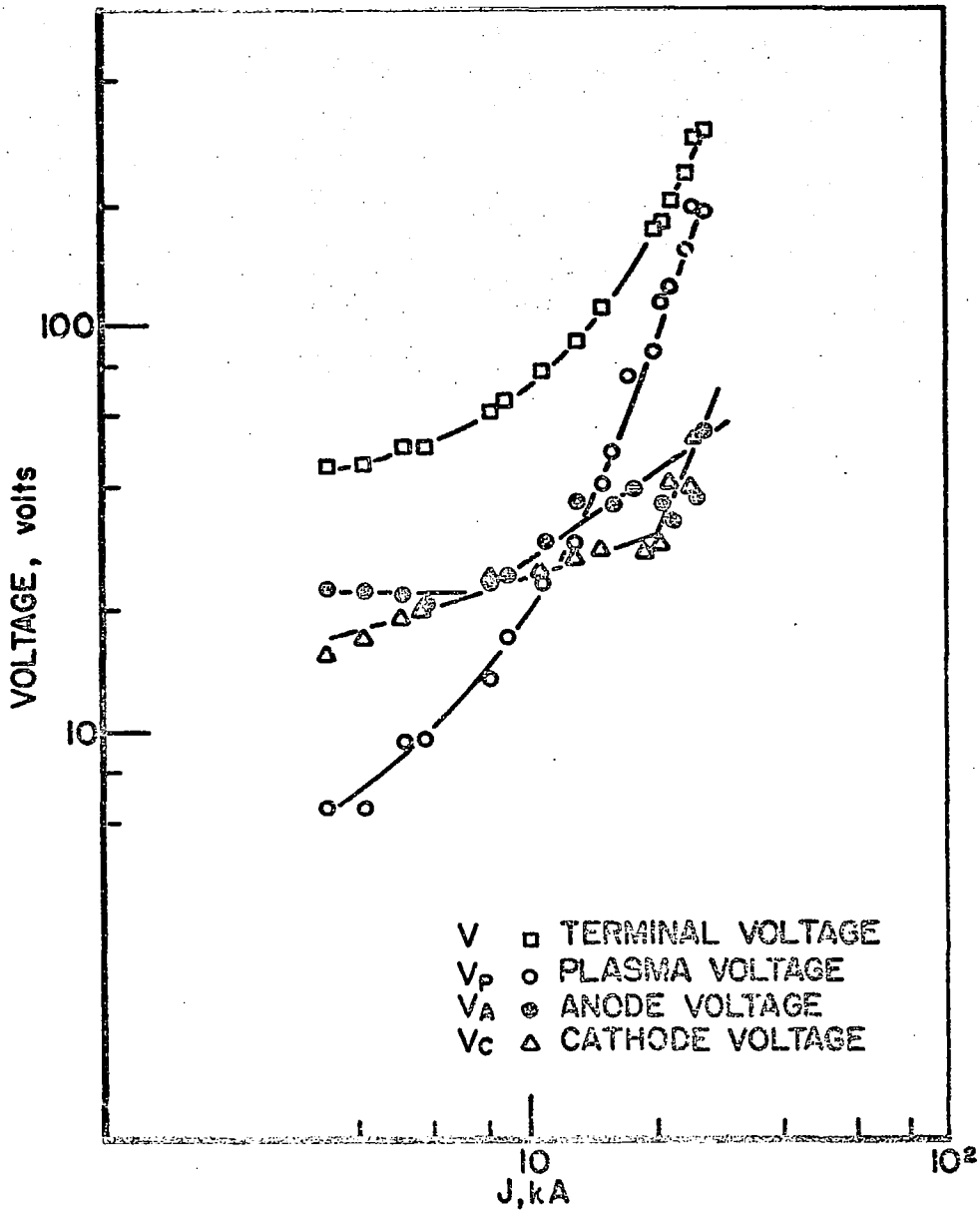

VOLTAGE COMPONENTS vs CURRENT

FIGURE 28
AP 25-L079

increases and becomes oscillatory. It is tempting to speculate that this critical voltage and the changes in the field properties about the cathode reflect a change in the local current emission processes. However, since the electron emission and current conduction processes in the cathode region of an arc discharge are extremely complex and pertinent experimental data do not presently exist, further clarification of this suggestion must await future work.

Finally, there is an indication that V^*-J^* phenomena may ultimately influence the performance characteristics of the quasi-steady MPD arcjet. Figure 29 illustrates the functional relationship between the thermal efficiency η_{th} and arc current for the above accelerator configuration. Assuming that JV_C and JV_A represent all the power that is deposited into the cathode and anode respectively, then the thermal arcjet efficiency neglecting radiation is defined as

$$\eta_{th} = \frac{V - V_A - V_C}{V} = \frac{V_P}{V}$$

Physically, η_{th} represents the fraction of input energy which appears as plasma enthalpy during the arc discharge. From a performance point of view, η_{th} equals the maximum attainable arcjet thrust efficiency for the ideal case wherein all the plasma enthalpy is converted into useful thrust. For arc currents less than J^*, η_{th} monotonically increases. Above J^*, however, the thermal efficiency assumes a constant value of approximately 65%. Whether or not this trend represents a fundamental limitation imposed by electrode phenomena upon quasi-steady arcjet performance deserves further attention.

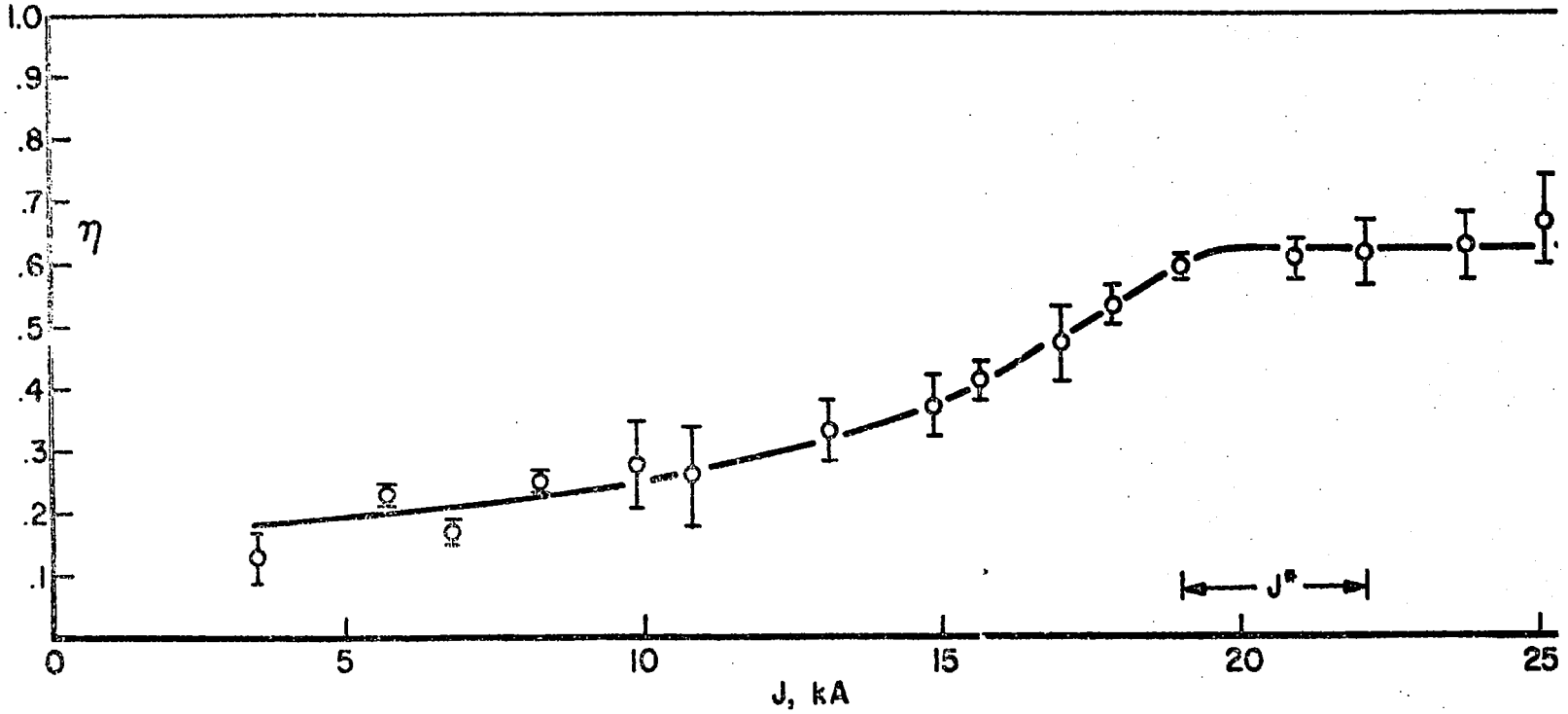

ARCJET THERMAL EFFICIENCY vs ARC CURRENT
$\dot{m}_T$ = 6g/sec, 50:50 FLOW DIVISION

FIGURE 29
AP25-5060

IV. PLASMADYNAMIC LASER STUDIES

MPD Discharge in a Laser Cavity (Dutt)

This section describes progress on a set of experiments intended to determine directly whether lasing can be sustained in the discharge and exhaust regions of an MPD accelerator. A direct evaluation of lasing is possible by placing the region of plasma under consideration within a resonant optical cavity. In order to minimize the variation of plasma properties along the optical axis of the resonant cavity, a two-dimensional discharge geometry was considered desirable.

The previous semi-annual report[155] described the important characteristics of the cavity. Progress described in this report includes a) the alignment of the cavity mirrors to form a resonant cavity; b) the measured distributions of radiance and current in an ambient two-dimensional discharge; and c) the design and calibration of a mass injection system capable of providing a short risetime, uniformly distributed mass pulse in the two-dimensional geometry.

Alignment of the Cavity Mirrors.

Two concave mirrors 1.5 cm in diameter with a radius of curvature of 67.5 cm constituted the resonant cavity. Their reflectivities were 97% and 99.7% in the wavelength range 430 nm to 530 nm, which includes many of the strong emission lines of ionized argon, krypton, xenon and many other elements.

An externally mounted helium-neon laser, wavelength 632.8 nm, was used to align initially the cavity. To ensure that the axes of the cavity and He-Ne laser were coincident and parallel to the supporting I-beam, adjustable irises mounted on an optical bench were used. For the initial alignment, the multiple reflections of the laser beam on the inner

reflecting surfaces of the mirrors were made to coincide. The He-Ne laser was then removed. Subsequently, a commercial argon ion laser, with its mirrors removed, was placed within the cavity (Fig. 30a). The laser tube was lined up with the cavity axis and the discharge initiated. Laser output was observed from the mirror of lower reflectivity. Minor adjustments in the mirror positions were made to obtain the brightest output. Each mirror could be rotated approximately 0.25^{o} about a diameter before lasing disappeared completely. The mirrors were easily adjustable to within 0.02^{o}. The argon ion laser tube was then removed.

Following alignment, the cavity can now be used to investigate whether conditions suitable for lasing (described in the previous semi-annual report[155]) exist in any medium within the cavity.

Two-dimensional MPD Discharge

Experimental arrangement. The coaxial geometry predominant in MPD arc work was considered inadequate to provide a lasing medium because of the large gradients of plasma properties along any line of sight perpendicular to the MPD axis. Specifically, the gain of an amplifying region could be masked by other absorbing regions elsewhere along the line of sight. In addition, a longer active medium is preferable because the overall gain (or loss) within the medium is correspondingly increased. This would also provide a more accurate determination of the gain per unit length.

To realize these advantages, a two-dimensional version of the MPD arc was designed and constructed with electrodes considerably wider than any previously used in this laboratory. This was intended to provide a long uniform plasma region with variations in the plasma properties confined to relatively small end regions.

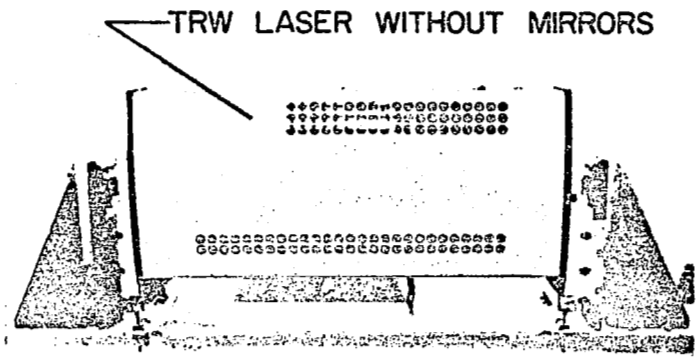

a) RESONANT CAVITY

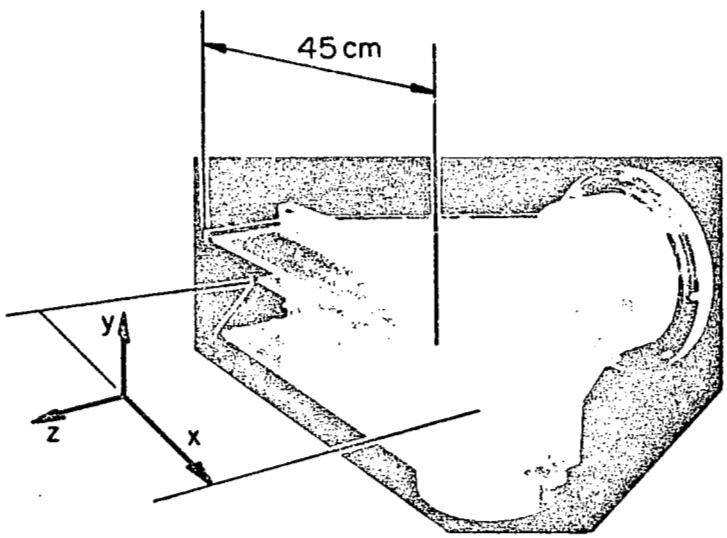

b) DISCHARGE APPARATUS

EXPERIMENTAL APPARATUS

FIGURE 30
AP25-P-533

The proposed discharge geometry was briefly described in the previous semi-annual report.[155] It consists of three aluminum parallel plates, 45-cm wide by 0.95-cm thick as shown in Fig. 30b. The upper and lower plates are anodes which extend 10 cm out of the backplate, while the center cathode plate extends only 5 cm from the backplate. The plates are tapered at their rear ends to fit into a 20-cm diameter Plexiglas cylinder which passes through the circular back access port in the large Plexiglas tank. Electrical contact to the plates from outside the tank is made by brass studs passing through the Plexiglas cylinder. Copper plates connect the brass studs to the capacitive pulse-forming network via a gas triggered switch.

When the assembly is in place within the vacuum tank, the electrode region lies in the line of sight of an opposing pair of tank windows. The resonant cavity may thus be placed with the mirrors outside the windows to contain various portions of the discharge region.

In order to provide a suitable lasing medium, the discharge must satisfy several criteria. One important requirement is that the components of the current to the two anodes be equal for the discharge to be horizontally symmetric. It should be noted that the two anodes are not physically connected inside the vacuum tank. Second, the current distribution must be diffuse and approximately uniform across the entire width of the electrodes with relatively small fringing effects. Finally, not only must the current be uniformly distributed but mass must also be injected uniformly across the electrode width in order to guarantee uniform plasma properties in the cavity.

In order to determine whether these criteria are satisfied for our discharge configuration, several experiments were conducted in an ambient gas discharge. This technique has been found useful in the past for examining the feasi-

bility of a particular experimental configuration without the added complexity of a mass injection system.

Ambient Gas Discharge Operation. For these initial tests, the vacuum tank was filled with argon to pressures varying between 25 μ and 300 μ of mercury. This is also the range of fill pressures for conventional argon ion lasers. During a discharge, the terminal voltage was measured using a Tektronix voltage probe. The current distribution between the two anodes was measured by passive integration of separate Rogowski coil signals.

Oscillogram traces of current and voltage are shown in Fig. 31 for a total current of 65 kA supplied for 200 μsec. The two uppermost traces represent the currents J_1 and J_2 to the upper and lower anodes, respectively. The other traces are voltage records for various ambient pressures.

Current measurement over a variety of operating conditions show the current division to be quasi-steady, and in all cases J_1 and J_2 differ by less than 5%. The device thus satisfies the important condition of equal division of current between the two anodes.

The voltage traces exhibit the familiar drop to a minimum after discharge initiation, followed by a rise to a quasi-steady voltage level. These features are usually associated with insulator ablation, in this case caused by operation in the ambient mode.

Photographic Study. Photographs of the discharge were taken for a limited range of conditions as indicated in the table below.

Table II. Photographs of Ambient Discharge

Figure Number	Current Amplitude	Current Duration	Camera Lens Aperture	Neutral Density Filter
32b	8.0 kA	0.92 msec	f/32	50%
32c	15.6	0.92	f/32	50
32d	15.6	0.92	f/11	10
32e	65.0	0.20	f/16	10
33b	15.6	0.92	f/11	10

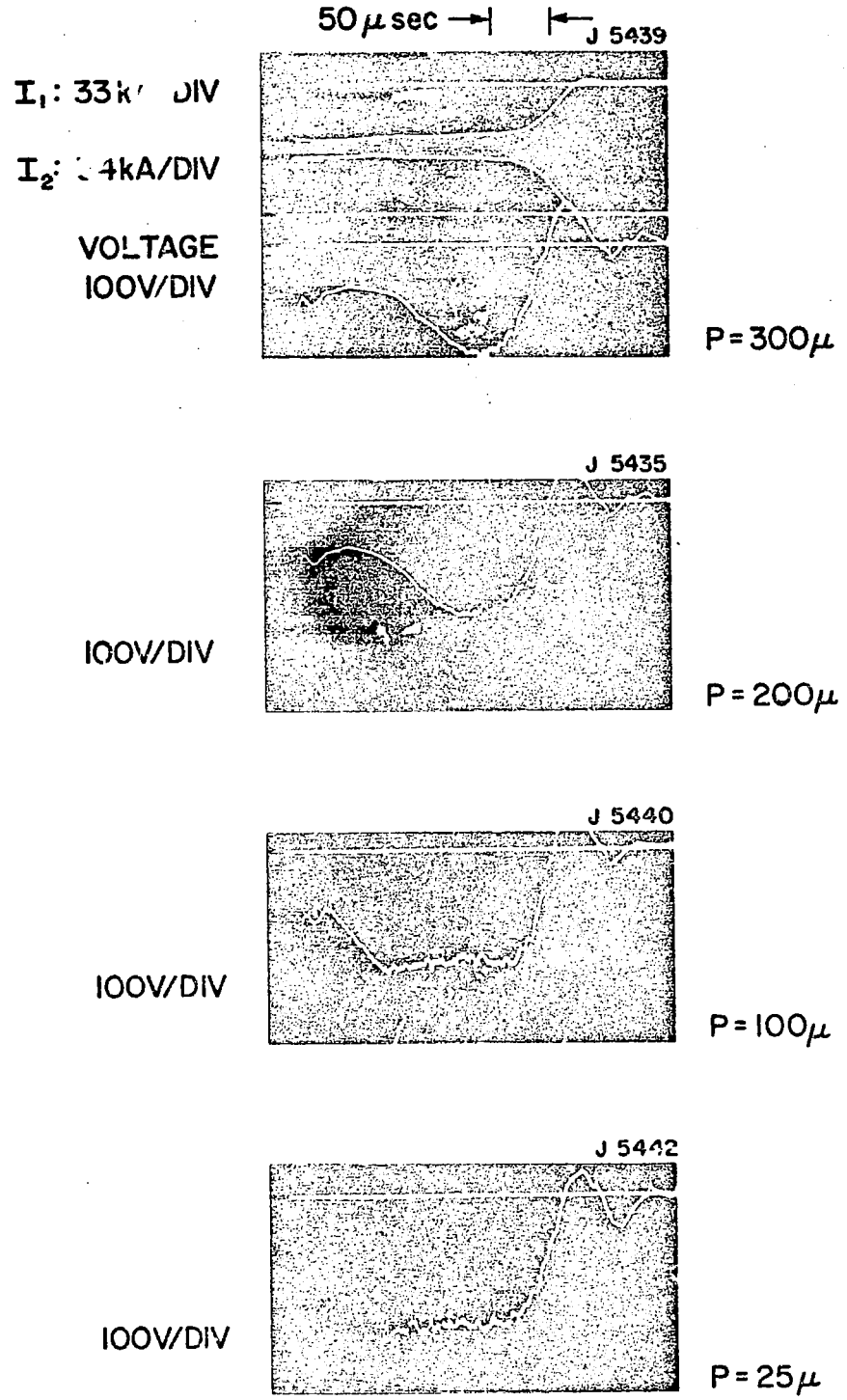

TERMINAL VOLTAGE

FIGURE 31
AP 25-P-534

At 8 kA the luminosity is confined to one-half of the discharge width (Fig. 32b) indicating that this current is inadequate to drive the 45-cm wide discharge. At a higher current of 15.6 kA the discharge appears to be distributed more evenly but it is still much brighter on one side, Fig. 32c. A different photograph of this same discharge in Fig. 32d taken at a different combination of lens aperture and neutral density filter shows it to be more uniform. When the current was increased substantially to 65 kA, the discharge appeared more laterally symmetric but exhibited bright areas near the ends of the electrodes, Fig. 32e.

A side view at 15.6 kA (Fig. 33b) shows the discharge to be horizontally symmetric. The bright radiance close to the ends of the electrodes originates on the surfaces of the insulating sidewalls, as can be seen by comparing this photograph with the no-discharge photograph shown in Fig. 33a.

The more uniform distribution of luminosity which is observed at the higher currents may be taken as an indication of a relatively uniform distribution of current and plasma parameters, but it is not in itself sufficient evidence of uniformity. It does suggest however, that the plasma properties are more uniform at higher current levels. This favors the choice of high current levels for a finer and more extensive mapping of the current distribution in the discharge.

Current Distribution. Measurements of magnetic field may be used to determine not only the uniformity of current distribution across the discharge but also to evaluate the current densities within the discharge regions.

To facilitate the reduction of magnetic field data a coordinate system shown in Fig. 30b was used with the origin centrally located on the cathode tip. Three similar probes were used, instead of one, to speed up the probing of such an

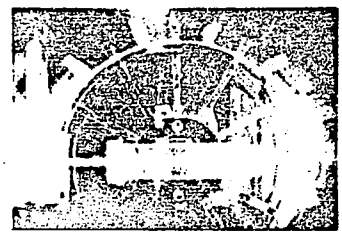

a) NO DISCHARGE

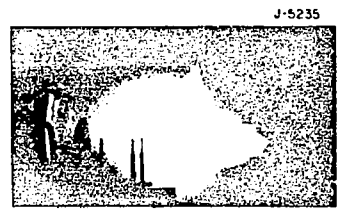

b) 8kA × 0.92 ms AT 200μ

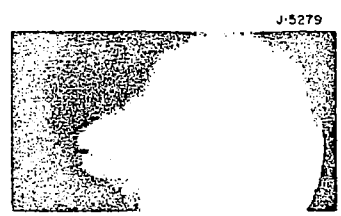

c) 15.6 kA × 0.92 ms AT 200μ

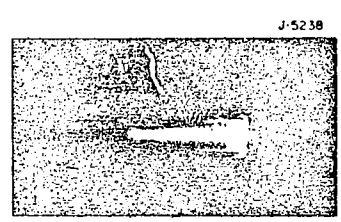

d) 15.6kA×0.92 ms AT 200μ

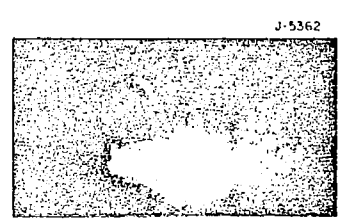

e) 65kA×0.2 ms AT 200μ

END VIEW OF DISCHARGE
FIGURE 32
AP25 P 535

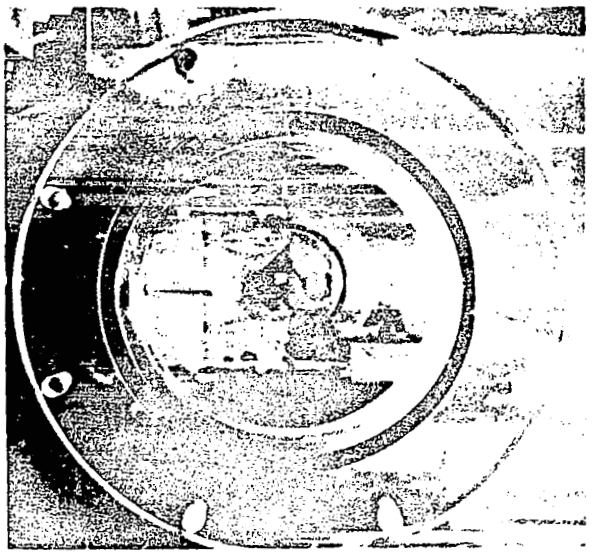

(a) NO DISCHARGE

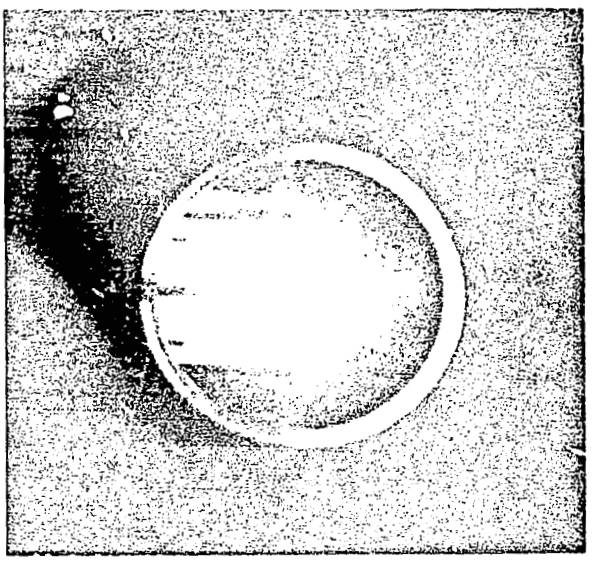

(b) 15.6 kA × 0.92 ms AT 200μ

SIDE VIEW OF DISCHARGE

FIGURE 33
AP25-P-536

extensive discharge region. The probes were mounted on a movable platform within the vacuum tank with their stems oriented parallel to each other and pointing in the negative z direction. The axes of the probe coils were in the x direction so that the component B_x of the magnetic field would be measured. This was expected to be the dominant component for the given orientation of electrodes. Probes #1 and 2 were on the same horizontal plane 21.6 cm apart while probe #3 was 5.7 cm directly below probe #2 (Fig. 34a). The probe coils were all at the same z value.

The magnetic field B_x was measured at a few locations in the discharge at the intermediate current level, 15.6 kA. Oscillograms reproduced in the left column of Fig. 34b represent magnetic probe signals at locations x = -21.6, 0 and +21.5 cm on the line y = 4 cm, Z=-3.8 cm. Corresponding oscillograms for the 65 kA case are shown in the right hand column of Fig. 34b. The traces indicate that at the lower current, the field component B_x and consequently the current distribution remain unsteady for a large part of the 0.9 msec pulse. At the higher current, 65 kA, the discharge becomes quasi-steady in about 120 μsec.

The distribution of the quasi-steady values of B_x in the x direction is shown in Fig. 35 for probing along three lines at the y = 2 cm plane. These locations correspond to the insulating backplate Z = 3.8 cm, the cathode front edge, Z = 0, and the anode front edge, Z = 5.1 cm, respectively.

The most important conclusion from these data is that the discharge is uniform across the entire 45-cm width of the electrodes at locations close to the insulating backplate. Further away from the backplate the profile is less uniform with a B_x of one-half its maximum value recorded at the edges of the electrodes. The reason for this decrease in the field may be

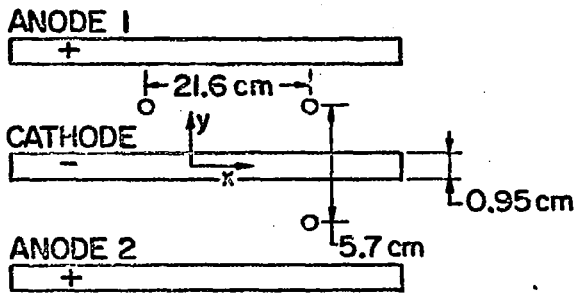

a) RELATIVE PROBE SPACING

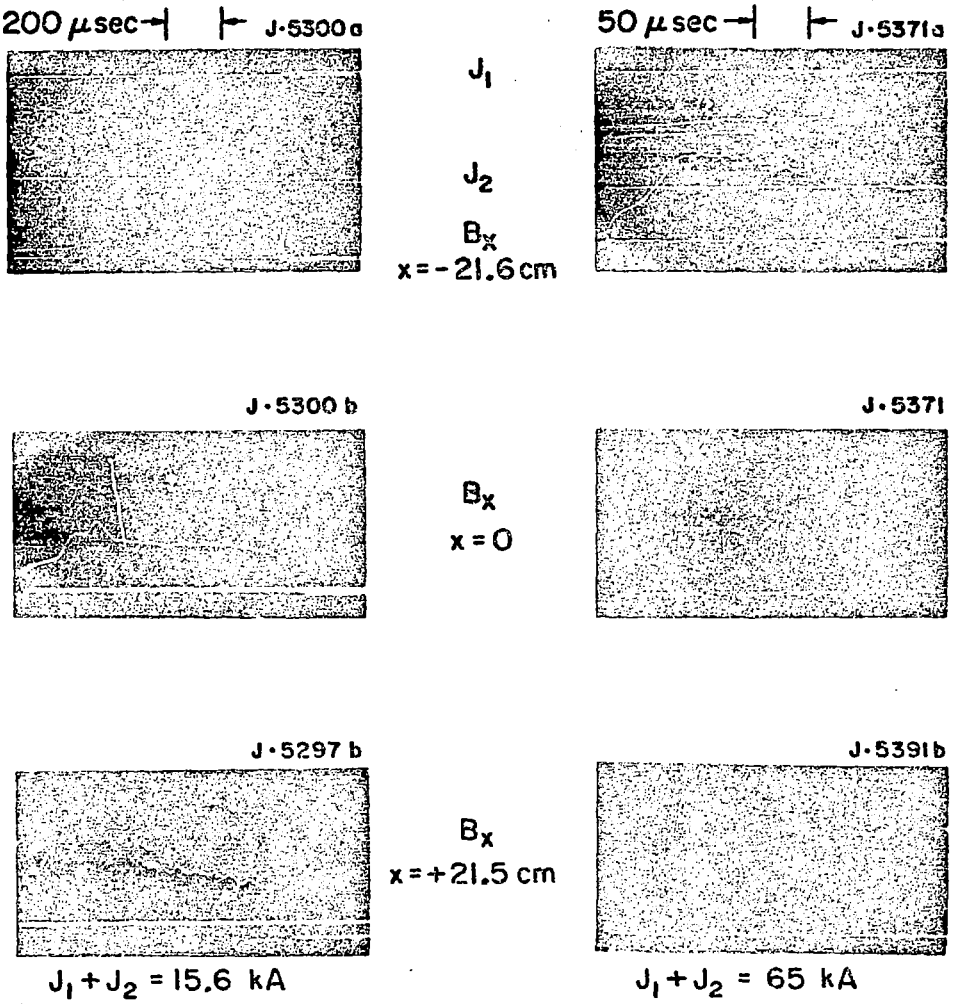

b) CURRENTS AND MAGNETIC FIELDS

DISCHARGE CURRENTS AND FIELD MEASUREMENTS

FIGURE 34

AP 25-P-537

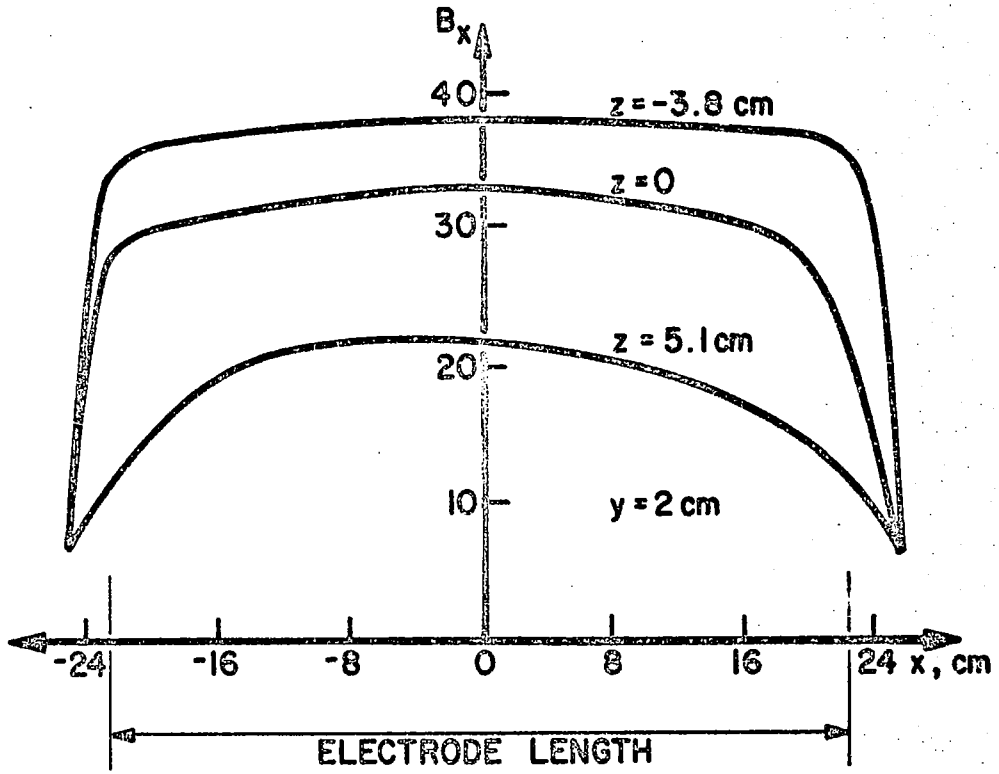

MAGNETIC FIELD B_x

FIGURE 35
AP 25-3060

that the insulating sidewalls, which are partially cut away (see Fig. 30b), permit the current to fringe near the ends of the electrodes. The lateral fringing of current contours is substantiated by measurements of B_y which have values comparable to B_x at the edges of the discharge, downstream from the backplate. It is expected that this small departure from uniformity will be corrected by using more extensive sidewalls.

To evaluate the vector current density $\bar{j}$, all the components of the magnetic field within the discharge must be known. However, in these initial experiments only B_x, the dominant component of the magnetic field, was measured in some detail over the entire region of the discharge. For a total current of 65 kA these measurements lead to an average value of $j = 93$ A/cm^2 between the cathode and anode in the plane containing the anode front edges about the symmetry, or z, axis. If the other components of B had been included, j would be somewhat larger. It should be noted that the value of j is in excess of the typical threshold current density, 50 A/cm^2, for conventional argon ion laser operation, although the significance of this comparison is not yet known for this discharge configuration.

The experiments with the ambient argon fill discharge operation show that a fairly uniform discharge of sufficiently high current density can be sustained. However, the voltage measurements indicate the possible presence of substantial ablation products in the discharge. In order to operate the discharge in a pure argon plasma, a means of injecting uniformly a sufficient mass flow of argon gas into the discharge must be provided. The design of such a system is presented in the following section.

Mass Injection System

Design. The mass injection system should provide a uniformly distributed quantity of gas into the discharge region at a

rate that enables a quasi-steady discharge to be maintained with minimal ablation. From previous experiments with a 15-cm wide parallel plate accelerator, the mass flow required for the highest current anticipated ($\approx$80 kA) may be greater than 100 g/sec.[128]

The risetime of the mass pulse is also crucial in that the mass injected prior to discharge initiation raises the background pressure in the vacuum tank. To the extent that this background pressure can be compared to the initial fill pressure of conventional argon ion lasers, the risetime takes on added significance. Conventional argon ion lasers operate with a cold gas filling pressure in the range from 25 to 300 μ. In comparison, a 100 g/sec mass pulse with a 10 msec risetime will raise the average pressure in the present vacuum tank to approximately 400 μ. Although a strict comparison between the two pressures is not warranted because of the differences between the conventional laser and the present dynamic system, it is nevertheless apparent that the risetime should be kept as small as possible.

The mass injection system is shown in Fig. 36a. A standard gas cylinder was positioned immediately outside the vacuum tank and connected with a tee arrangement to the two solenoid valves fixed to the side of the insulating backplate. The valves are Skinner type V52 with a nominal diameter of 0.8 cm. Holes drilled through the side of the insulating backplate connect the valves to two plena which run across the backplate. Each plenum is a 0.95-cm square channel machined out of the Plexiglas backplate. The plena are closed by two rectangular plates (0.63-cm thick) which cover the interelectrode region. There are nine equidistant holes of 0.159-cm diameter on each plate directly in front of the plenum.

The solenoid valves are opened by discharging an 850 μF capacitor through them. Earlier experiments have shown that the

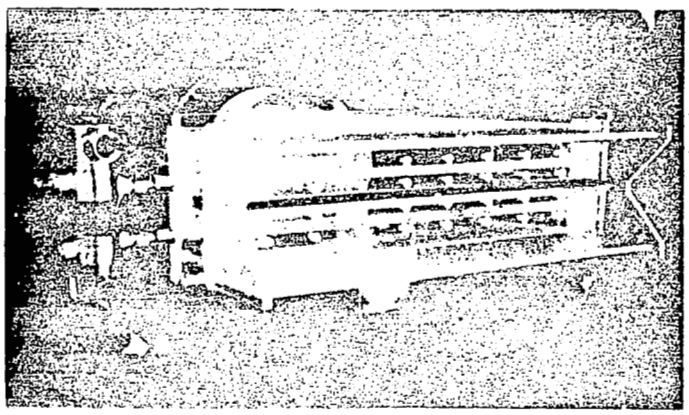

a) MASS INJECTION SYSTEM

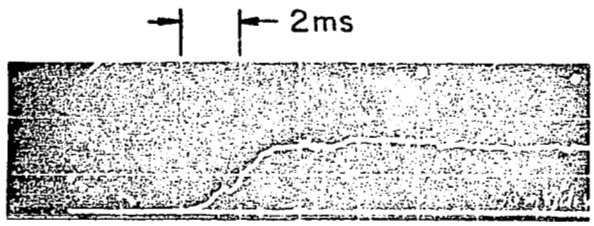

b) PRESSURE SIGNAL

MASS INJECTION

FIGURE 36
AP25-P-538

two valves open almost simultaneously, delivering gas into the two plena. The nine holes in each plenum allow the gas to escape and fill the discharge chamber.

The effective choking area of each valve is 0.196 cm^2. The total area of the 9 holes is 0.181 cm^2. Thus, irrespective of the discharge coefficient C_D of the holes, the flow when steady will choke at the nine exit holes. The advantage of such an arrangement is that when the discharge commences the flow adjustment time is small, thus allowing quasi-steady operation to be reached in a shorter time.

Performance. A fast ionization gauge (Varian Millitorr) was placed at various locations within the tank in order to determine the uniformity of the cold flow. The time for the flow to reach a quasi-steady state was measured in addition to the distribution of pressure once the steady state was reached.

A representative oscillogram of the ionization gauge output is shown in Fig. 36b. The pressure at the anode region reaches a steady value in about 2 msec. A profile of steady state pressure distribution at y = 3 cm, Z = 5.1 cm is shown in Fig. 37. The peak-to-trough variation is $\pm 15\%$ about the mean, while the decrease in the average pressure from the left to right is $\approx 8\%$ consistent with the valve location on the left or negative x end. These data show that the flow reaches a steady state quickly and is reasonably uniform in the x direction.

Calibration of the Mass Flow Rate. The mass flow was calibrated as described in earlier semi-annual reports.[119,146] A Hewlett Packard Pulse Generator was used to generate a square wave lasting 2.5 to 10.1 msec. The square wave was differentiated, with the resultant positive and negative spikes used to tailor the voltage pulse to the valves. The positive spike allows the previously charged 850 μF capacitor to discharge

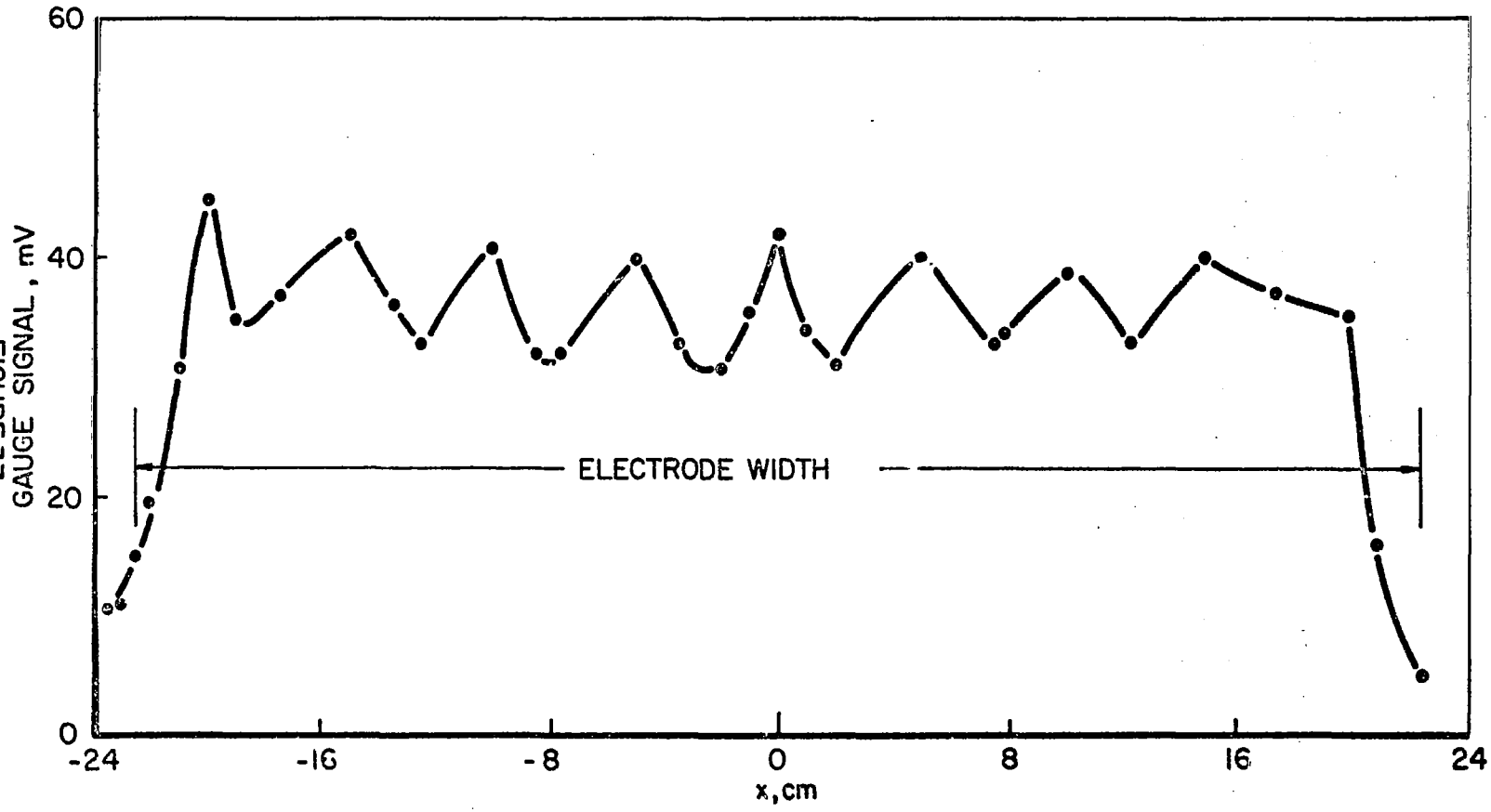

FIGURE 37
AP25-5081

PRESSURE DISTRIBUTION

into the valves, opening them after a small delay. The negative spike shorts out the capacitor allowing the valves to close. With the vacuum pumps isolated, the pressure rise in the tank due to the injected mass pulse is measured using a McLeod gauge.

By altering the length of the square wave and thus the time interval between the spikes, the mass of gas admitted into the vacuum chamber can be varied. A minimum pulse length t_{min} exists below which the valve never fully opens and thus the flow rate through the valve does not reach the choked flow rate associated with the particular stagnation pressure. For pulse lengths greater than the minimum, a fixed mass flow is obtained, and the tank pressure increases linearly with $t - t_{min}$. The slope of the tank pressure rise vs. pulse length for time greater than the minimum thus yields the mass flow rate.

A typical calibration curve gives an average pressure rise of 1.81 μ/msec for a stagnation pressure of $1.34(10^5)$ N/m^2 (5 psig). Using the tank volume of 1.22 m^3 and an assumed ambient temperature of 295 ^{o}K, the mass flow is calculated to be 4.74 g/sec. Similar measurements at double the absolute pressure give twice the mass flow verifying the choked flow assumption.

Summary.

The results and conclusions of the experiments described in this report may be summarized as follows.

Alignment of the constructed optical cavity with a commercial argon ion laser source is readily accomplished. This cavity is now being adapted for first experiments with the large Plexiglas vacuum tank.

The two-dimensional discharge geometry was constructed and tested in ambient argon at pressures around 200 μ. Rogowsky coil measurements showed that in all cases the current was distributed evenly between the two anodes. In addition, for

sufficiently large currents the discharge distributed itself to provide a uniform luminosity and magnetic field along the width of the electrodes. The magnetic field distribution was less uniform away from the insulating backplate, probably because restraining sidewalls were absent there. Large sidewalls are presently under construction.

For a total current of 65 kA the current density in the middle of the discharge was estimated to be twice the threshold current density required for argon ion laser operation in thin tubes. About half of the total current was found to attach on the outer surfaces of the anodes. This suggests that the current density could be increased in some parts of the discharge by insulating the outer surfaces of the anodes.

As was expected, ablation of the Plexiglas insulators occurred during the discharge, especially at the larger currents. These insulators will be replaced or covered with some refractory material such as quartz or boron nitride. This will reduce the contamination and allow a clearer interpretation of the observed phenomena.

A mass injection system was designed and constructed. Measurement of cold flow pressure distribution across the discharge region showed it to be reasonably uniform. The mass outflow was experimentally determined. Sufficiently high mass flows can be obtained at stagnation pressures of several atmospheres with the possible addition of two other valves.

These results show that a quasi-steady uniform two-dimensional discharge can be obtained over wide plates, accompanied by uniform gas injection at desired levels. Experiments can thus be performed to determine whether lasing is possible in the medium under various conditions.

V. HOLLOW CATHODE STUDIES (Krishnan)

Advantage was taken of the recent move of the Electric Propulsion Laboratory to redesign the pulse-forming network to generate longer current pulses. The new pulse lengths are 500 μsec in the parallel and 2 msec in the series configurations as compared with 200 μsec and 800 μsec, respectively, from the previous arrangement. The discharge chamber and its supporting equipment were also rearranged to allow greater accessibility for photographic and spectroscopic study of the hollow cathode discharge.

In earlier studies the distributions of current and potential within and about hollow cathodes of different configurations, designated as HC-I to HC-VIII, were determined in order to establish some of the characteristics of typical hollow cathode operation.[151,155] These studies have been continued with two additional hollow cathodes, designated HC-X and HC-XI, in order to determine the distributions of current and potential which distinguish typical hollow cathode operation in a high current discharge. For reasons of expediency, the most recent two hollow cathodes HC-X and HC-XI were manufactured of stainless steel instead of tungsten as were all the previous configurations. Therefore, in order to compare the experimental results with those acquired previously, one additional stainless steel cathode, HC-IX, of the same dimensions as the tungsten HC-VIII, was manufactured to record any differences in its electrical characteristics, as well as to check out the operation of the improved facility in the relocated laboratory.

This report describes in its first section the modifications and improvements of the hollow cathode facility. The second section presents the results of studies with the two additional new hollow cathode configurations. These studies bring to a conclusion the first phase of the investigation of the characteristics of hollow cathode operation in a high current discharge.

Expanded Hollow Cathode Discharge Facility

The major change in the hollow cathode facility is an extension of the pulse-forming network to provide longer current pulses at the same current levels as before. The previous pulse-forming network provided approximately 4 to 20 kA for 200 μsec when arranged in the parallel configuration or 1 to 5 kA for 800 μsec when in the series configuration. The old facility, which was described in a previous report,[143] consisted of 4 rows of individual transmission lines of 9 capacitors each, giving the capacitor bank a total capacitance of 940 μF.

The new facility consists of 4 individual transmission lines, each assembled from 21 equal sections of 6.6 μH series inductors and 27.1 μF shunt capacitors as shown in Fig. 38. The total capacitance of this new bank is 2.35 mF. With this larger network the line segments can be arranged in parallel to provide approximately 4 to 20 kA for 500 μsec or in series to provide 1 to 5 kA for 2 msec, thus yielding current pulses 2-1/2 times as long at the same current levels as the older and smaller capacitor bank. A photograph of the capacitor bank is shown in Fig. 39.

Voltage reversal across any of the capacitors in the pulse forming network must be avoided to prevent damage. In addition, even a low level of reversed current is undersirable since it

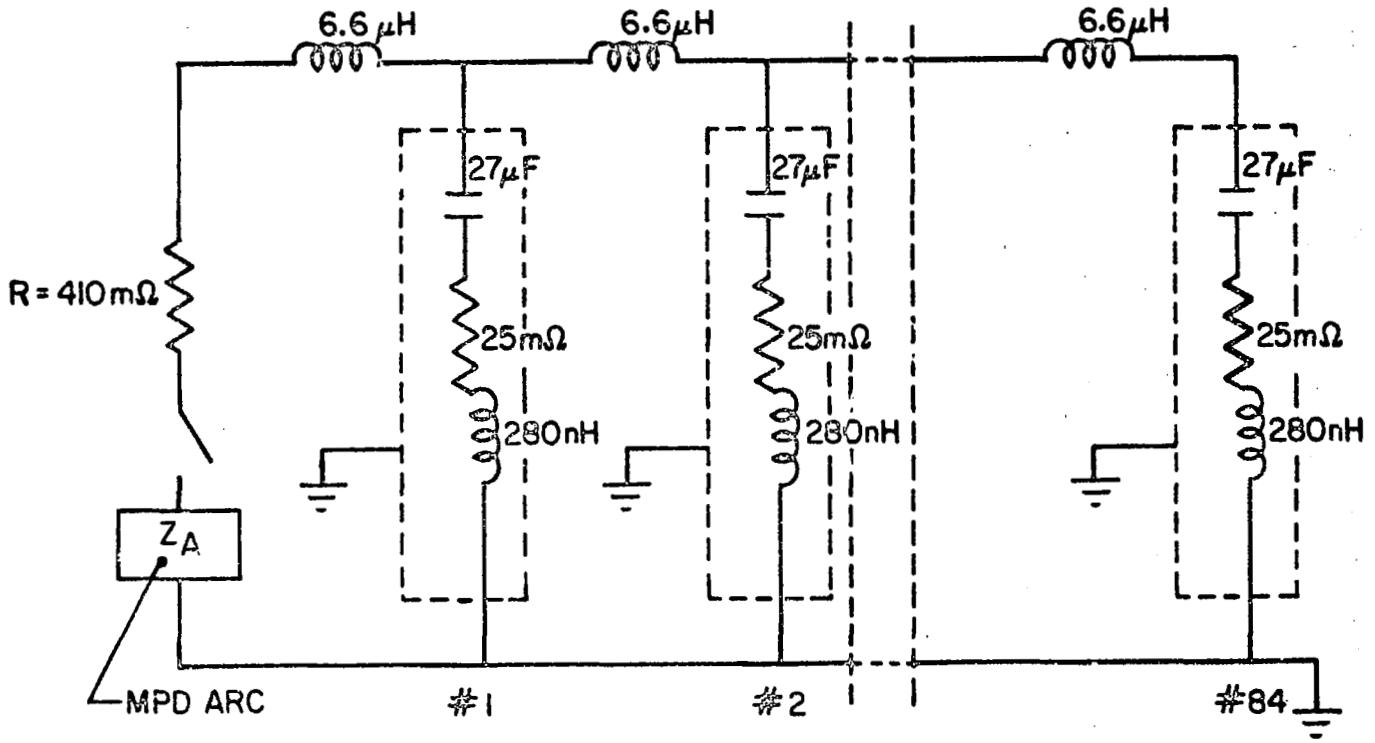

PULSE FORMING NETWORK, SCHEMATIC

FIGURE 38
AP25-5002

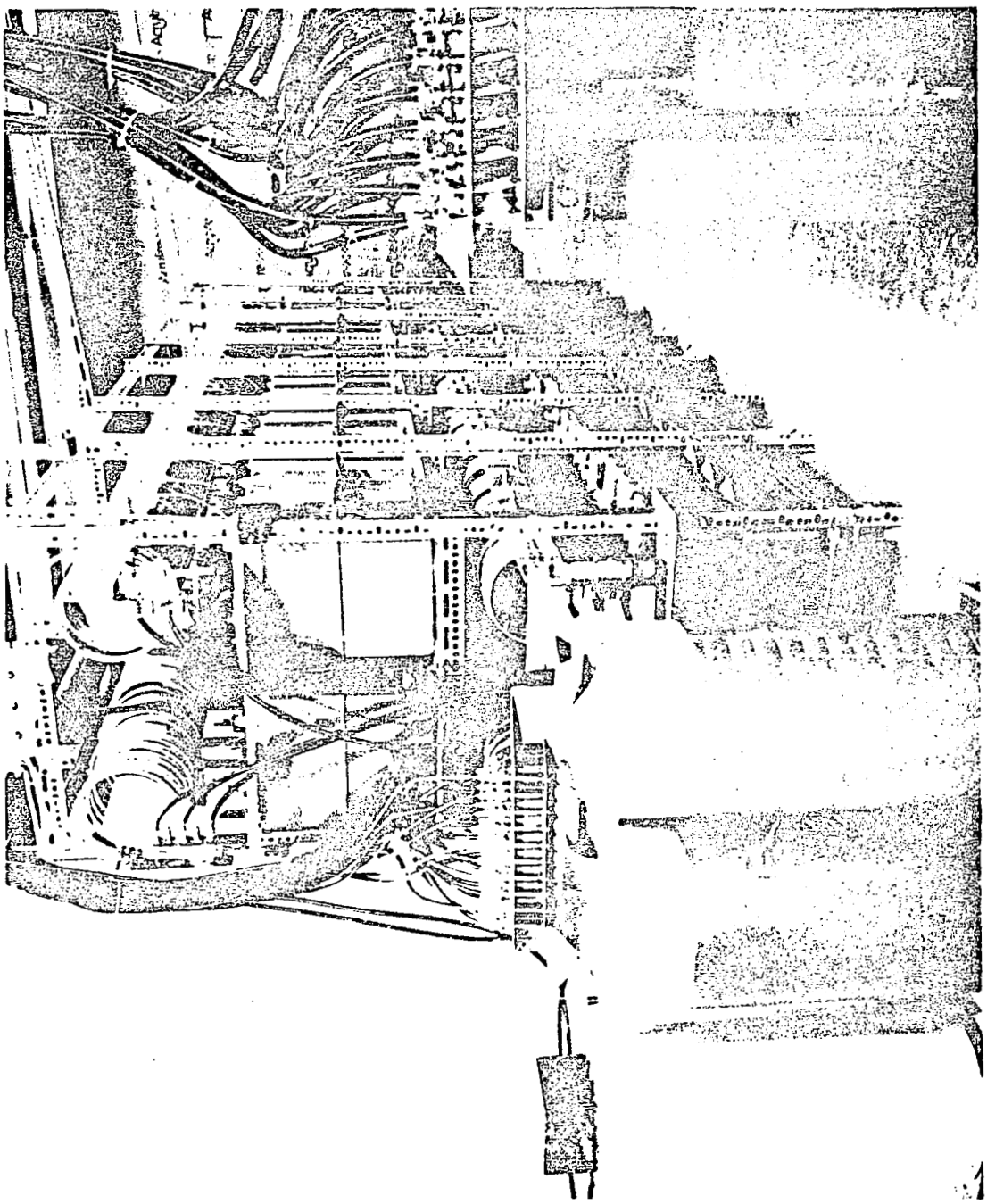

VIEW OF PULSE FORMING NETWORK

FIGURE 39
AP25-P-540

changes the polarity of the electrodes of the MPD apparatus. The resulting change in the distribution of radiance from the discharge completely masks the actual quasi-steady state of the discharge in photography and spectroscopy unless high speed resolution techniques are used.

To prevent a voltage reversal in the network due to the mismatch between the network impedance Z_N and the 10 mΩ accelerator impedance Z_A, a resistor R must be connected in series between the network and the accelerator as shown in Fig. 38. If the value of the resistor $R = Z_N - Z_A$, then the load formed by the accelerator and the resistor is effectively matched to the network and no appreciable voltage reversal occurs when the network is discharged across the load.

The series and parallel configurations of the ladder network use electrolytic load resistors of 410 mΩ and 122 mΩ respectively. These resistors, shown in the lower left of Fig. 39, consist of 2 copper plates 0.08 cm thick, 33 cm x 63 cm, with a separation of 5 cm suspended in a polyethylene tub filled with 56 liters of cupric sulphate electrolyte. Besides their simplicity and low initial cost, these resistors are particularly advantageous for this application due to the very large heat capacity of the liquid. It is estimated that the temperature of the solution rises by less than 0.50 ^{o}C during the 20 kA x 500 μsec pulse.

The discharge chamber, glass vacuum tank and associated electronics are positioned on a table in the middle of a separate room as shown in Fig. 40, thus giving easy access from every direction for spectroscopy and photography. Furthermore, the connection between the gas triggered switch of the discharge apparatus and the wall outlet of the power supply network is made by ten flexible low inductance RG14-A/U coaxial cables, shown in Fig. 40, of sufficient length to allow the entire accelerator

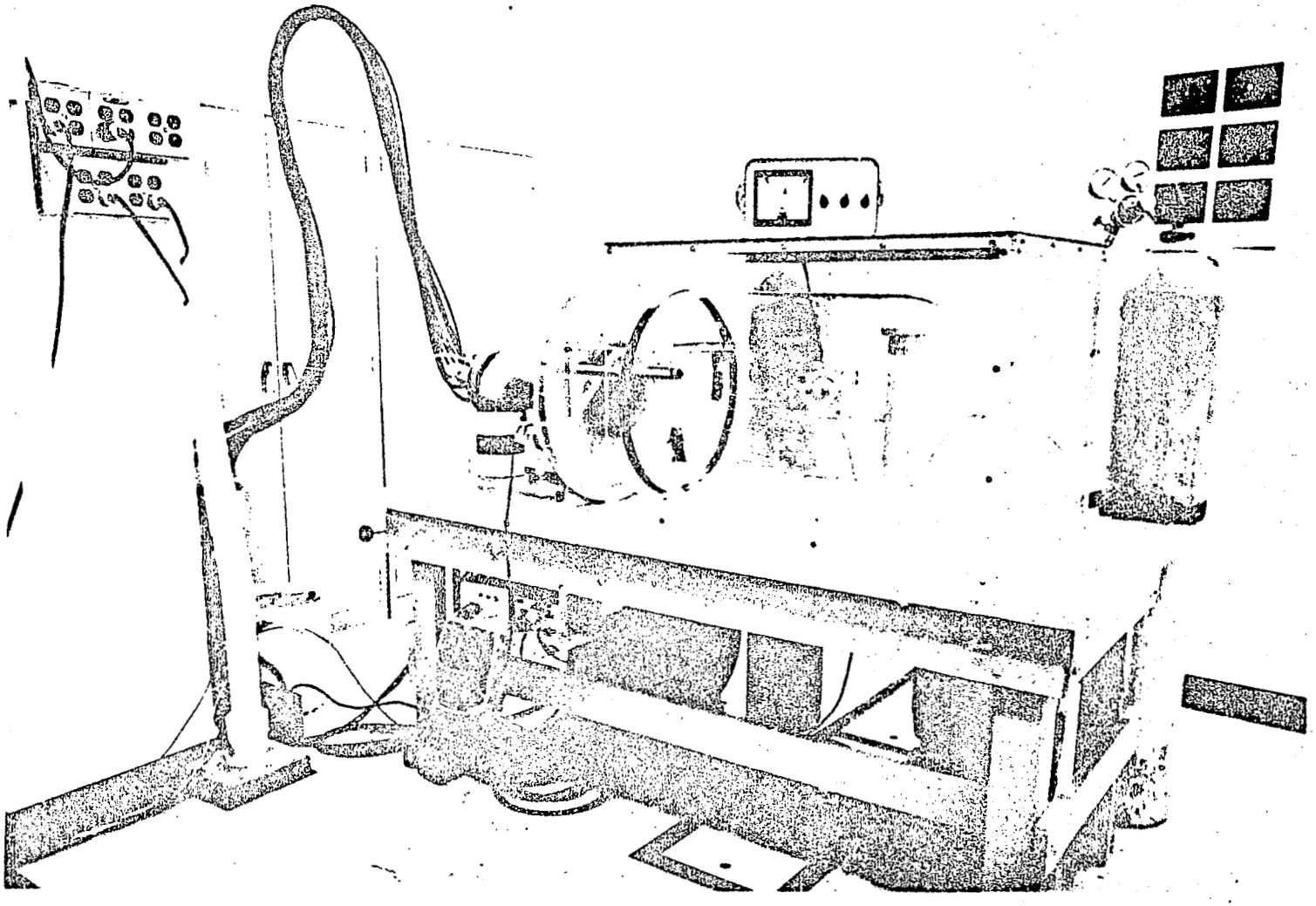

FIGURE 40
AP25-P-541

VIEW OF HOLLOW CATHODE FACILITY

assembly, including the table, to be rotated by up to 90° when needed for diagnostic study of the discharge.

Two typical oscillograms of the current pulse from the new pulse forming network are displayed in Fig. 41. The upper trace, Fig. 41a, shows the 6 kA x 500 μsec pulse when the parallel network is initially charged to 1.7 kV. The droop of the 2.9 kA x 2 msec current pulse from the series network in Fig. 41b is due to the relatively short time constant, ≈ 4 μsec, of the R-C integrator which was used for recording the signal from the Rogowski coil.

Experimental

Previous semi-annual reports contained the results of detailed experimental investigations of eight different insulated hollow cathode configurations designated HC-I to HC-VIII. Before describing recent work with the new hollow cathode configurations, designated HC-IX, X and XI and shown in Fig. 42, it may be worthwhile to recall the important results of the studies of cathodes I to VIII in order to understand the need for further alterations of the cathode geometry. These features are: a) Electron number densities in excess of $10^{17} cm^{-3}$ prevail in the cavity of the hollow cathode; b) A field free region with a weak potential gradient of less than 10 V/cm exists in the same region of the cavity where current densities of typically 1500 A/cm^2 are extracted from the wall; c) The observed correlation of axial electric field E in the insulated channel with area A of the insulated channel

$$E\ (V/cm) = 6.15/A\ (cm^2) \qquad (V\text{-}1)$$

lends credence to the assumption of constant electrical conductivity in the channel of 10^4 mho/m which corresponds to an electron temperature of 3 to 4 electron volts at any substantial ionization level.

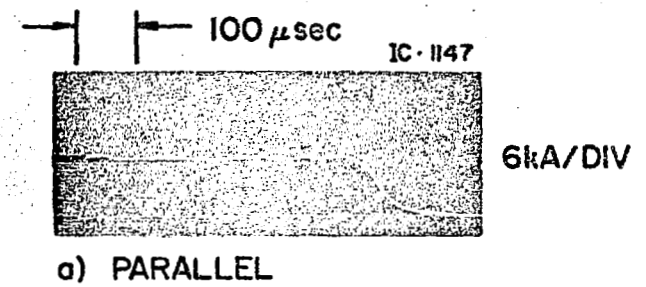

a) PARALLEL

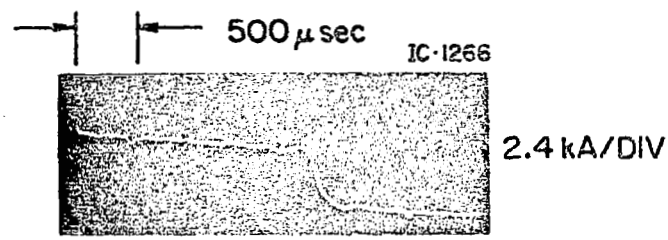

b) SERIES

CURRENT SIGNATURES

FIGURE 41
AP25-P-542

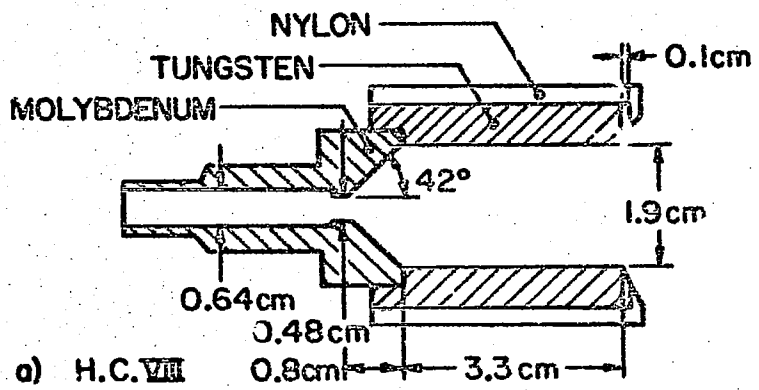

a) H.C. VIII

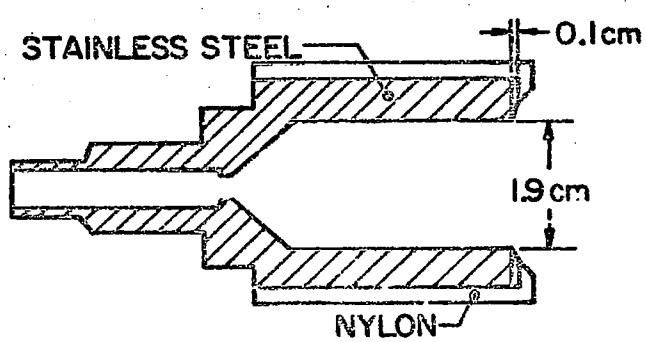

b) H.C. IX

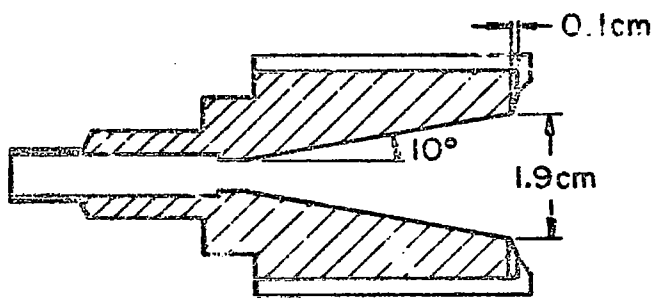

c) H.C. X

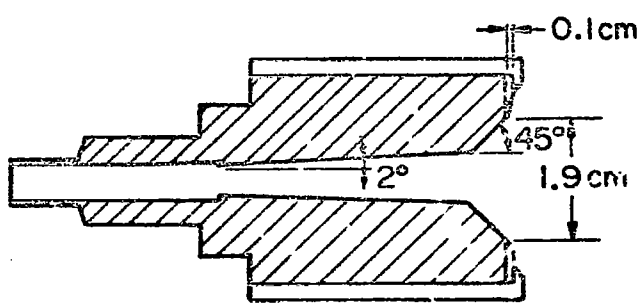

d) H.C. XI

HOLLOW CATHODE CONFIGURATIONS

FIGURE 42
AP25-5083

While these are interesting observations they do not yet establish a complete set of criteria for hollow cathode operation. In an effort to identify the principal characteristics of hollow cathode discharges, a few additional hollow electrode configurations have been constructed and their performance examined in the laboratory.

Effect of Cathode Material. Figures 42a and 42b show the previous tungsten hollow cathode HC-VIII and the new stainless steel cathode HC-IX of identical cavity dimensions. For this latter electrode, the profiles of enclosed current characteristic, were determined. As in previous studies, a current of 7 kA and argon mass flow of 4 g/sec entirely through the cathode cavity were maintained, but now with the extended capacitor bank the duration of the discharge was 0.5 msec instead of 0.2 msec. All experimental studies in this report were undertaken at these discharge conditions.

For the survey of current distribution, the magnetic probe was translated at a radius of 0.8 cm. The measured enclosed current profiles for the tungsten electrode HC-VIII and for the stainless steel electrode HC-IX are compared in Fig. 43. The current was normalized to the 3 kA value measured at the downstream cavity end at $r = 0.8$ cm (0.15 cm from the cathode surface). The relative current distribution inside both cathode cavities is seen to be identical, with more than 90% of the measured current attaching over the last 1 cm of cavity. The data for the steel cathode extend 2 cm downstream, exhibiting a pinch at 0.3 cm followed by a rapid expansion of the current downstream.

Axial potential profiles were determined experimentally with a floating Langmuir probe. The floating potential relative to the anode was subtracted from the terminal voltage signal with an accurately balanced difference amplifier, leaving the

C-2

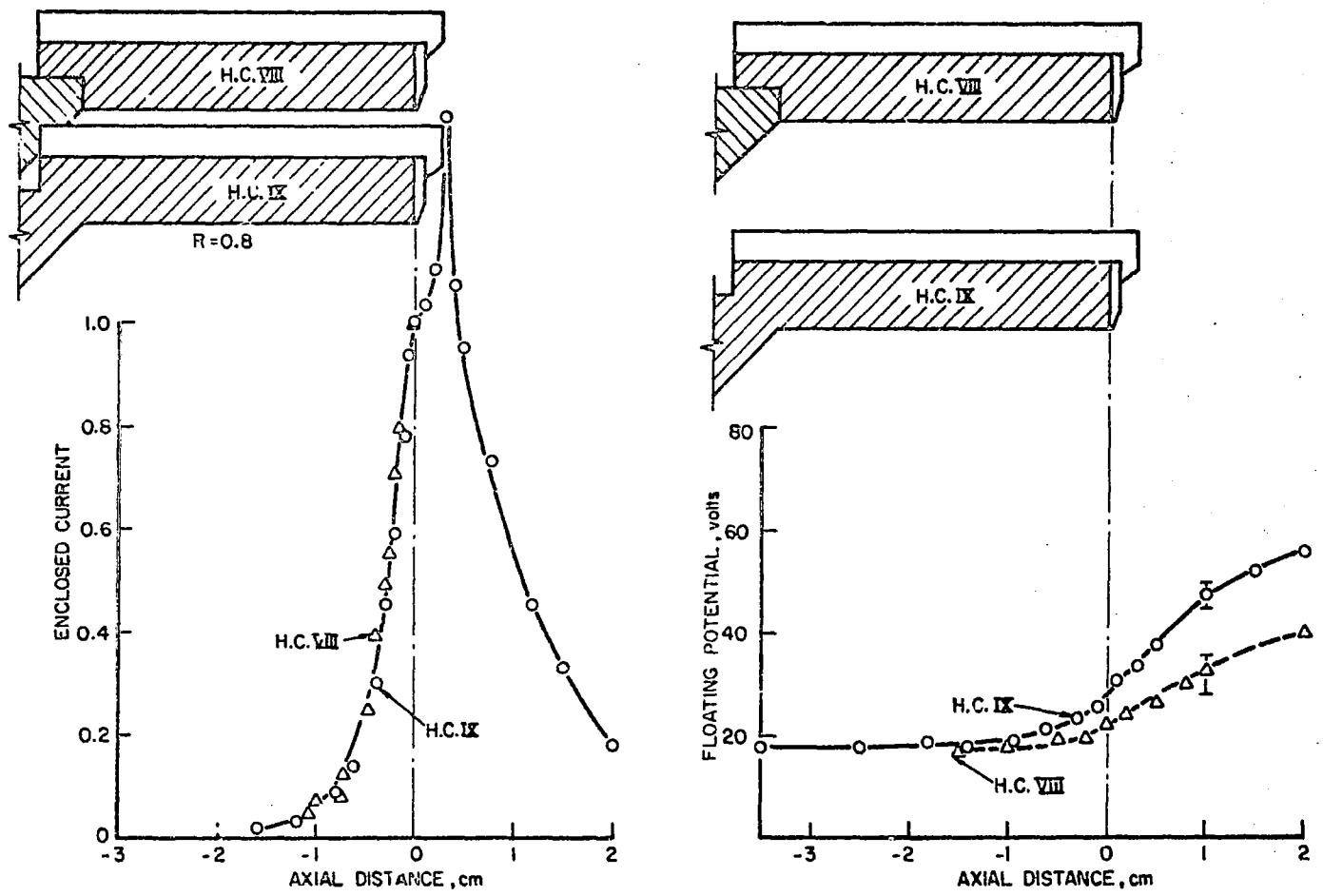

FIGURE 43
AP25-5086

CURRENTS AND POTENTIALS IN H.C. VIII AND H.C. IX

floating potential relative to the cathode. The measured axial potential profiles for the tungsten HC-VIII and the steel HC-IX are compared in Fig. 43. The cavity is essentially field-free up to 1 cm from its end, the region of primary current attachment. Over this last 1 cm of the cavity the tungsten cathode shows a small average field of a few volts/cm, while the steel cathode shows a slightly greater average field of 10 V/cm. The difference in potential increases to approximately 15 volts at an axial location 2 cm downstream of the cathode.

These observations can be summarized in the statement that the change of cathode material from tungsten to steel produces only marginal changes in the measured enclosed current and potential distributions.

In addition to the surveys of current distributions and floating potentials for HC-VIII and HC-IX, their voltage-current characteristics have also been recorded over a discharge current range from 2 to 16 kA. The characteristics are exhibited in Fig. 44 and are seen to coincide within experimental error. At approximately 10 kA both characteristics show a relatively abrupt change in their slopes. The nature of this transition is not being pursued further in these investigations of hollow cathodes at this time; the interested reader is referred to an earlier discussion of such transitions in the slope of the characteristics, which have been observed previously for MPD discharges with solid cathodes.[146,155]

New Hollow Cathode Configurations. In addition to the previously reported results of the studies with the hollow cathode configurations HC-I through HC-VIII, two new configurations designated HC-X and HC-XI, shown in Fig. 42, were manufactured and their operation investigated in the laboratory. The cavity configurations were changed significantly in these

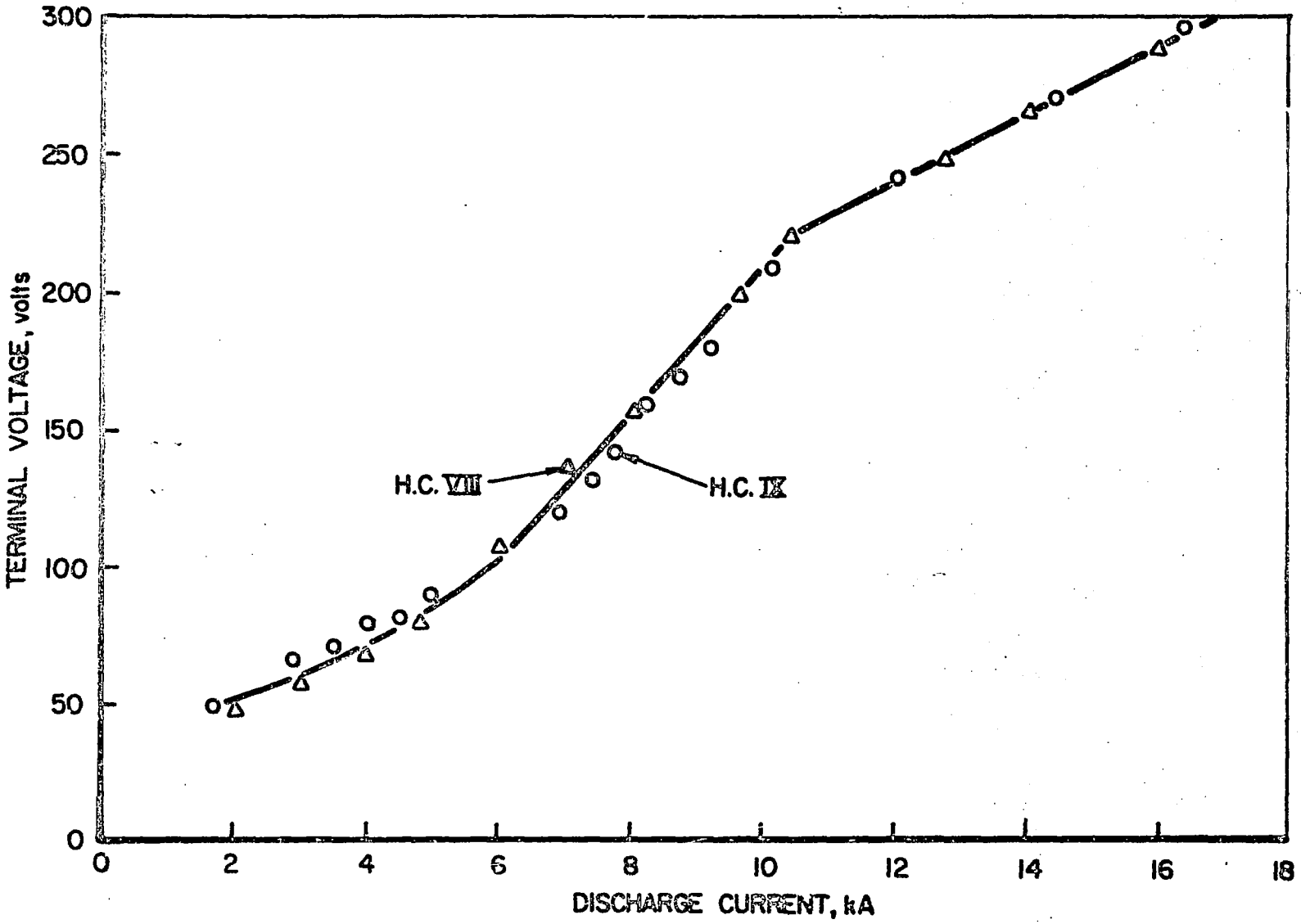

FIGURE 4.4
AP23-9087

CHARACTERISTICS OF H.C. VIII AND H.C. IX

two models in order to observe differences in the characteristic features of current and potential distributions which distinguish typical hollow cathode operation from discharges with solid cathodes.

In both of these cathodes the diameter of the orifice in the face of the cathode and the diameter of the upstream entrance to the cavity, as well as the length of the electrode have been retained as they were in the preceding configurations, HC-VII to HC-IX. However, the previously cylindrical cavity now takes the shape of a right circular cone with a half angle of 10^{o} in HC-X, while the cavity of HC-XI is formed by a shallow conical chamfer of 45^{o} half-angle, fed by the upstream orifice through a relatively narrow, slightly expanding (2^{c}) channel. These two configurations may be considered as steps in the transition from a hollow cathode with a cylindrical cavity to a compact electrode with a flat face. Furthermore, the current distribution in conical cavities of increasing half-angles can be expected to contain decreasing components of radial current density if the attachment at the electrode cavity wall is assumed to remain normal to it. Excluding the thin cathode fall region, this assumption of normal attachment may be justified by the high conductivity of steel and tungsten, 1.3×10^{6} mhos/m and 2×10^{7} mhos/m respectively, which exceeds by at least two orders of magnitude the estimated plasma conductivity in the cavity of 10^{4} mhos/m. Therefore, if the plasma conductivity is scalar, then the current attachment can indeed be assumed normal.

With smaller radial current components a decreased axial component of the Lorentz body force is then available to retard the plasma flow in the cavity. The current and potential profiles for hollow cathodes HC-X and HC-XI are therefore expected to exhibit a redistribution of currents and potentials as a consequence of the decreased retardation of the plasma flow. The magnetic field was surveyed with a small magnetic probe of

≈ 0.3 cm diameter containing 56 turns of #38 wire, and a single Langmuir probe was used to record the floating potential. The results of these experiments are presented and discussed in the following paragraphs.

The magnetic probe survey of cathode HC-X was carried out in steps of 0.1 cm, and in regions of large gradients in 0.05 cm steps, over an axial extent from -0.5 cm to + 1.0 cm and at radial positions from 0.5 cm to 0.95 cm. The floating potential was measured on the cavity centerline. Figure 45 compares enclosed current and floating potential profiles of HC-X with those of HC-IX, reproduced from Fig. 43. The outline of the two electrodes is sketched in the top right of Fig. 45 for reference.

Looking first at the current distribution, the origin of the abscissa is the downstream end of the cavity, where the normalization current of 3 kA was measured. Because of the 0.3-cm probe diameter, the closest possible approach of the probe to the cavity surface was 0.15 cm. The distributions in Fig. 45 were obtained at this local maximum radius. It is seen that the distribution of current attachment in these two electrodes is practically identical within experimental error, i.e. the change of the cylindrical cavity configuration to that of a 10° cone has no recognizable effect on the current distribution.

The enclosed current and floating potential profiles for HC-XI with the 45° chamfered cavity were similarly determined and are shown in Fig. 46, again with the corresponding profiles of HC-IX. It should be noted in this figure that the enclosed current is plotted with the coordinate Y as abscissa. This coordinate Y, which is indicated in the succeeding Fig. 47, is again the line of closest approach of the magnetic probe to the cavity surface (0.15 cm). The current profile of HC-IX is

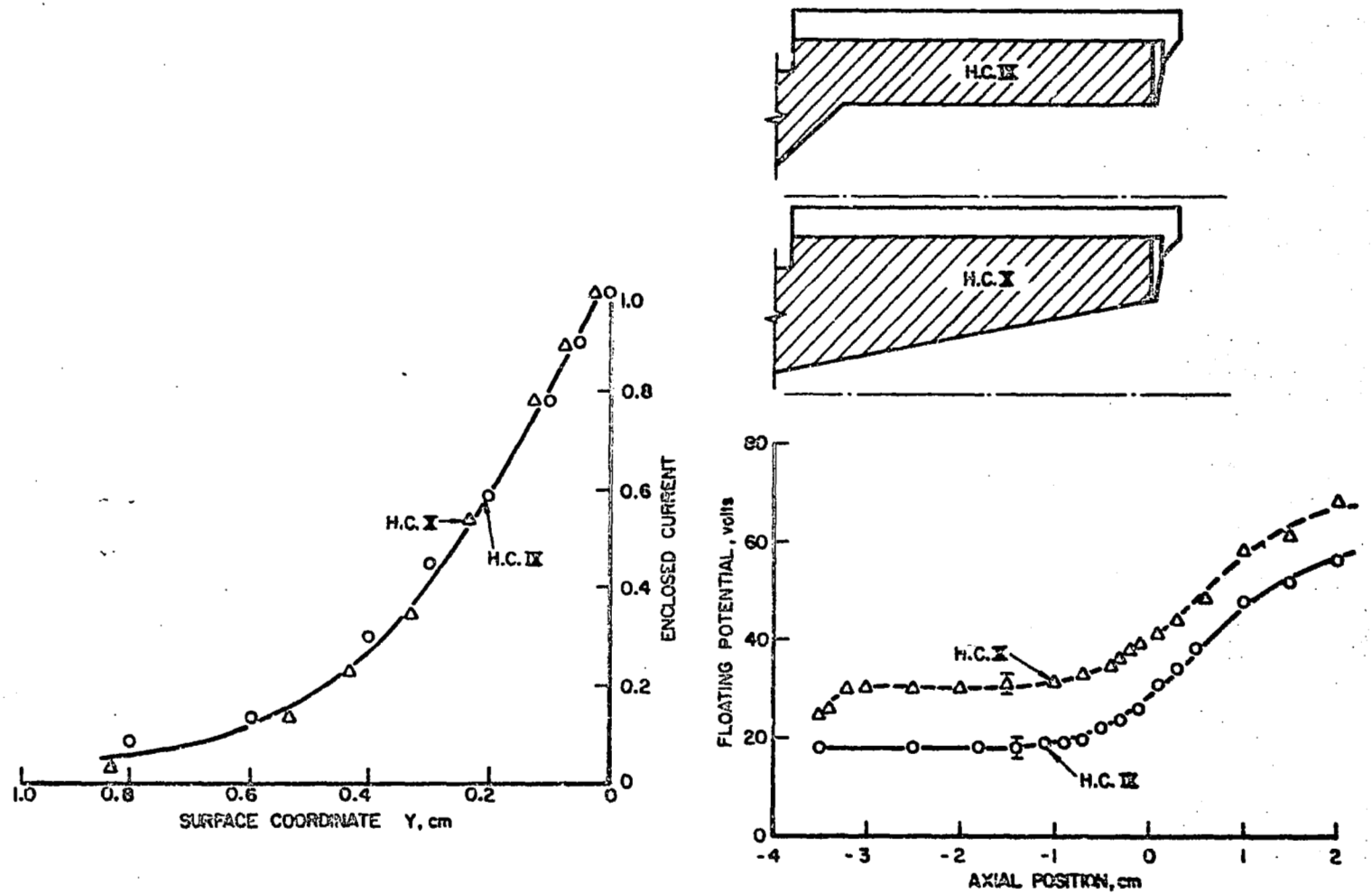

FIGURE 45
AP25-5088

CURRENTS AND POTENTIALS IN H.C. IX AND X

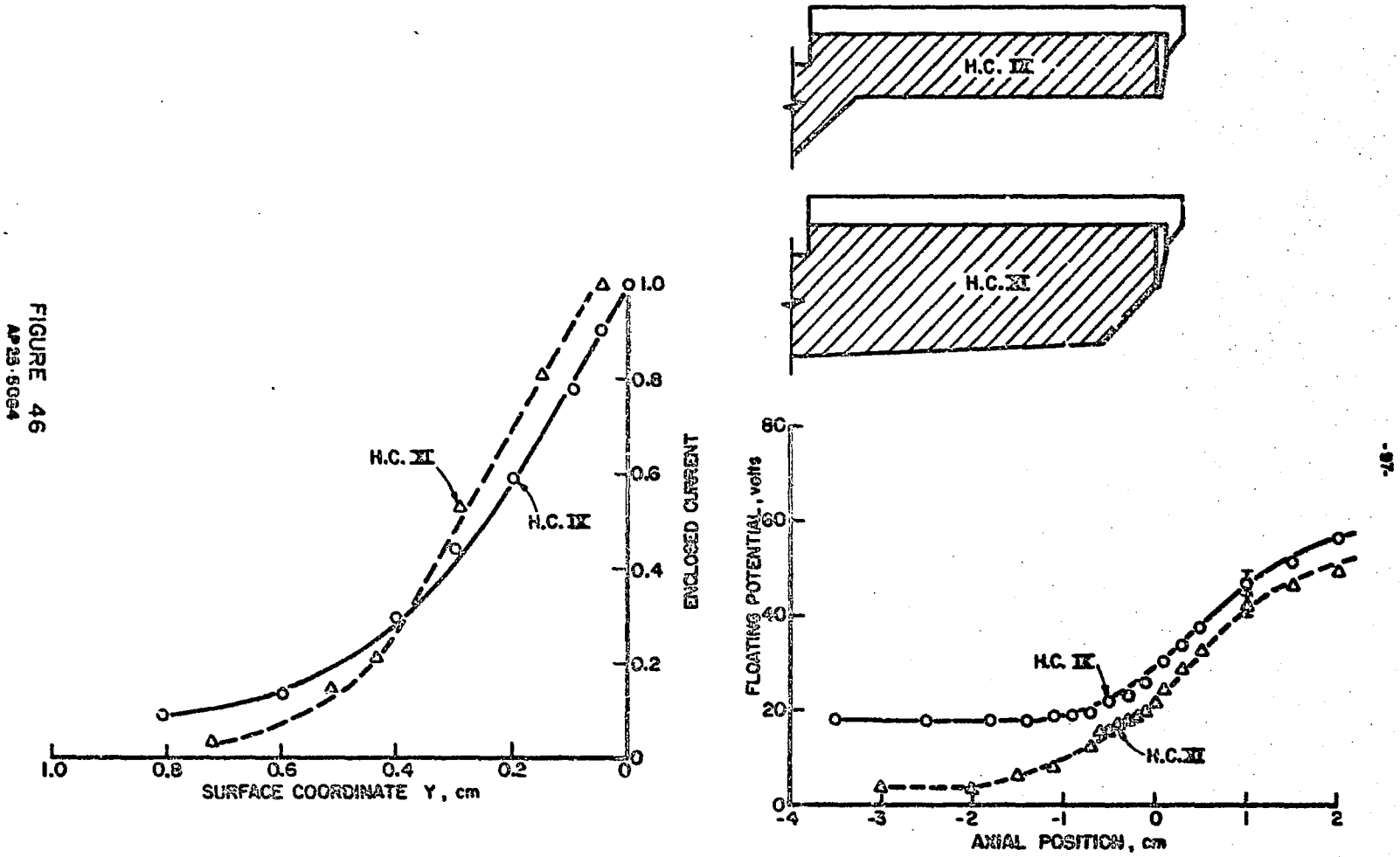

FIGURE 46
AP23-6064

CURRENTS AND POTENTIALS IN HOLLOW CATHODES H.C. IX AND H.C. XI

normalized with 3.0 kA as before while that of HC-XI is normalized with 45 kA, which is the value measured at approximately 0.05 cm from the origin of the coordinate Y.

The enclosed current profile of HC-XI in Fig. 46 is seen to decrease approximately linearly at a slightly more rapid rate than HC-IX and then to start levelling off beyond Y = 0.4 cm.

The linear portion indicates equal enclosed current increments for equal increments of the surface coordinate Y. However, because the conical surface area increments are decreasing as Y increases, the local current density must be increasing. The current density thus reaches a maximum and then drops as the enclosed current profile levels off at low current values. A plot of the entire enclosed current pattern for HC-XI, Fig. 47, shows this maximum current density as a bunching of the enclosed current contours on the 45° probing surface. The enclosed current contour pattern for HC-X, also presented for comparison in Fig. 47, does not show a pronounced maximum because of its small 10° conical angle. The cause and significance of this current density maximum on the face of the conical cathode HC-X are not yet understood.

Referring back to Figs. 45 and 46, the axial floating potential profiles relative to the cathode are presented for HC-X and HC-XI together with the profile for HC-IX. HC-X shows in its long cavity a potential plateau of 30 volts, while HC-XI shows a short potential plateau of a mere 4 volts in the upstream portion of the narrow cavity. More detailed potential measurements are required in order to establish the significance of these features.

Following these tests with other geometries, one cathode has been selected for a more detailed series of diagnostic tests.

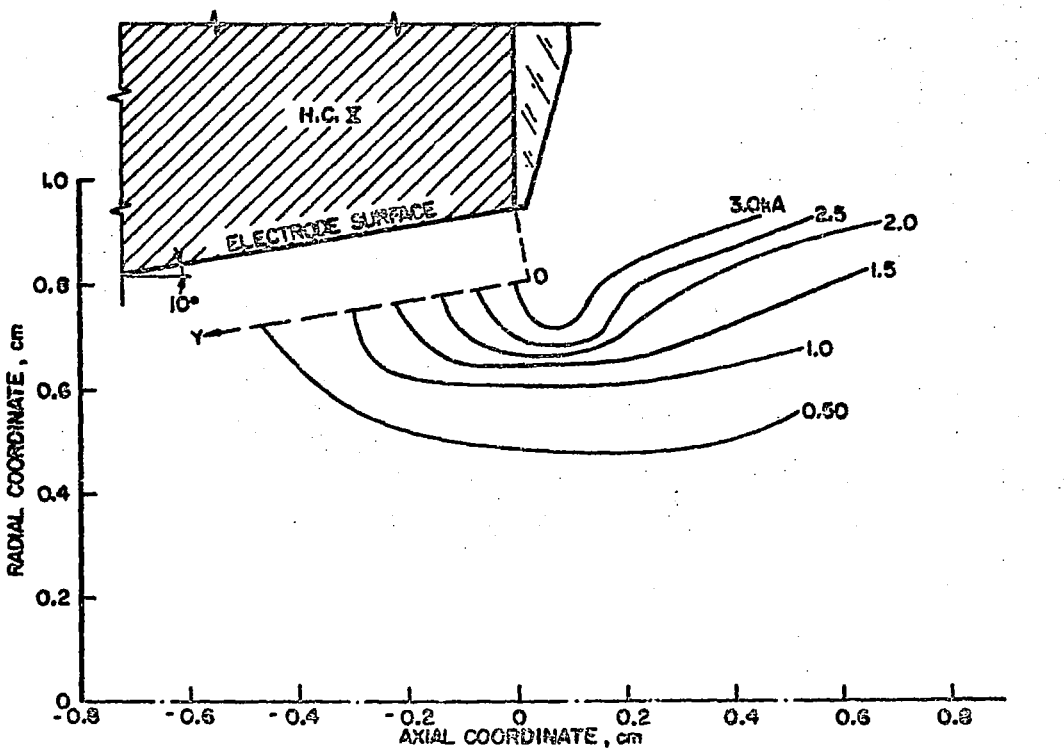

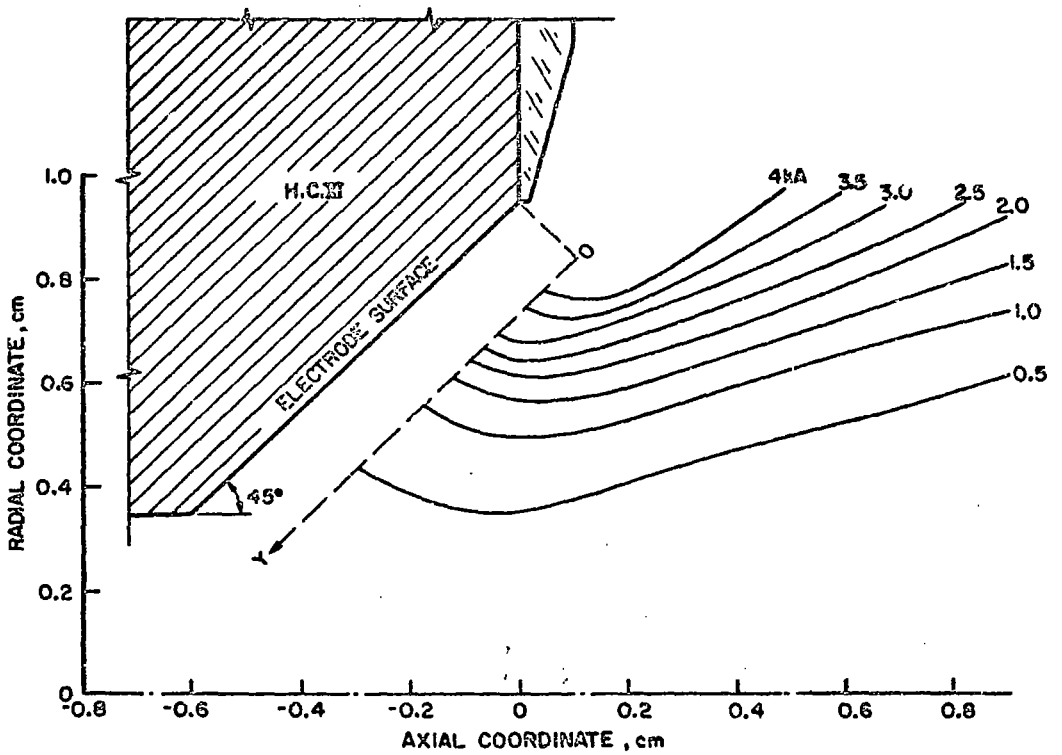

ENCLOSED CURRENT CONTOURS IN H.C. X AND H.C. XI

FIGURE 47

AP25-5083

Because geometry does not appear to be a major factor in altering the key features of the current and potential distributions, the cathode design selected was similar to HC-VIII, i.e., one with a large constant diameter cavity making it most accessible for probing. Detailed current density and potential surveys are now underway over a wide range of operating conditions with a refractory insulator coated version of this cathode.

PROJECT REFERENCES

[1]Jahn, R. G., Bernstein, I. B. and Kunen, A. E., "Proposed Studies of the Formation and Stability of an Electromagnetic Boundary in a Pinch," Proposal for NASA Research Grant NsG-306-63, Mar. 5, 1962, Princeton Univ., Princeton, N. J.

[2]Jahn, R. G. and von Jaskowsky, W. F., "Pulsed Electromagnetic Gas Acceleration," NASA NsG-306-63 progress report for the period 1 July 1962 to 31 December 1962, Aeron. Eng. Rept. No. 634, Jan. 1963, Princeton Univ., Princeton, N. J.

[3]Jahn, R. G. and von Jaskowsky, W. F., "The Plasma Pinch as a Gas Accelerator," A.I.A.A. Preprint 63013, A.I.A.A. Electric Propulsion Conference, Colorado Springs, Colo., 11-13 Mar. 1963.

[4]Jahn, R. G. and von Jaskowsky, W. F., "Pulsed Electromagnetic Gas Acceleration," NASA NsG-306-63 progress report for the period 1 January 1963 to 30 June 1963, Aeron. Eng. Report No. 634a, June 1963, Princeton Univ., Princeton, N. J.

[5]Jahn, R. G. and von Jaskowsky, W. F., "Structure of a Large-radius Pinch Discharge," A.I.A.A. Journal, Vol. 1, No. 8, Aug. 1963, pp. 1809-1814.

[6]Jahn, R. G., von Jaskowsky, W. F. and Casini, A. L., "A Gas-triggered Inverse Pinch Switch," NASA NsG-306-63, Aeron. Eng. Tech. Note No. 660, Aug. 1963, Princeton Univ., Princeton, N. J.

[7]Jahn, R. G., von Jaskowsky, W. F. and Casini, A. L., "Gas triggered Inverse Pinch Switch," The Review of Scientific Instruments, Vol. 34, No. 12, Dec. 1963, pp. 1439-1440.

[8]Jahn, R. G. and von Jaskowsky, W. F., "Pulsed Electromagnetic Gas Acceleration," (Paper delivered at the 4th NASA Intercenter Conference on Plasma Physics, Washington, D. C., 2-4 Dec. 1963), p. 8.

[9]Jahn, R. G. and von Jaskowsky, W. F., "Pulsed Electromagnetic Gas Acceleration," NASA NsG-306-63 progress report for period 1 July 1963 to 31 December 1963, Aeron. Eng. Rept. No. 634b, Dec. 1963, Princeton Univ., Princeton, N. J.

PROJECT REFERENCES

[10]Jahn, R. G. and von Jaskowsky, W. F., "Current Distributions in Large-radius Pinch Discharges," A.I.A.A. Preprint 64-25, A.I.A.A. Aerospace Sciences Meeting, New York, N. Y., 20-22 Jan. 1964.

[11]Jahn, R. G. and von Jaskowsky, W. F., "Current Distributions in Large-radius Pinch Discharges," A.I.A.A. Bulletin, Vol. 1, No. 1, Jan. 1964, p. 12.

[12]Jahn, R. G. and von Jaskowsky, W. F., "Pulsed Electromagnetic Gas Acceleration," NASA NsG-306-63 renewal proposal for 15-months extension, Jan. 15, 1964, Princeton Univ., Princeton, N. J.

[13]Jahn, R. G. and von Jaskowsky, W. F., "Pulsed Electromagnetic Gas Acceleration," NASA NsG-306-63 progress report for the period 1 January 1964 to 30 June 1964, Aeron. Eng. Rept. No. 634c, July 1964, Princeton Univ., Princeton, N. J.

[14]Jahn, R. G., von Jaskowsky, W. F. and Casini, A. L., "Gas-triggered Pinch Discharge Switch," NASA NsG-306-63, Aerospace and Mechanical Sciences Tech. Note No. 101, July 1964, Princeton Univ., Princeton, N. J.

[15]Corr, J. M., "Double Probe Studies in an 8" Pinch Discharge," M.S.E. thesis, Sept. 1964, Princeton Univ., Princeton, N. J.

[16]Jahn, R. G. and von Jaskowsky, W. F., "Exhaust of a Pinched Plasma From an Axial Orifice," A.I.A.A. Bulletin, Vol. 1, No. 10, Oct. 1964, p. 570.

[17]Jahn, R. G. and von Jaskowsky, W. F., "Current Distributions in Large-radius Pinch Discharges," A.I.A.A. Journal, Vol. 2, No. 10, Oct. 1964, pp. 1749-1753.

[18]Jahn, R. G., von Jaskowsky, W. F. and Casini, A. L., "Gas-triggered Pinch Discharge Switch", The Review of Scientific Instruments, Vol. 36, No. 1, Jan. 1964, pp. 101-102.

[19]Jahn, R. G. and von Jaskowsky, W. F., "Exhaust of a Pinched Plasma from an Axial Orifice," A.I.A.A. Paper 65-92, A.I.A.A. 2nd Aerospace Sciences Meeting, New York, N. Y., 25-27 Jan. 1964.

PROJECT REFERENCES

[20]Jahn, R. G. and von Jaskowsky, W. F., "Pulsed Electromagnetic Gas Acceleration," NASA NsG-306-63 progress report for the period 1 July 1964 to 31 December 1964, Aerospace and Mechanical Sciences Rept. No. 634d, Jan. 1965, Princeton Univ., Princeton, N. J.

[21]Wright, E. S., "The Design and Development of Rogowski Coil Probes for Measurement of Current Density Distribution in a Plasma Pinch," M.S.E. thesis, May 1965, Princeton Univ., Princeton, N. J.

[22]Jahn, R. G. and von Jaskowsky, W. F., "Pulsed Electromagnetic Gas Acceleration," NASA NsG-306-63 renewal proposal for 12-months extension, June 7, 1964, Princeton Univ., Princeton, N. J.

[23]Jahn, R. G. and Black, N. A., "On the Dynamic Efficiency of Pulsed Plasma Accelerators," A.I.A.A. Journal, Vol. 3, No. 6, June 1965, pp. 1209-1210.

[24]Black, N. A., "Linear Pinch Driven by a High-current Pulse-forming Network," A.I.A.A. Bulletin, Vol. 2, No. 6, June 1965, p. 309.

[25]Wright, E. S. and Jahn, R. G., "The Design and Development of Rogowski Coil Probes for Measurement of Current Density Distribution in a Plasma Pinch," NASA NsG-306-63, Aerospace and Mechanical Sciences Rept. No. 740, June 1965, Princeton Univ., Princeton, N. J.

[26]Rowell, G. A., "Cylindrical Shock Model of the Plasma Pinch," M.S.E. thesis, July 1965, Princeton Univ., Princeton, N. J.

[27]Black, N. A., "Linear Pinch Driven by a High-current Pulse-forming Network," A.I.A.A. Paper 65-336, A.I.A.A. 2nd Annual Meeting, San Francisco, Calif., 26-29 July 1965.

[28]Jahn, R. G. and von Jaskowsky, W. F., "Pulsed Electromagnetic Gas Acceleration," NASA NsG-306-63 progress report for the period 1 January 1965 to 30 June 1965, Aerospace and Mechanical Sciences Rept. No. 634e, July, 1965, Princeton Univ., Princeton, N. J.

[29]Jahn, R. G. and Ducati, A. C., "Design and Development of a Thermo-Ionic Electric Thrustor," 5QS 085-968 Interim Report, NASA Contract NASw-968, Aug. 1965, Giannini Scientific Corp., Santa Ana, Calif.

PROJECT REFERENCES

[30]Jahn, R. G., von Jaskowsky, W. F. and Burton, R. L., "Ejection of a Pinched Plasma From an Axial Orifice," A.I.A.A. Journal, Vol. 3, No. 10, Oct. 1965, pp. 1862-1866.

[31]Jahn, R. G. and Wright, E. S., "Miniature Rogowski Coil Probes for Direct Measurement of Current Density Distribution in Transient Plasmas," The Review of Scientific Instruments, Vol. 36, No. 12, Dec. 1965, pp. 1891-1892.

[32]Jahn, R. G. and von Jaskowsky, W. F., "Pulsed Electromagnetic Gas Acceleration," NASA NsG-306-63 progress report for the period 1 July 1965 to 31 December 1965, Aerospace and Mechanical Sciences Rept. No. 634f, Jan. 1966, Princeton Univ., Princeton, N. J.

[33]Burton, R. L. and Jahn, R. G., "Electric and Magnetic Field Distributions in a Propagating Current Sheet," A.I.A.A. Bulletin, Vol. 3, No. 1, Jan. 1966, p. 35.

[34]Rowell, G. A., Jahn, R. G. and von Jaskowsky, W. F., "Cylindrical Shock Model of the Plasma Pinch," NASA NsG-306-63, Aerospace and Mechanical Sciences Rept. No. 742, Feb. 1966, Princeton Univ., Princeton, N. J.

[35]Burton, R. L. and Jahn, R. G., "Electric and Magnetic Field Distributions in a Propagating Current Sheet," A.I.A.A. Paper 66-200, A.I.A.A. 5th Electric Propulsion Conference, San Diego, Calif., 7-9 Mar. 1966.

[36]Black, N. A., "Pulse-forming Networks for Propulsion Research," Proceedings of the 7th Symposium on Engineering Aspects of Magnetohydrodynamics, Princeton Univ., Princeton, N. J., Mar. 30-April 1, 1966, pp. 10-11.

[37]Jahn, R. G., "Electromagnetic Propulsion," Astronautics and Aeronautics, Vol. 4, No. 2, February, 1966, pp. 73-75.

[38]Black, N. A., "Dynamics of a Pinch Discharge Driven by a High-current Pulse-forming Network," Ph.D. thesis, May 1966, Princeton Univ., Princeton, N. J.

[39]Black, N. A. and Jahn, R. G., "Dynamics of a Pinch Discharge Driven by a High-current Pulse-forming Network," NASA NsG-306-63, Aerospace and Mechanical Sciences Rept. No. 778, May 1966, Princeton Univ., Princeton, N. J.

PROJECT REFERENCES

[40]Jahn, R. G., "Pulsed Plasma Propulsion," Proceedings of the 5th NASA Intercenter and Contractors Conference on Plasma Physics, Washington, D. C., 24-26 May 1966, pt. V, pp. 75-81.

[41]Jahn, R. G. and von Jaskowsky, W. F., "Pulsed Electromagnetic Gas Acceleration," NASA NsG-306-63 renewal proposal for 24-months extension, May 25, 1966, Princeton Univ., Princeton, N. J.

[42]Ducati, A. C., Jahn, R. G., Muehlberger, E. and Treat, R. P., "Design and Development of a Thermo-Ionic Electric Thrustor," FR-056-968 Final Report, NASA CR-54703, May 1966, Giannini Scientific Corp., Santa Ana, Calif.

[43]Jahn, R. G. and Clark, K. E., "A Large Dielectric Vacuum Facility," A.I.A.A. Journal, Vol. 4, No. 6, June 1966, p. 1135.

[44]John, R. R., Bennett, S. and Jahn, R. G., "Current Status of a Plasma Propulsion," A.I.A.A. Bulletin, Vol. 3, No. 5, May 1966, p. 264.

[45]John, R. R., Bennett, S. and Jahn, R. G., "Current Status of a Plasma Propulsion," A.I.A.A. Paper 66-565, A.I.A.A. 2nd Propulsion Joint Specialist Conference, Colorado Springs, Colo., 13-17 June 1966.

[46]Jahn, R. G. and von Jaskowsky, W. F., "Pulsed Electromagnetic Gas Acceleration," NASA NsG-306-63 progress report for the period 1 January 1966 to 30 June 1966, Aerospace and Mechanical Sciences Rept. No. 634g, July 1966, Princeton Univ., Princeton, N. J.

[47]Burton, R. L., "Structure of the Current Sheet in a Pinch Discharge," Ph.D. thesis, Sept. 1966, Princeton Univ., Princeton, N. J.

[48]Burton, R. L. and Jahn, R. G., "Structure of the Current Sheet in a Pinch Discharge," NASA NsG-306-63, Aerospace and Mechanical Sciences Rept. No. 783, Sept. 1966, Princeton Univ., Princeton, N. J.

[49]Jahn, R. G. and von Jaskowsky, W. F., "Pulsed Electromagnetic Gas Acceleration," NASA NsG-306-63 progress report for the period 1 July 1966 to 31 December 1966, Aerospace and Mechanical Sciences Rept. No. 634h, Jan. 1967, Princeton Univ., Princeton, N. J.

PROJECT REFERENCES

[50]Burton, R. L. and Jahn, R. G., "Structure of the Current Sheet in a Pinch Discharge," Bulletin of the American Physical Society, Vol. 12, Ser. II, Paper L1, May 1967, p. 848.

[51]Jahn, R. G., "Plasma Propulsion for Deep Space Flight," Bulletin of the American Physical Society, Vol. 12, Ser. II, Paper BC-1, May 1967, p. 646.

[52]Ellis, W. R., Jr., "An Investigation of Current Sheet Structure in a Cylindrical Z-Pinch," Ph.D. thesis, July 1967, Princeton Univ., Princeton, N. J.

[53]Ellis, W. R., Jr. and Jahn, R. G., "An Investigation of Current Sheet Structure in a Cylindrical Z-Pinch," NASA NsG-306-63, Aerospace and Mechanical Sciences Rept. No. 805, July 1967, Princeton Univ., Princeton, N. J.

[54]Jahn, R. G. and von Jaskowsky, W. F., "Pulsed Electromagnetic Gas Acceleration," NASA NsG-306-63 progress report for the period 1 January 1967 to 30 June 1967, Aerospace and Mechanical Sciences Rept. No. 634i, July 1967, Princeton Univ., Princeton, N. J.

[55]Clark, K. E. and Jahn, R. G., "The Magnetoplasmadynamic Arc," Astronautica Acta, Vol. 13, No. 4, 1967, pp. 315-325.

[56]Jahn, R. G., "The MPD Arc," NASA Contract NASw-1513, Aug. 1967, Giannini Scientific Corp., Santa Ana, Calif.

[57]Eckbreth, A. C., Clark, K. E. and Jahn, R. G., "Current Pattern Stabilization in Pulsed Plasma Accelerators," A.I.A.A. Bulletin, Vol. 4, No. 9, Sept. 1967, p. 433.

[58]Clark, K. E., Eckbreth, A. C. and Jahn, R. G., "Current Pattern Stabilization in Pulsed Plasma Accelerators," A.I.A.A. Paper 67-656, A.I.A.A. Electric Propulsion and Plasmadynamics Conference, Colorado Springs, Colo., 11-13 Sept. 1967.

[59]Jahn, R. G. and von Jaskowsky, W. F., "Pulsed Electromagnetic Gas Acceleration," NASA NsG-306-63 progress report for the period 1 July 1967 to 31 December 1967, Aerospace and Mechanical Sciences Rept. No. 634j, Jan. 1968, Princeton Univ., Princeton, N. J.

PROJECT REFERENCES

[60]Ducati, A. C., Jahn, R. G., Muehlberger, E. and Treat, R. P., "Exploratory Electromagnetic Thruster Research," TR 117-1513 Annual Report, NASA CR 62047, Feb. 1968, Giannini Scientific Corp., Santa Ana, Calif.

[61]Jahn, R. G., PHYSICS OF ELECTRIC PROPULSION, McGraw-Hill Book Company, New York, 1968.

[62]Burton, R. L. and Jahn, R. G., "Acceleration of Plasma by a Propagating Current Sheet," The Physics of Fluids, Vol. 11, No. 6, June 1968, pp. 1231-1237.

[63]Jahn, R. G. and von Jaskowsky, W. F., "Pulsed Electromagnetic Gas Acceleration," NASA NGR 31-001-005 step-funding renewal proposal for the period 1 October 1968 to 30 September 1971, June 1, 1968, Princeton Univ., Princeton, N. J.

[64]Jahn, R. G. and von Jaskowsky, W. F., "Pulsed Electromagnetic Gas Acceleration," NASA NsG-306/31-001-005 progress report for the period 1 January 1968 to 30 June 1968, Aerospace and Mechanical Sciences Rept. No. 634k, July 1968, Princeton Univ., Princeton, N. J.

[65]Wilbur, P. J., "Energy Transfer from a Pulse Network to a Propagating Current Sheet," Ph.D. thesis, Sept. 1968, Princeton Univ., Princeton, N. J.

[66]Wilbur, P. J. and Jahn, R. G., "Energy Transfer from a Pulse Network to a Propagating Current Sheet," NASA NGR 31-001-005, Aerospace and Mechanical Sciences Rept. No. 846, Sept. 1968, Princeton Univ., Princeton, N. J.

[67]Ducati, A. C., Jahn, R. G., Muehlberger, E. and Treat, R. P., "Exploratory Electromagnetic Thruster Research, Phase II," 2SS108-1513 Interim Report, NASA Contract NASw-1513, Oct. 1968, Giannini Scientific Corp., Santa Ana, Calif.

[68]Eckbreth, A. C., Clark, K. E. and Jahn, R. G., "Current Pattern Stabilization in Pulsed Plasma Accelerators," A.I.A.A. Journal, Vol. 6, No. 11, Nov. 1968, pp. 2125-2132.

PROJECT REFERENCES

[69]Eckbreth, A. C., "Current Pattern and Gas Flow Stabilization in Pulsed Plasma Accelerators," Ph.D. thesis, Dec. 1968, Princeton Univ., Princeton, N. J.

[70]Eckbreth, A. C. and Jahn, R. G., "Current Pattern and Gas Flow Stabilization in Pulsed Plasma Accelerators," NASA NGL 31-001-005, Aerospace and Mechanical Sciences Rept. No. 857, Dec. 1968, Princeton Univ., Princeton, N. J.

[71]York, T. M., "Pressure Distribution in the Structure of a Propagating Current Sheet," Ph.D. thesis, Dec. 1968, Princeton Univ., Princeton, N. J.

[72]York, T. M. and Jahn, R. G., "Pressure Distribution in the Structure of a Propagating Current Sheet," NASA NGL 31-001-005, Aerospace and Mechanical Sciences Rept. No. 853, Dec. 1968, Princeton Univ., Princeton, N. J.

[73]Eckbreth, A. C. and Jahn, R. G., "Current Pattern and Gas Flow Stabilization in Pulsed Plasma Accelerators," A.I.A.A. Bulletin, Vol. 5, No. 12, Dec. 1968, p. 730.

[74]Wilbur, P. J. and Jahn, R. G., "Energy Transfer From a Pulse Network to a Propagating Current Sheet," A.I.A.A. Bulletin, Vol. 5, No. 12, Dec. 1968, p. 730.

[75]Ellis, W. R. and Jahn, R. G., "Ion Density and Current Distributions in a Propagating Current Sheet, Determined by Microwave Reflection Technique," Rept. No. CLM-P-187, Dec. 1968, Culham Laboratory, Abingdon, Berkshire, Great Britain.

[76]Jahn, R. G. and von Jaskowsky, W. F., "Pulsed Electromagnetic Gas Acceleration," NASA NGL 31-001-005 progress report for the period 1 July 1968 to 31 December 1968, Aerospace and Mechanical Sciences Rept. No. 634, Jan. 1969, Princeton Univ., Princeton, N. J.

[77]Eckbreth, A. C. and Jahn, R. G., "Current Pattern and Gas Flow Stabilization in Pulsed Plasma Accelerators," A.I.A.A. Paper 69-112, A.I.A.A. 7th Aerospace Sciences Meeting, New York, N. Y., 20-22 Jan. 1969.

PROJECT REFERENCES

[78]Wilbur, P. J. and Jahn, R. G., "Energy Transfer From a Pulse Network to a Propagating Current Sheet," A.I.A.A. Paper 69-113, A.I.A.A. 7th Aerospace Sciences Meeting, New York, N. Y., 20-22 Jan. 1969.

[79]Ellis, W. R. and Jahn, R. G., "Ion Density and Current Distributions in a Propagating Current Sheet, Determined by Microwave Reflection Technique," Journal of Plasma Physics, Vol. 3, Pt. 2, 1969, pp. 189-213.

[80]York, T. M. and Jahn, R. G., "Pressure Distribution in the Structure of a Propagating Current Sheet," A.I.A.A. Bulletin, Vol. 6, No. 2, Feb. 1969, p. 75.

[81]Clark, K. E. and Jahn, R. G., "Quasi-steady Plasma Acceleration," A.I.A.A. Bulletin, Vol. 6, No. 2, Feb. 1969, p. 75.

[82]York, T. M. and Jahn, R. G., "Pressure Distribution in the Structure of a Propagating Current Sheet," A.I.A.A. Paper 69-264, A.I.A.A. 7th Electric Propulsion Conference, Williamsburg, Va., 3-5 Mar. 1969.

[83]Clark, K. E. and Jahn, R. G., "Quasi-steady Plasma Acceleration," A.I.A.A. Paper 69-267, A.I.A.A. 7th Electric Propulsion Conference, Williamsburg, Va., 3-5 Mar. 1969.

[84]Jahn, R. G. and Mickelsen, W. R., "Electric Propulsion Notebook," A.I.A.A. Professional Study Series, Williamsburg, Va., 1-2 Mar. 1969.

[85]Boyle, M. J., "Plasma Velocity Measurements with Electric Probes," B.S.E. thesis, April 1969, Princeton Univ., Princeton, N. J.

[86]Clark, K. E., "Quasi-steady Plasma Acceleration," Ph.D. thesis, May 1969, Princeton Univ., Princeton, N. J.

[87]Clark, K. E. and Jahn, R. G., "Quasi-steady Plasma Acceleration," NASA NGL 31-001-005, Aerospace and Mechanical Sciences Rept. No. 859, May 1969, Princeton Univ., Princeton, N. J.

PROJECT REFERENCES

[88]Boyle, M. J., "Plasma Velocity Measurements with Electric Probes," Paper No. 4 (Paper presented at the Northeastern Regional Student Conference, Princeton Univ., Princeton, N. J., 9-10 May 1969).

[89]Mickelsen, W. R. and Jahn, R. G., "Status of Electric Propulsion," A.I.A.A. Bulletin, Vol. 6, No. 6, June 1969, p. 257.

[90]Mickelsen, W. R. and Jahn, R. G., "Status of Electric Propulsion," A.I.A.A. Paper 69-497, A.I.A.A. 5th Propulsion Joint Specialist Conference, U. S. Air Force Academy, Colo., 9-13 June 1969.

[91]Ducati, A. C. and Jahn, R. G., "Electron Beam from a Magnetoplasmadynamic Arc," The Physics of Fluids, Vol. 12, No. 6, June 1969, pp. 1177-1181.

[92]Jahn, R. G. and von Jaskowsky, W. F., "Pulsed Electromagnetic Gas Acceleration," NASA NGL 31-001-005 progress report for the period 1 January 1969 to 30 June 1969, Aerospace and Mechanical Sciences Rept. No. 634m, July 1969, Princeton Univ., Princeton, N. J.

[93]Jahn, R. G. and von Jaskowsky, W. F., "Pulsed Electromagnetic Gas Acceleration," NASA NGR 31-001-005 step-funding renewal proposal for the period 1 October 1969 to 30 September 1970, July 1, 1969, Princeton Univ., Princeton, N. J.

[94]Jahn, R. G., Clark, K. E., Oberth, R. C. and Turchi, P. J., "Acceleration Patterns in Quasi-steady MPD Arcs," A.I.A.A. Bulletin, Vol. 6, No. 12, Dec. 1969, p. 701.

[95]Ducati, A. C. and Jahn, R. G., "Repetitively Pulsed, Quasi-steady Vacuum MPD Arc," A.I.A.A. Bulletin, Vol. 6, No. 12, Dec. 1969, p. 701.

[96]Jahn, R. G., von Jaskowsky, W. F. and Clark, K. E., "Pulsed Electromagnetic Gas Acceleration: Acceleration Processes in Quasi-steady Arcs," (Paper delivered at the 6th NASA Intercenter and Contractors Conference on Plasma Physics, NASA Langley Research Center, Hampton, Va., 8-10 Dec. 1969), pp. 8-15.

PROJECT REFERENCES

[97] Jahn, R. G., von Jaskowsky, W. F. and Clark, K. E., "Pulsed Electromagnetic Gas Acceleration," NASA NGL 31-001-005 progress report for the period 1 July 1969 to 31 December 1969, Aerospace and Mechanical Sciences Rept. No. 634n, Jan. 1970, Princeton Univ., Princeton, N. J.

[98] Eckbreth, A. C. and Jahn, R. G., "Current Pattern and Gas Flow Stabilization in Pulsed Plasma Accelerators," A.I.A.A. Journal, Vol. 8, No. 1, Jan. 1970, pp. 138-143.

[99] Jahn, R. G., Clark, K. E., Oberth, R. C. and Turchi, P. J., "Acceleration Patterns in Quasi-steady MPD Arcs," A.I.A.A. Paper 70-165, A.I.A.A. 8th Aerospace Sciences Meeting, New York, N. Y., 19-21 Jan. 1970.

[100] Ducati, A. C. and Jahn, R. G., "Repetitively Pulsed, Quasi-steady Vacuum MPD Arc," A.I.A.A. Paper 70-167, A.I.A.A. 8th Aerospace Sciences Meeting, New York, N. Y., 19-21 Jan. 1970.

[101] Wilbur, P. J. and Jahn, R. G., "Energy Transfer from a Pulse Network to a Propagating Current Sheet," A.I.A.A. Journal, Vol. 8, No. 1, Jan. 1970, pp. 144-149.

[102] Clark, K. E. and Jahn, R. G., "Quasi-steady Plasma Acceleration," A.I.A.A. Journal, Vol. 8, No. 2, Feb. 1970, pp. 216-220.

[103] York, T. M. and Jahn, R. G., "Pressure Distribution in the Structure of a Propagating Current Sheet," The Physics of Fluids, Vol. 13, No. 5, May 1970, pp. 1303-1309.

[104] Jahn, R. G., "Pulsed Electromagnetic Gas Acceleration," NASA NGL 31-001-005 step-funding renewal proposal for period 1 October 1970 to 30 September 1971, June 11, 1970, Princeton Univ., Princeton, N. J.

[105] Jahn, R. G., von Jaskowsky and Clark, K. E., "Pulsed Electromagnetic Gas Acceleration," NASA NGL 31-001-005, progress report for the period 1 January 1970 to 30 June 1970, Aerospace and Mechanical Sciences Rept. No. 634o, July 1970, Princeton Univ., Princeton, N. J.

PROJECT REFERENCES

[106] Turchi, P. J. and Jahn, R. G., "The Cathode Region of a Quasi-steady MPD Arcjet," A.I.A.A. Bulletin, Vol. 7, No. 9, Sept. 1970, p. 449.

[107] Clark, K. E., DiCapua, M. S., Jahn, R. G. and von Jaskowsky, W. F., "Quasi-steady Magnetoplasmadynamic Arc Characteristics," A.I.A.A. Bulletin, Vol. 7, No. 9, Sept. 1970, p. 449.

[108] Turchi, P. J. and Jahn, R. G., "The Cathode Region of a Quasi-steady MPD Arcjet," A.I.A.A. Paper 70-1094, A.I.A.A. 8th Electric Propulsion Conference, Stanford, Calif., 31 Aug.-2 Sept. 1970.

[109] Clark, K. E., DiCapua, M. S., Jahn, R. G. and von Jaskowsky, W. F., "Quasi-steady Magnetoplasmadynamic Arc Characteristics," A.I.A.A Paper 70-1095, A.I.A.A. 8th Electric Propulsion Conference, Stanford, Calif., 31 Aug.-2 Sept. 1970.

[110] Turchi, P. J., "The Cathode Region of a Quasi-steady Magnetoplasmadynamic Arcjet," Ph.D. thesis, Sept. 1970, Princeton Univ., Princeton, N. J.

[111] Turchi, P. J. and Jahn, R. G., "The Cathode Region of a Quasi-steady Magnetoplasmadynamic Arcjet," NASA NGL 31-001-005, Aerospace and Mechanical Sciences Rept. No. 940, Oct. 1970, Princeton Univ., Princeton, N. J.

[112] Oberth, R. C., "Anode Phenomena in High-Current Discharges," Ph.D. thesis, Dec. 1970, Princeton Univ., Princeton, N. J.

[113] Oberth, R. C. and Jahn, R. G., "Anode Phenomena in High-Current Discharges," NASA NGL 31-001-005, Aerospace and Mechanical Sciences Rept. No. 961, Dec. 1970, Princeton Univ., Princeton, N. J.

[114] Di Capua, M. S. and Jahn, R. G., "Voltage-Current Characteristics of Parallel-Plate Plasma Accelerators," A.I.A.A. Bulletin, Vol. 8, No. 1, Jan. 1971, p. 40.

[115] Oberth, R. C. and Jahn, R. G., "Anode Phenomena in High-Current Accelerators," A.I.A.A. Bulletin, Vol. 8, No. 1, Jan. 1971, p. 40.

[116] Di Capua, M. S. and Jahn, R. G., "Energy Deposition in Parallel-Plate Plasma Accelerators," A.I.A.A. Paper 71-197, A.I.A.A. 9th Aerospace Sciences Meeting, New York, N. Y., 25-27 Jan. 1971.

PROJECT REFERENCES

[117]Oberth, R. C. and Jahn, R. G., "Anode Phenomena in High-Current Accelerators," A.I.A.A. Paper 71-198, A.I.A.A. 9th Aerospace Sciences Meeting, New York, N. Y., 25-27 Jan. 1971.

[118]Jahn, R. G., Clark, K. E., Oberth, R. C. and Turchi, P. J., "Acceleration Patterns in Quasi-steady MPD Arcs," A.I.A.A. Journal, Vol. 9, No. 1, Jan. 1971, pp. 167-172.

[119]Jahn, R. G., von Jaskowsky, W. F. and Clark, K. E., "Pulsed Electromagnetic Gas Acceleration," NASA NGL 31-001-005, semi-annual report for period 1 July 1970 to 31 December 1970, Aerospace and Mechanical Sciences Rept. No. 634p, January 1971, Princeton University, Princeton, N. J.

[120]Jahn, R. G., von Jaskowsky, W. F. and Clark, K. E., "Pulsed Electromagnetic Gas Acceleration," NASA NGL 31-001-005 step-funding renewal proposal for the period 1 October 1971 to 30 September 1972, June 16, 1971, Princeton Univ., Princeton, N. J.

[121]Clark, K. E., Jahn, R. G. and von Jaskowsky, W. F., "Exhaust Characteristics of a Quasi-steady MPD Accelerator," DGLR Symposium on Electric Space Thruster System, Braunschweig, Germany, June 22-23, 1971, DLR Mitt. 71-21, Teil 1, pp. 81-100.

[122]Turchi, P. J. and Jahn, R. G., "Cathode Region of a Quasi-steady MPD Arcjet," A.I.A.A. Journal, Vol. 9, No. 7, July 1971, pp. 1372-1379.

[123]Jahn, R. G., von Jaskowsky, W. F. and Clark, K. E., "Pulsed Electromagnetic Gas Acceleration," NASA NGL 31-001-005, semi-annual report for period 1 January 1971 to 30 June 1971, Aerospace and Mechanical Sciences Dept. No. 634q, July 1971, Princeton University, Princeton, N. J.

[124]Cory, John S., "Mass,Momentum and Energy Flow from an MPD Accelerator," Ph.D. thesis, August 1971, Princeton University, Princeton, N. J.

PROJECT REFERENCES

[125]Cory, J. S. and Jahn, R. G., "Mass, Momentum and Energy Flow from an MPD Accelerator," NASA NGL 31-001-005, Aerospace and Mechanical Sciences Rept. No. 999, September 1971, Princeton University, Princeton, N. J.

[126]Jahn, R. G., von Jaskowsky, W. F. and Clark, K. E., "Quasi-steady Plasma Acceleration," International Symposium on Dynamics of Ionized Gases, University of Tokyo, September 1971.

[127]Di Capua, M. S., "Energy Deposition in the Parallel-Plate Plasma Accelerator," Ph.D. thesis, November 1971, Princeton University, Princeton, N. J.

[128]Di Capua, M. S. and Jahn, R. G., "Energy Deposition in Parallel-Plate Plasma Accelerators," NASA 31-001-005, Aerospace and Mechanical Sciences Rept. No. 1015, December 1971, Princeton University, Princeton, N. J.

[129]Parmentier, N., "Hollow Cathode, Quasi-steady MPD Arc," M.S.E. thesis, December 1971. Princeton University, Princeton, N. J.

[130]Parmentier, N. and Jahn, R. G., "Hollow Cathode, Quasi-steady MPD Arc," NASA NGL 31-001-005, Aerospace and Mechanical Sciences Rept. No. 1023, December 1971, Princeton University, Princeton, N. J.

[131]Jahn, R. G., von Jaskowsky, W. F. and Clark, K. E., "Pulsed Electromagnetic Gas Acceleration," NASA NGL 31-001-005, semi-annual report for period 1 July 1971 to 31 December 1971, Aerospace and Mechanical Sciences Report No. 634r, January 1972, Princeton University, Princeton, N. J.

[132]Oberth, R. C. and Jahn, R. G., "Anode Phenomena in High-Current Accelerators," A.I.A.A. Journal, Vol. 10, No. 1, January 1972, pp. 86-91.

[133]Clark, K. E., "Electric Propulsion," Astronautics and Aeronautics, Vol. 10, No. 2, February 1972, pp. 22-23.

[134]Hixon, T. L., "Near-Ultraviolet Spectroscopic Studies of a Quasi-Steady Magnetoplasmadynamic Arc,"B.A. thesis, April 1972, Princeton University, Princeton, N. J.

[135]Hixon, T. L., "Near-Ultraviolet Spectrographic Studies of AIII in an MPD Arc Discharge," Paper presented at the Northeastern Regional Student Conference, Rutgers University, New Brunswick, N. J., April 29, 1972.

PROJECT REFERENCES

[136]Clark, K. E., Jahn, R. G. and von Jaskowsky, W. F., "Distribution of Momentum and Propellant in a Quasi-Steady MPD Discharge," A.I.A.A. Bulletin, Vol. 9, No. 4, April 1972, p. 165.

[137]Bruckner, A. P. and Jahn, R. G., "Exhaust Plume Structure in a Quasi-steady MPD Arc," A.I.A.A. Bulletin, Vol. 9, No. 4, April 1972, p. 166.

[138]Clark, K. E., Jahn, R. G. and von Jaskowsky, W. F., "Measurements of Mass, Momentum and Energy Distributions in a Quasi-Steady MPD Discharge," A.I.A.A. Paper 72-497, A.I.A.A. 9th Electric Propulsion Conference, Bethesda, Md., 17-19 April 1972.

[139]Bruckner, A. P. and Jahn, R. G., "Exhaust Plume Structure in a Quasi-Steady MPD Arc," A.I.A.A. Paper 72-499, A.I.A.A. 9th Electric Propulsion Conference, Bethesda, Md., 17-19 April, 1972.

[140]Bruckner, A. P., "Spectroscopic Studies of the Exhaust Plume of a Quasi-steady MPD Accelerator," Ph.D. thesis, May 1972, Princeton University, Princeton, N. J.

[141]Bruckner, A. P. and Jahn, R. G., "Spectroscopic Studies of the Exhaust Plume of a Quasi-steady MPD Accelerator," NASA NGL 31-001-005, Aerospace and Mechanical Sciences Rept. No. 1041, May, 1972, Princeton University, Princeton, N. J.

[142]Jahn, R. G., von Jaskowsky, W. F. and Clark, K. E., "Pulsed Electromagnetic Gas Acceleration," NASA NGL 31-001-005 step-funding renewal proposal for the period 1 October 1972 to 30 September 1973, June 1972, Princeton University, Princeton, N. J.

[143]Jahn, R. G., von Jaskowsky, W. F. and Clark, K. E., "Pulsed Electromagnetic Gas Acceleration," NASA NGL 31-001-005, semi-annual report for period 1 January 1972 to 30 June 1972, Aerospace and Mechanical Sciences Report No. 634s, July 1972, Princeton University, Princeton, N. J.

[144]Kelly, A. J. and Clark, K. E., "Plasma Propulsion Systems," Aerospace and Mechanical Sciences Rept. No. 1074, September 1973, Princeton University, Princeton, N. J.

[145]Greco, R. V., Bliss, J. R., Murch, C. K., Clark, K. E., and Kelly, A. J., "Resistojet and Plasma Propulsion System Technology," AIAA Paper 72-1124 (1972).

PROJECT REFERENCES

[146] Jahn, R. G., von Jaskowsky, W. F. and Clark, K. E., "Pulsed Electromagnetic Gas Acceleration," NASA NGL 31-001-005, semi-annual report for period 1 July 1972 to 31 December 1972, Aerospace and Mechanical Sciences Report No. 634t, January 1973, Princeton University, Princeton, N. J.

[147] Fradkin, D. B., "Analysis of Acceleration Mechanisms and Performance of an Applied Field MPD Arcjet," Ph.D. thesis, March 1973, Princeton University, Princeton, N. J.

[148] Jahn, R. G., von Jaskowsky, W. F. and Clark, K. E., "Quasi-Steady Plasma Acceleration," in Dynamics of Ionized Gases, Proceedings of the International Symposium on Dynamics of Ionized Gases sponsored by the International Union of Theoretical and Applied Mechanics, Tokyo, Japan, September 13-17, 1971, University of Tokyo Press, 1973, Edited by M. J. Lighthill, I. Imai and H. Sato.

[149] von Jaskowsky, W. F., Jahn, R. G., Dutt, G. S. and Clark, K. E., "Impact Pressure Measurements in a Quasi-Steady MPD Discharge," Paper dedicated to Prof. H. Maecker, Technical University, Munich, Germany (April 1973).

[150] Jahn, R. G., von Jaskowsky, W. F. and Clark, K. E., "Pulsed Electromagnetic Gas Acceleration," renewal proposal for the period 1 October 1973 to 30 September 1974, June 1973, Princeton University, Princeton, N. J.

[151] Jahn, R. G., von Jaskowsky, W. F. and Clark, K. E., "Pulsed Electromagnetic Gas Acceleration, NASA NGL 31-001-005 semi-annual report for period 1 January 1973 to 30 June 1973, Aerospace and Mechanical Sciences Report No. 634u, July 1973, Princeton University, Princeton, N. J.

[152] Boyle, M. J., and Jahn, R. G., "Effects of Insulator Ablation on the Operation of a Quasi-Steady MPD Arc," A.I.A.A. Paper 73-1090, A.I.A.A. 10th Electric Propulsion Conference, Lake Tahoe, Nev., Oct. 31-Nov. 2, 1973.

[153] Saber, A. J. and Jahn, R. G., "Anode Power Deposition in Quasi-Steady MPD Arcs," A.I.A.A. Paper 73-1091, A.I.A.A. 10th Electric Propulsion Conference, Lake Tahoe, Nev., Oct. 31-Nov. 2, 1973.

PROJECT REFERENCES

[154] von Jaskowsky, W. F., Krishnan, M., Jahn, R. G. and Clark, K. E., "The Hollow Cathode in the Quasi-Steady MPD Discharge," A.I.A.A. Paper 73-1092, A.I.A.A. 10th Electric Propulsion Conference, Lake Tahoe, Nev., Oct. 31-Nov. 2, 1973.

[155] Jahn, R. G., von Jaskowsky, W. F. and Clark, K. E., "Pulsed Electromagnetic Gas Acceleration," NASA NGL 31-001-005, semi-annual report for period 1 July 1973 to 31 December 1973, Aerospace and Mechanical Sciences Report No. 634v, January 1974, Princeton University, Princeton, N. J.

[156] Saber, A. J., "Anode Power in the Quasi-Steady MPD Thruster," Ph.D. thesis, May 1974, Princeton University, Princeton, N. J.

[157] Jahn, R. G., von Jaskowsky, W. F. and Clark, K. E., "Pulsed Electromagnetic Gas Acceleration," renewal proposal for the period 1 October 1974 to 30 September 1975, June 1974, Princeton University, Princeton, N. J.

[158] Boyle, M. J., "Acceleration Processes in the Quasi-Steady Magnetoplasmadynamic Discharge," Ph.D. thesis (to be published), Princeton University, Princeton, N. J.

GENERAL REFERENCES

A-1 Malliaris, A. C., John, R. R., Garrison, R. L. and Libby, D. R., "Performance of Quasi-steady MPD Thrusters at High-Powers," A.I.A.A. Journal, Vol. 10, No. 2, February 1972, pp. 121-122.

A-2 Shapiro, A. H., The Dynamics and Thermodynamics of Compressible Fluid Flow, Vol. I, Ronald Press Company, New York, 1953.

A-3 Baum, E. and Cann, G. L., "Thermodynamic Properties of Argon," ARL 63-133, Electro-Optical Systems, Inc., Pasadena, California, August, 1963.

A-4 Spitzer, L., Physics of Fully Ionized Gases, Interscience Publishers, New York, 1962.

A-5 Liepmann, H. W. and Roshko, A., Elements of Gasdynamics, John Wiley and Sons, Inc., New York, 1957.

A-6 Bates, D. R., Kingston, A. E. and McWhirter, R. W. P., "Recombination between electrons and atomic ions," Proceedings of the Royal Society, A 267, January, 1962.

APPENDIX A: Semi-annual Statement of Expenditures

PULSED ELECTROMAGNETIC GAS ACCELERATION

NASA NGL 31-001-005

1 January 1974 to 30 June 1974

DIRECT COSTS			
I.	Salaries		
	A. Professional	$18,337	
	B. Technicians	11,814	
	C. Students	2,770	
	D. Supporting Staff	2,364	
			$35,285
II.	Employee Benefits (21%)		6,828
III.	Equipment		0
IV.	Materials and Services		7,678
V.	Travel		0
VI.	Tuition		2,320
	Total Direct Costs		$52,111
INDIRECT COSTS			
VII.	Overhead (80%)		28,228
	Total		$80,339

END

DATE

FILMED

JAN 24 1975